Available online at www.sciencedirect.com
ScienceDirect
Surface Science Reports 62 (2007) 63–109
surface science reports
www.elsevier.com/locate/surfrep

Surface composition analysis by low-energy ion scattering

H.H. Brongersma[a,b,*], M. Draxler[c], M. de Ridder[a], P. Bauer[c]

[a] *Calipso B.V., P.O. Box 513, 5600 MB Eindhoven, The Netherlands*
[b] *Department of Applied Physics, Eindhoven University of Technology, P.O. Box 513, 5600 MB Eindhoven, The Netherlands*
[c] *Institut für Experimentalphysik, Johannes Kepler Universität Linz, A-4040 Linz, Austria*

Received 7 December 2006; accepted 11 December 2006

Dedicated to the memory of Arnoud W. Denier van der Gon

Abstract

Low-energy ion scattering (LEIS) is an analytical tool that provides information on the atomic composition of the outer surface, when noble gas ions are used as projectiles. In fact, quantitative composition analysis is currently done on a huge variety of materials, including catalysts and organic materials. The information on the surface composition is contained in the signal of backscattered ions (typically 1–3 keV He^+, Ne^+). In order to translate the LEIS signal to an elemental surface concentration all factors determining the LEIS signal must be known. These are in particular the scattering cross section and the ion fraction of the backscattered particles. The scattering cross section, which is due to the screened electrostatic potential between target atom and projectile, is well-known for the prevailing conditions of LEIS. It is an intriguing fact that, despite the large quantity of successful applications, the charge exchange processes in LEIS are not yet fully understood. It is e.g. not known why in LEIS for a given atomic species on the surface the signal usually does not depend on which other species are present (absence of matrix effects). Significant progress has recently been made in the understanding of the underlying charge exchange processes.

Therefore, the aim of this review is twofold: on the one hand, to summarize the present understanding of the factors that determine the ion fraction of the scattered projectiles in LEIS, i.e. charge exchange processes. On the other hand, to summarize how quantitative surface composition analysis can be accomplished.

In addition, we critically review publications that deal with surface composition analysis by LEIS, and analyze in which cases and by what means this was achieved and where and why it was successful or failed. After reading this review the reader will be able to deal with the pitfalls encountered in LEIS and to choose preferred experimental conditions for quantitative surface composition analysis.

Keywords: LEIS; ISS; Quantitative surface composition analysis

Contents

* Corresponding author at: Calipso B.V., P.O. Box 513, 5600 MB Eindhoven, The Netherlands. Tel.: +31 40 247 4281; fax: +31 40 245 3587.
E-mail address: H.Brongersma@calipso.nl (H.H. Brongersma).

0167-5729/$ - see front matter © 2006 Elsevier B.V. All rights reserved.
doi:10.1016/j.surfrep.2006.12.002

1. Introduction

Low-Energy Ion Scattering (LEIS), also called Ion Scattering Spectroscopy (ISS), is a unique tool in surface analysis, since it provides the atomic composition of the outer atomic layer. To take full advantage of this feature, it is important that the results can be quantified, which can be a nontrivial problem. The objective of this review is to describe relevant fundamental processes in LEIS, indicate cases where quantification is straightforward and where it is not, and to obtain guidelines for experimental conditions, which enable a reliable quantification. The outer surface atoms dominate many processes such as adhesion, catalysis, electron emission, growth and wetting. It is, therefore, not surprising that in 80%–90% of the challenges facing chemical and electronic industry relate to surfaces. In the case of poor adhesion they relate to the surfaces that are exposed after failure. While for other surface analytic techniques the composition analysis is an average over a few or generally even over many atomic layers, for LEIS the analysis is selective for the outer atoms. Nowadays LEIS is just as easy to apply to conductors as to insulators, to atomically flat single crystals as well as highly dispersed amorphous materials, and at any temperature of the sample. Thus, all kinds of materials are studied, including metals, semiconductors, ceramics, organics and polymers. The only major restriction being, similar to the other beam techniques in surface analysis, which need vacuum, that the materials vapor pressure is low enough to sustain the vacuum. In addition to the exploitation of the surface sensitivity mentioned above, it is also possible to obtain in-depth information on the composition of the outer few nm. This non-destructive analysis relies on the use of a specific property of the ions (reionization). Typical applications of this feature include ultra-thin layers (0–10 nm). This progress in combination with the surface selectivity has widened the scope of applications tremendously.

Thus, nowadays typical applications of LEIS include:

Adhesion:	Origin of pinholes in thin layers, improvement of primers
Catalysis:	Understanding and improvement of catalysts, site of poisoning, quantification of promoters, size of nanoclusters
Electron emission:	Understanding low work function materials, development of new cathodes
Wetting:	Development of new anti-wetting surfaces
Biology/ medicine:	Biocompatibility, biosensors, bone growth
Semiconductors:	Thickness distribution, high-k dielectrics, diffusion barriers.

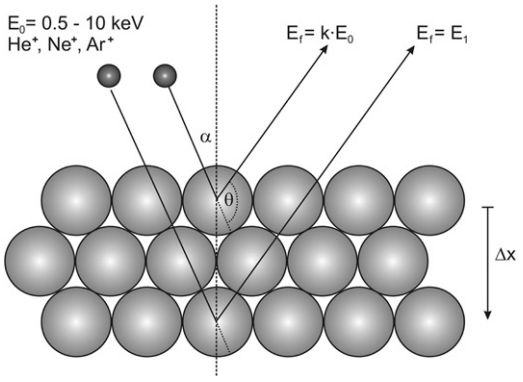

Fig. 2.1. Schematic of experimental conditions in LEIS.

Since the aim of the present paper is to develop a reliable framework for quantitative composition analysis of the outer surface, we restrict ourselves to experimental conditions that simplify this.

In particular this review is mainly limited to:

- Energy range: 500–10 000 eV
- Use of noble gas ions (He^+, Ne^+, Ar^+).
- Angles $>30°$ with the surface for both the in- and outgoing ions.

This choice of experimental conditions is thus very different from those that are favored for surface structure analysis.

2. Fundamentals of LEIS and composition analysis

In LEIS a sample (target) is bombarded with noble gas ions (He^+, Ne^+ or Ar^+) with energies (E_0) between 0.5 and 10 keV. The incident ion beam is directed towards the surface at an angle α with respect to the surface normal; typically, α is smaller than 60°. Only projectiles that are backscattered into a certain solid angle element $d\Omega$ (at a scattering angle θ; typically 140°) are analyzed (Fig. 2.1). For quantitative surface analysis, only the signal of scattered ions, S^+, is analyzed. It may also be advantageous to analyze the signal of backscattered neutrals, S^0 (see also Sections 6 and 8).

In this regime, projectiles are scattered from surface atoms almost exclusively by binary collisions, with an energy $E_f = kE_0$ ($k < 1$, see Eq. (2.1) and Fig. 2.2). Ions that have penetrated the target up to a depth Δx will leave the surface with an energy $E_1 < kE_0$.

2.1. Binary collision peak

In an elastic binary collision of a projectile of mass m_1 and primary energy E_0 with a target atom of mass m_2 at rest, the energy transfer only depends on the scattering angle θ. The kinematic factor k, which is defined as the ratio E_f/E_0, can be

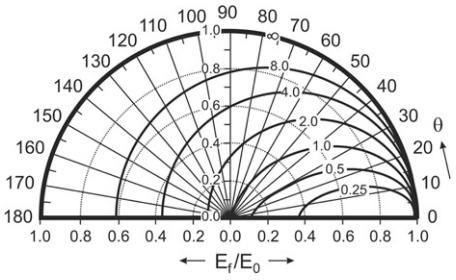

Fig. 2.2. Polar diagram representing Eq. (2.1). The energy ratio E_f/E_0 is given for mass ratios $q = m_2/m_1 = 0.25, 0.5, 1, 2, 4, 8$ and ∞ as a function of the scattering angle θ. For $\theta > 90°$ there is only one value for the energy ratio.

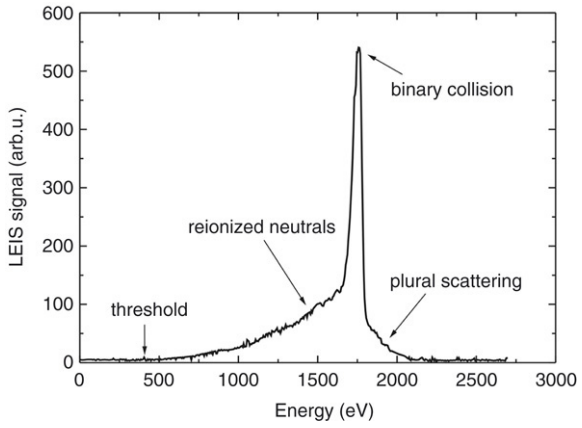

Fig. 2.3. LEIS spectrum of 3 keV He^+ scattered over 142° by polycrystalline aluminum [116].

calculated from energy and momentum conservation and yields (for a detailed derivation see for instance [1])

$$E_f = k \cdot E_0 = \left(\frac{\cos\theta \pm \sqrt{\left(\frac{m_2}{m_1}\right)^2 - \sin^2\theta}}{1 + \frac{m_2}{m_1}} \right)^2 \cdot E_0 \qquad (2.1)$$

where the positive sign applies to $m_2/m_1 \geq 1$ while both positive and negative signs are solutions if $1 \geq m_2/m_1 \geq |\sin\theta|$.

From Eq. (2.1) it becomes obvious that for scattering angles above 90° E_f is a unique function of m_2. Eq. (2.1) is also depicted in Fig. 2.2 as a polar diagram. Here, E_f/E_0 is used as the polar axis but sometimes it is advantageous to use the square root of E_f/E_0 as the polar axis in such a diagram [2]. It is seen that backscattering ($\theta > 90°$) for a mass ratio $q = m_2/m_1 < 1$ is not possible. Consequently, hydrogen is the only element that cannot be directly detected in backscattering (see also Section 8). Mass separation deteriorates rapidly for small scattering angles and for $q > 10$. It is also influenced by other factors like energy spread of the primary ions, energy resolution of the analyzer, thermal vibrations of the target atoms and finite acceptance angle of the analyzer. In practice, values of $q > 2$ are preferred, since for $q < 2$ the final energy of the projectile is very low and neutralization so efficient that detection becomes difficult.

A typical LEIS spectrum for 3 keV He^+ ions scattered by a pure Al target is given in Fig. 2.3 ($\theta = 142°$, $\alpha = 0°$). The (binary collision or surface) peak is due to He^+ ions that are backscattered in a single collision from an Al atom at the surface of the target. The signal at higher energies originates from double and multiple scattering of He^+ ions. The background at energies lower than that of the elastic peak (the "low-energy tail") is a result from backscattering in deeper layers. Its intensity is mainly due to a reionization process (Section 3.1.2). This tail provides non-destructive in-depth information. The onset of the tail gives the reionization threshold (Section 6.3).

For a multi-component sample the masses of the different target atoms can be derived from the positions of the binary collision peaks; the intensities of these surface peaks are a measure for the atomic surface concentrations.

2.2. Determination of the atomic surface concentration

The yield of ions, S_i, backscattered from a surface atom of mass m_i, is a measure for the atomic surface concentration N_i (see also Section 4.2) according to:

$$S_i = \frac{I_p}{e} \cdot t \cdot \xi \cdot R \cdot \eta_i \cdot N_i. \qquad (2.2)$$

Here, the following symbols have been used

- I_p, the primary ion beam current and e the elementary charge,
- t, the acquisition time,
- ξ, an instrumental factor including detector solid angle, detector efficiency and analyzer transmission (see also Section 5),
- R, a factor, which takes the surface roughness and the shielding by neighboring atoms into account (see also Section 8.2),
- η_i, the elemental sensitivity factor, given by

$$\eta_i = P_i^+ \cdot \frac{d\sigma_i}{d\Omega}, \qquad (2.3)$$

with the ion fraction $P_i^+ = S_i^+/(S_i^+ + S_i^0)$ (see also Sections 3, 4 and 7) and the differential scattering cross section $\frac{d\sigma_i}{d\Omega}$, which can be calculated for a given scattering potential [3].

In the regime of high energy ion backscattering (Rutherford backscattering, RBS) the Coulomb repulsion between two nuclei $V_C(r)$ is a reasonable choice for the scattering potential. In the LEIS regime, screening of the nuclear charges by electrons bound to the target atom and to the ion becomes important. There are various representations of the resulting screened scattering potential [4] available, like the Thomas–Fermi–Molière (TFM) potential or the "universal potential" (ZBL) [3], which are a reasonable basis to calculate $d\sigma/d\Omega$ in the LEIS regime (see Fig. 2.4). Both types of potentials are of the form $V_C(r) \cdot \Phi(r/a)$ with screening functions Φ that are represented by a sum of single exponentials with prefactors that sum up to unity and screening lengths a

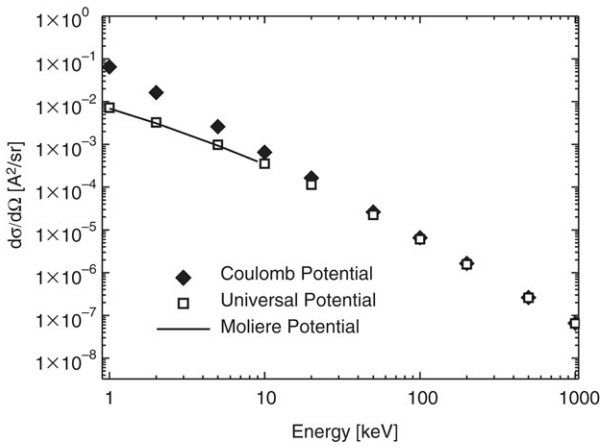

Fig. 2.4. Differential scattering cross sections for $^4He^+$ and Cu and a scattering angle $\theta = 129°$ for various potentials.

that depend on the atomic numbers of scattering centre and projectile [4].

In principle, either the peak area or height can be used as LEIS signal for surface composition analysis, but the peak area is the more appropriate physical quantity. Quantitative surface composition analysis is based on Eq. (2.2). However, the elemental sensitivity factor is only known for a few combinations of elements, incident ions, ion energies and scattering angles [5,6]. Therefore, quantitative analysis is often based on calibration against reference samples with known surface concentrations. A good example of a quantitative determination of the surface composition with LEIS is given for a $Cu_{55}Pd_{45}$ alloy sample [6]. Three different groups have sputter-cleaned the sample using the same procedure and subsequently measured the surface composition using $^4He^+$ ion scattering at various energies. Calibration was done via pure Pd and Cu reference samples which have been measured under identical conditions. The three groups involved obtained concordant values of the surface composition, i.e. 58 ± 3 at.% Cu.

Generally, the elemental sensitivity factor is a smooth function of the incident ion energy (at a fixed scattering geometry). There are, however, also a few projectile–target combinations that exhibit a more complex energy dependence of the sensitivity factor. For example, for He^+ projectiles and Pb the sensitivity factor shows an oscillatory behavior as a function of the incident ion energy [7]. These oscillations are caused by resonant neutralization effects (see Section 3).

The surface sensitivity of LEIS is largely due to the fact that only scattered ions are analyzed. In general, most of the incoming ions are neutralized upon impact. Therefore, knowledge about neutralization is a necessary requirement for the understanding of the sensitivity factor. Neutralization introduces interesting physics and insight into this physics helps in choosing experimental conditions which allow for quantitative analysis of the surface composition with LEIS.

3. Charge exchange processes

The inelastic interaction of low energy ions with surfaces is quite a complex subject which has manifold aspects depending on the specific type of projectile and primary energy [8]. Here, we review the present knowledge about charge exchange processes of noble gas ions at energies ∼100 eV–10 keV, in particular of He^+ and Ne^+, backscattered from solid surfaces at a large angle (>90°). In this regime, backscattering occurs via binary collisions between the projectile and a surface atom.

3.1. Noble gas projectiles

At these low velocities, the equilibrium charge state of projectiles moving in matter is a dynamic one, i.e. the projectile charge state fluctuates due to continuous electron *capture* and *loss* processes along the trajectory [9]. The charge state of noble gas ions is close to neutral due to their large excitation energy. In LEIS, the projectile first passes the electron gas in front of the surface, and then is backscattered in a collision with a surface atom. During the collision process, additional mechanisms of charge exchange become possible, due to the interaction of projectile levels with target electrons. This is discussed in more detail in the following sections.

3.1.1. Shift and broadening of electronic levels during interaction

When discussing electronic transitions from a target to an ion moving in front of the sample surface (and vice versa), one has to be aware of the fact that the electronic levels of projectile and surface atoms are modified with respect to the static levels at infinite distance: the projectile levels shift (and broaden) during the surface collision, due to the interaction of the projectile states with the conduction band and with the bound electrons of the target.

For sufficiently large distances, the force experienced by the ion and the shift of its electron levels in front of a surface are described by the image potential, which leads to attraction of the ion. For a positive ion, the binding energy of occupied levels is lowered, due to the repulsion by the (negative) image charge [10,11]. When the distances between projectile and scattering center becomes sufficiently small, the projectile levels interact with the valence and core electrons of the target, and the situation is much more complex. Let us, e.g., consider a He^+ ion in front of an Al surface [12]: at a distance of about 6 atomic units (a.u.) (≈3 Å) first deviations from the simple image charge picture occur already, due to electrostatic interaction of the He 1s level with the Al conduction electrons, leading to an upwards shift of the He level. At a distance of about 2 a.u. (≈1 Å) the overlap with the Al core electrons (2p) becomes significant and will promote the He 1s level so high that it becomes resonant with the conduction band at distances smaller than ≈1 a.u. (0.5 Å), see Fig. 3.1.

In general, it depends on the binding energies and on the symmetries of the electronic levels involved, whether promotion of projectile levels occurs. Calculations are commonly performed using the molecular orbitals (MO) approach, based on the pioneering work on diabatic correlation diagrams by Fano and Lichten [13], extended to asymmetric target–projectile combinations by Barat and Lichten [14].

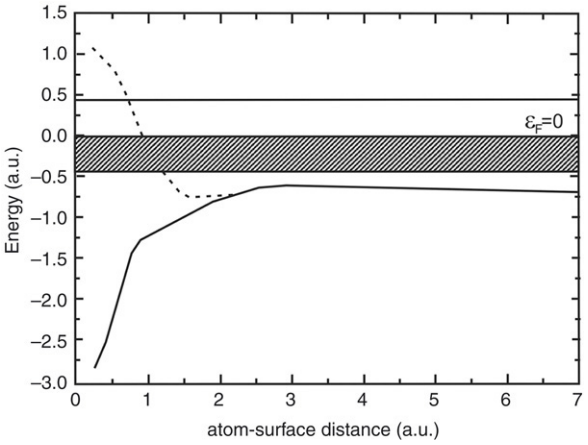

Fig. 3.1. The adiabatic energy level of He in front of Al (dashed line) is shown together with the diabatic level (continuous line). The top and the bottom of the conduction band of Al are schematically drawn as two horizontal straight lines. The Fermi level ε_F corresponds to zero energy so that the hatched region represents the occupied part of the band. Due to the interaction between He and the core electrons of Al, the He-1s level is promoted and resonates with the conduction band close to the surface [170].

Tsukada and coworkers have performed Hartree–Fock self-consistent field calculations to investigate how MO energy levels behave when a He^+ ion approaches an atom [15].

Connected with the shift, there is also a resonant broadening of the projectile levels due to their finite interaction time. First studies of atomic levels in front of a surface were performed within perturbation theory, following the original work of Gadzuk [16,17].

3.1.2. Charge exchange processes in front of a surface

In the following, we will discuss the relevant charge exchange processes, and will combine them to a coherent model of ion fractions in LEIS. The relevant processes are (i) resonant processes, (ii) Auger processes, (iii) collision induced processes.

(i) Resonant processes

(a) *Transitions involving the target conduction band (C–RN)*:

Resonant processes between states in the target conduction band and weakly bound states of the projectile may occur, when a projectile moves in front of a surface. This leads to neutralization (RN), if the electron tunnels from the conduction band to the projectile, or to ionization (RI) in the reverse case (see Fig. 3.2).

Since resonant processes proceed via electron tunneling, their probabilities depend strongly on the projectile–surface distance and on the binding energies of the levels. In a resonant transition only one electron is involved; therefore the corresponding transition rates (i.e. the probability for a resonant transition per time unit), $1/\tau_R$, are (within linear theory) proportional to the density of involved electronic states and they are commonly assumed to be 'high', so that resonance processes are assumed to be dominant at atomic distances, whenever they are possible.

For metals it was found that the dependence of $1/\tau_R$ on the distance from the surface plane, z, may be described by a single

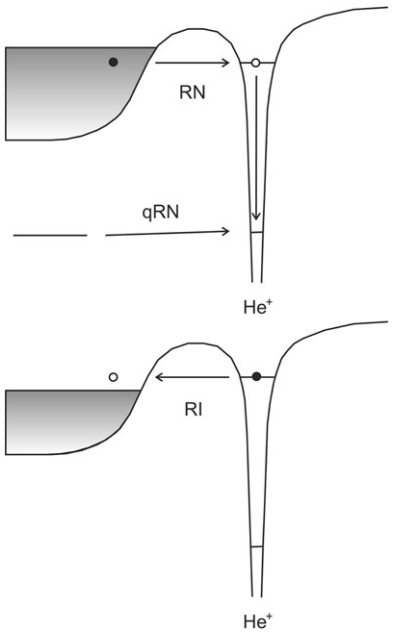

Fig. 3.2. Visualization of Resonance Neutralization (RN) and of Resonance Ionization (RI). Also shown is the quasiresonant neutralization (qRN).

exponential, multiplied by a polynomial (both in z) [18,19]. In view of the fact that neutralization occurs over a limited z range, the following simplified ansatz for $1/\tau_R$ is justified [20]:

$$\frac{1}{\tau_R(z)} = A_R \cdot \exp^{-a_R z} . \tag{3.1}$$

Here, the parameter A_R represents a characteristic transition rate (at $z = 0$), and a_R is the reciprocal interaction length.

First-principles calculations solve the time-dependent quantum mechanical problem, using the position dependent ground state energy of the projectile and the hopping integrals between the target orbitals and the projectile level as input data. From this, the occupancy of the final states is obtained after scattering; the mean occupancy of the charge state +1 is the relevant quantity to be compared to the experimental ion fraction [21].

(b) *Transitions involving bound levels of the target (B–RN):*

Charge transfer from a target atom to the ground state of a noble gas ion via a resonant transition may occur at larger distances (typically >1 Å) only if the electron originates from an atomic level of the target. This is possible only for specific elements with electronic levels at appropriate energy. Erickson and Smith were the first to observe very pronounced resonances in the scattered ion yields for scattering of He^+ ions by elements such as Pb [7] and Brongersma and Buck found oscillations in the scattering of Ne^+ by Au [22]. Since there is rarely a perfect match between the levels of the atom and ion, the neutralization is only quasiresonant (qRN, see Fig. 3.2). The energy defect (ΔE) between the initial and final states has a strong influence on the damping and thus on the quality of the resonance. In practice clear resonances are only observed when $\Delta E \leq 10$ eV, while strong resonances only occur for $\Delta E \leq 5$ eV. Another requirement for oscillatory behavior is the symmetry of the atomic orbital from which the electron

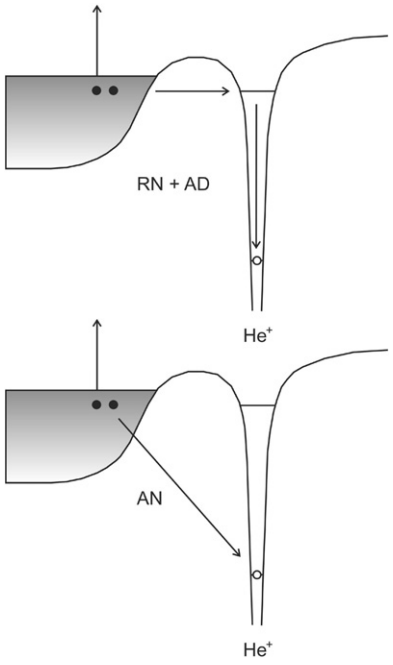

Fig. 3.3. Visualization of Auger De-excitation (AD) (after RN) and of Auger Neutralization (AN).

is transferred. Strong oscillations are only observed when the electron originates from a localized d-level.

The chemical environment of a surface atom will influence the binding energies of the relevant atomic levels (*chemical shift*, as in X-ray Photoelectron Spectroscopy XPS). This should thus also affect the oscillations. Subtle differences have indeed been observed [23–25], for instance for scattering of He^+ by In in $ZnIn_2S_4$, InP and In [23]. Zartner et al. [26] also demonstrated the differences in the oscillatory behavior for metallic and atomic Pb. Practically all known oscillatory combinations relate to He^+ ions. For Ne^+ only Au [22] gives a clear oscillation, while for Ne^+ and Ga an oscillatory behavior has also been observed [27], but the oscillations are weak (although the non-monotonic structure is clear [28]).

(ii) Auger neutralization (AN)

Auger transitions are possible for many ion–target combinations, with several processes contributing to the total Auger rate:

- *direct* AN of the incoming He^+ ion to the ground state by a metal electron, with excitation of another metal electron or a plasmon (with transition rate $1/\tau_{DA}$),
- *direct Auger de-excitation*, where a metastable He atom is first formed by tunneling of a metal electron to singlet states (2^1S–2^1P), which then decays to the ground state (1^1S), with excitation of a metal electron or a plasmon (with transition rate $1/\tau_{AD}$),
- *indirect Auger de-excitation (Penning de-excitation)*, where a metal electron fills the 1s hole of a He atom that is excited in a triplet state, with emission of the He $n = 2$ electron.

For Auger neutralization the first two processes (illustrated in Fig. 3.3) are dominant. Therefore, we may write the Auger transition rate, $1/\tau_A$, as

$$\frac{1}{\tau_A(z)} = \frac{1}{\tau_{DA}(z)} + \frac{1}{\tau_{AD}(z)}. \tag{3.2}$$

The transition rates for the Auger processes listed above are commonly calculated within the electron gas model [29–33], the description within the jellium model was found appropriate for perpendicular energies >100 eV [34]. Since in Auger processes two electrons are involved, the corresponding transition rates are usually lower than the transition rates of resonant processes. This is reflected by a smaller characteristic Auger rate, A_A, in the exponential ansatz, in analogy to Eq. (3.1):

$$\frac{1}{\tau_A(z)} = A_A \cdot \exp^{-a_{Az}}. \tag{3.3}$$

(iii) Collision induced processes

There is ample experimental evidence that incident neutrals can be ionized in the surface collision [35–37]. Of course, also incident ions can be reionized, after neutralization while approaching the surface. The term 'reionization' (ReI) refers to this situation. Since the reionization process is possible only in a close collision, it is also called collision induced reionization (CIR). Two different processes lead to collision induced reionization: (a) excitation of one projectile electron due to electron promotion, and (b) double excitation of the projectile during the close collision with the target atom and subsequent autoionization (see below). Let us discuss these processes in the following:

(a) *Collision induced reionization and neutralization*

It has been shown by ab initio Hartree–Fock calculations that *collision induced reionization* can be caused by level crossings of the He 1s level with open valence levels of the target, as a consequence of the antibonding interaction of the He 1s level with target core levels [15]. This process is illustrated in Fig. 3.4. At large distances from the surface, the total electronic energy of an ionized He atom ($He^+ + e^-$)

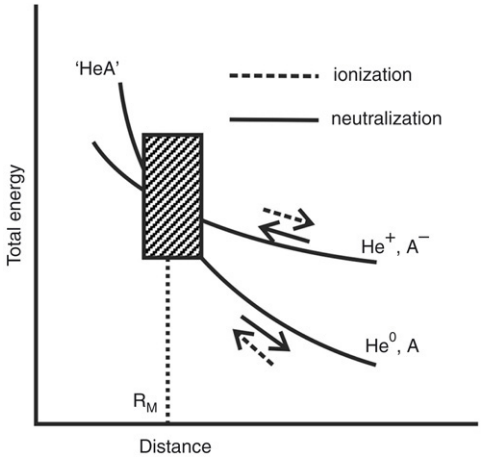

Fig. 3.4. Visualization of the reionization process ($He^0 \rightarrow He^+$) and of collision induced neutralization ($He^+ \rightarrow He^0$) by transfer of one electron. R_M denotes the distance at which the unperturbed potential energy surfaces would cross.

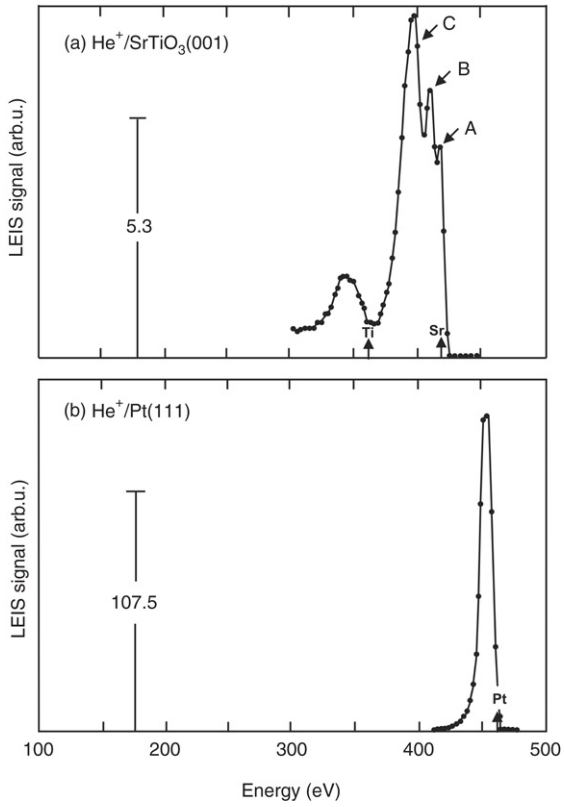

Fig. 3.5. Energy spectra for 500 eV He^+ ions scattered from (a) a $SrTiO_3$(001) surface and (b) from a Pt(111) surface. Peak positions of Ti, Sr, and Pt according to Eq. (2.1) are indicated. In (a) peak *A* refers to elastic scattering without inelastic losses, peak *B* refers to electron–hole pair excitation and peak *C* corresponds to either reionization or excitation of the Sr 4p electrons [38].

is larger than that of a neutral He projectile in the ground state (He^0). When the projectile approaches the surface, the interaction with target core levels may lead to a promotion of the He 1s level, if the principal quantum number of the molecular orbital formed is higher than that of the separated atoms. There is a critical distance, R_M, where the promoted level crosses levels of excited states, and transitions become possible, i.e. *(re)ionization* ($He^0 \rightarrow He^+ + e^-$). For positive ions incident, e.g. He^+, reionized projectiles have undergone a complete charge changing cycle $He^+ \rightarrow He^0 \rightarrow He^+$ which for He projectiles costs $\sim$20 eV + ε to move the electron to a level higher by ε than the Fermi level. This energy shift due to reionization has been observed for numerous projectile types and ionic compounds by Souda et al. [38] (see Fig. 3.5).

By exchange of the incoming and the outgoing particle in Fig. 3.4 (or the arrows of motion) it becomes clear that at R_M also a second process becomes possible [5]: *collision induced neutralization (CIN)*: $He^+ + e^- \rightarrow He^0$.

For a given scattering angle R_M is related to threshold energies, E_{th}, for both reionization and collisional resonant neutralization. Extensive experimental studies of the reionization threshold are listed in Ref. [39] and Table 6.1. The probability of reionization has been measured for He projectiles and many elemental surfaces [40]. Theoretical reionization probabilities for selected elements, calculated by solving the time dependent collision process, agree well with these data [41].

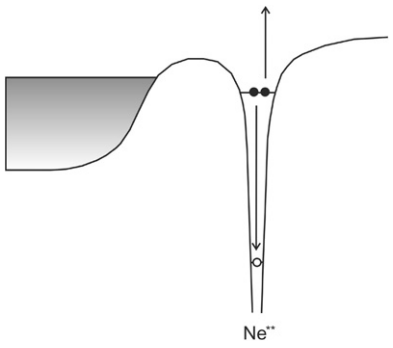

Fig. 3.6. Visualization of AU to Ionization (AuI).

The relative importance of collision induced reionization and of collision induced neutralization has been analyzed theoretically for the He–Al system [42] and experimentally for the He–Cu system [43]. The calculation showed, that in collision with an Al atom the promotion of the He 1s level is so strong that during the collision it becomes resonant with the Al conduction band, opening the resonance neutralization channel, even if in this case the levels at infinite separation are far from being resonant. The probabilities deduced from experiment made clear that CIN is by far more probable than CIR. This can be qualitatively understood on the basis that even after a CIR process, CIN is possible when projectile and atom are subsequently separating again.

(b) *Autoionization after double excitation (AuI)*

As mentioned above, a second mechanism can lead to reionization, i.e. double excitation of the projectile during the close collision with the target atom and subsequent autoionization [44]. For heavy projectiles like Ne^+, there are many ways how reionization via double excitation can be realized [45]. One typical example is the following (see Fig. 3.6):

- while approaching the surface, an impinging Ne^+ projectile is neutralized by AN ($Ne^+ \rightarrow Ne^0$),
- during the close encounter two electrons are promoted to exited states ($Ne^0 \rightarrow Ne^{**}$),
- while leaving the surface, the electronic excitation relaxes ($Ne^{**} \rightarrow Ne^+$). Similarly, triple excitation can lead to double ionization. Since these ions have the double charge, the peaks appear at half the deflection voltage in an electrostatic analyzer.

These autoionization processes are accompanied by pronounced inelastic energy losses, which are $\sim$54 eV for de-excitation of a Ne ($2p^{-2}$) configuration and $\sim$106 eV for Ne ($2s^{-2}$) (see Fig. 3.7 [46]). Note that the value observed in the laboratory frame for an inelastic energy loss in a collision between two atomic species may be considerably smaller than the corresponding value in the centre of mass system since the masses of the collision partners influence the conversion (see e.g., [45]).

For both mechanisms of reionization, energy is needed to promote the projectile electron(s). This energy is supplied by the projectile, by reduction of its kinetic energy, and represents an inelastic energy loss. In energy dependent measurements,

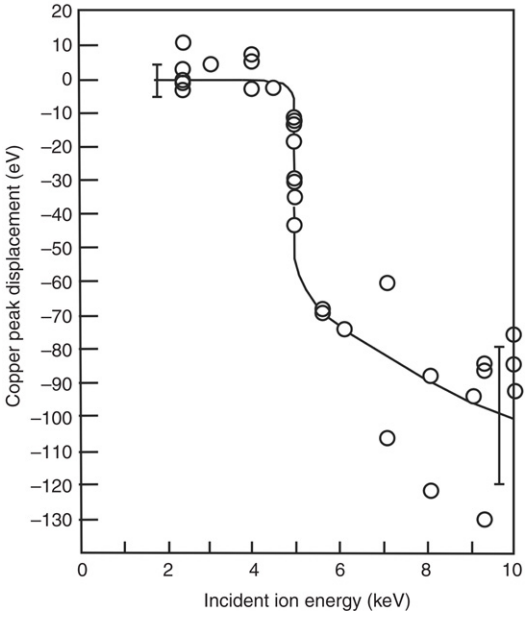

Fig. 3.7. Measured energy displacement of the Cu binary collision peak as determined from Ne^+ scattering by $Cu_3Au(100)$. A displacement of 0 eV corresponds to the energy predicted for ideal elastic scattering [46].

the identical threshold behavior as for reionization is also seen in the inelastic energy loss [45,46]. The experimental results are well reproduced by theory by tracing back the inelastic energy loss to the diabatic promotion of specific MOs to the continuum [47].

3.1.3. Scaling properties of individual charge exchange processes

In the following we describe how individual charge exchange processes depend on the projectile velocity (energy) and on the trajectory.

(a) *Transitions from the conduction band to the projectile (RN and AN)*

In the preceding section we have introduced the transition rates $1/\tau_R$ and $1/\tau_A$, for resonance neutralization from the conduction band and for Auger processes, respectively. For both processes, the transition probability (or the mean number of transitions), $\mathrm{d}P_{i,t}$, in the interval $\mathrm{d}z$ at the distance z on incoming or outgoing trajectory (the index i stands for in or out) is obtained from the transition rate τ:

$$\mathrm{d}P_{i,t} = \frac{\mathrm{d}t}{\tau(z)} = \frac{\mathrm{d}z}{\tau(z)} \cdot \frac{1}{v_{i,\perp}(z)}. \tag{3.4}$$

In Eq. (3.4), $v_{i,\perp}$ is the perpendicular velocity, i.e. the component of the ion velocity perpendicular to the surface on the way in or out. From this, the transition probability $\mathrm{d}P_i^+$ in a distance interval $\mathrm{d}z$, is given by $\mathrm{d}P_i^+ = -P_i^+ \cdot \mathrm{d}P_{i,t}^+$. The probability $P_{\mathrm{surv},i}^+$ that the ion does not get neutralized along the incoming or outgoing part of the trajectory is obtained by:

$$\begin{aligned} P_{\mathrm{surv},i}^+ &= \exp\left[-\int \mathrm{d}P_{i,t}\right] \\ &= \exp\left[-\int_{z_{\min}}^{\infty} \mathrm{d}z \frac{1}{v_{i,\perp}} \frac{1}{\tau(z)}\right]. \end{aligned} \tag{3.5}$$

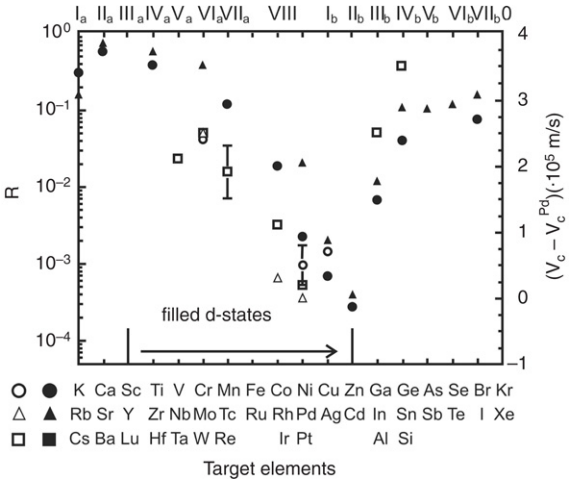

Fig. 3.8. Values for v_c relative to that of Pd for a number of different elements (open symbols. . . [5]) compared to the ionization probability (R) measured by Souda et al. (closed symbols . . . [48]).

In Eq. (3.5), the first equals sign is rigorously valid within the concept of Poissonian statistics, without any further assumptions. The second equals sign rests upon the additional assumption of non-local character of the neutralization process. Usually, additional assumptions are made to arrive at a simple evaluation of $P_{\mathrm{surv},i}^+$: the perpendicular velocity $v_{i,\perp}$ is taken constant along the integration path and $z_{\min} = 0$, leading to

$$P_{\mathrm{surv},i}^+ = \exp\left[-\frac{1}{v_{i,\perp}} \int_0^{\infty} \mathrm{d}z \frac{1}{\tau(z)}\right] = \exp\left[-\frac{v_c}{v_{i,\perp}}\right]. \tag{3.6}$$

In Eq. (3.6), the first equals sign necessarily represents an approximation, but is mathematically correct for an appropriate effective value $\langle 1/v_{i,\perp}\rangle$. The second equals sign defines the characteristic velocity v_c, commonly used in the context of neutralization, as the integral of the transition rate from zero distance to infinity ($v_c = A/a$). Mikhailov et al. have obtained experimental v_c values for He^+ ions and numerous elements [5] and found a correlation of the v_c values with the reionization probabilities measured by Souda [48] (see Fig. 3.8). Thus in contrast to what one might expect, higher reionization probability leads to a lower scattered ion signal (stronger neutralization).

The fact that $z_{\min}$ is finite leads to a systematic error in v_c, which is small as long as $z_{\min} \ll 1/a$. The approximation $v_\perp =$ constant is never applicable, since it changes its direction during the close collision. As a consequence, transition rates deduced from experimental data via Eq. (3.6) are subject to a systematic error, which may easily exceed 10% [49]. Neglecting collision induced processes, the survival probability along the total trajectory, P_{surv}^+, is then given by

$$P_{\mathrm{surv}}^+ = \exp\left[-\frac{v_c}{v_{0,\perp}} - \frac{v_c}{v_{f,\perp}}\right] = \exp\left[-\frac{v_c}{v_\perp}\right], \tag{3.7}$$

where $1/v_\perp$ stands for $1/v_{0,\perp} + 1/v_{f,\perp}$ to take incoming and outgoing parts of the trajectory into account.

(b) *Transitions of valence electrons from a specific atom to the projectile (RN, AN)*

We face quite a different situation if we regard the case where the electron can tunnel only from one specific surface atom to the projectile. Even if the transition rate concept remains unchanged, we have to replace the distance from the surface, z, by the distance from the specific atom, r. Consequently, replacement of the time integration by integration over the distance leads to $\mathrm{d}t = \mathrm{d}r/v$, where v is the projectile velocity. Finally, the survival probability, P_{at}^{+}, reads

$$P_{at}^{+} = \exp\left[-\int_0^{\infty} \mathrm{d}t \frac{1}{\tau(r)}\right] = \exp\left[-\frac{1}{v}\int_{r\,\min}^{\infty} \mathrm{d}r \frac{1}{\tau(r)}\right] = \exp\left[-\frac{v_{at}}{v}\right], \tag{3.8}$$

where $1/v \equiv 1/v_0 + 1/v_f$. This local model was introduced by Godfrey and Woodruff [50,51] and successfully applied to describe neutralization of low energy He^+ ions by oxygen and carbon adsorbates on Ni and Cu surfaces. In analogy to Eq. (3.6), a characteristic velocity, v_{at}, is defined, which relates to an atom, and the *velocity* v enters the expression for P_{at}^{+}. Note that the limitations discussed for Eq. (3.6) are also valid for Eq. (3.8). Verbist et al. have extended this local model [52] to neutralization of an ion by a square lattice with N atoms per unit cell at positions $\vec{u}_j$, $j = 1, \ldots, N$. Then the survival probability is given by

$$P^{+} = \exp\left[-\sum_{j=1}^{N} f_j\right],$$

$$f_j = A_j \cdot \exp\left[\int \mathrm{d}t \sum_{h,k=-\infty}^{\infty} \mathrm{e}^{-a_j|\vec{r}(t)-\vec{R}_{h,k}-\vec{u}_j|}\right]. \tag{3.9}$$

Here, A_j and a_j are the neutralization constants for the jth atom and $\vec{R}_{h,k}$ are the lattice vectors. Eq. (3.9) can be solved for the asymptotic [52] and for the Coulomb trajectory [53]. This model is useful if the surface consists of a regular lattice that contains different atoms in its unit cell. Especially if these atoms are chemically different, their electron density is not homogeneous parallel to the surface and the Hagstrum model does not apply.

Furthermore, one can modify the ansatz for the transition rate, and add one more parameter, e.g., by replacing the preexponential factor by a linear polynomial in the distance, r, or by a hyperbolic term [54]. Those authors have shown that also for these modified transition rates the neutralization integral can be solved analytically, and applied this lattice model to NaCl(001), yielding a fair agreement of the calculated angular dependence with experimental data. Also an azimuthal dependence of the scattered He^+ signal scattered from NaCl by Na atoms was observed (see Fig. 3.9 and [55]). Note that such an azimuth dependence could not have been obtained within the electron gas model.

(c) *Transitions from bound electrons to the projectile (B–RN)*

In B–RN, the oscillations observed are typical quantum mechanical phase oscillations [27,56]. A general analytic molecular orbital model, based on the work of Landau, Zener and Stückelberg in 1932 (see e.g. [57,58]) treats the transitions where a crossing of two quasimolecular states occurs at finite

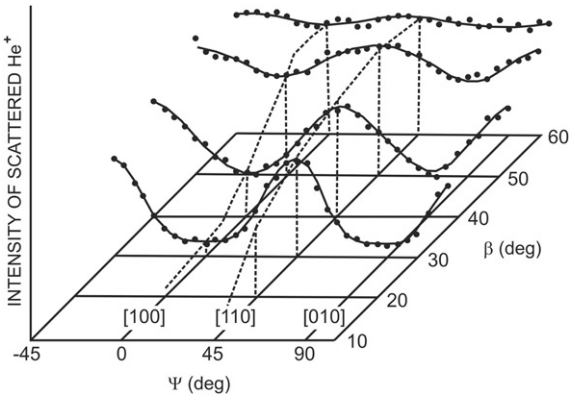

Fig. 3.9. Intensity of 1 keV He^+ ions scattered over 90° by Na at the NaCl(001) surface as a function of the exit angle β (measured with respect to the surface plane!) and the azimuth Ψ [55].

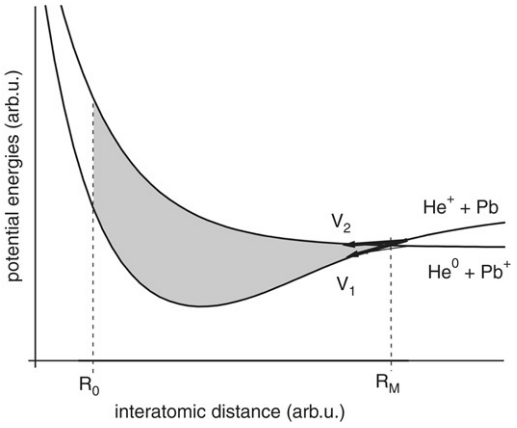

Fig. 3.10. 1D potential energy curves for He^++Pb (V_1) and for He^0+Pb (V_2). R_M denotes the distance at which the unperturbed potential energy surfaces would cross; R_0 denotes the minimum distance between the collision partners.

internuclear distance. Many features of the oscillatory behavior can be understood using the model shown in Fig. 3.10. The ion yield passes a maximum whenever $\int \mathrm{d}t\,\Delta V = n\hbar$, i.e. when the time integral (from the crossing on the inward trajectory to the crossing on the outward trajectory) over the difference in the potential curves between He^+ and He^0, $\Delta V = V_2 - V_1$, is a multiple of Planck's constant. It is again convenient to replace time integration by integration over the internuclear distance, r, via $\mathrm{d}t = \mathrm{d}r/v$. From this discussion it becomes clear why the oscillations are not equidistant in energy, but as a function of reciprocal velocity (see Fig. 3.11 where the ion yield for He^+ and Ge is shown as a function of the primary energy). It should be noted that the total ion yield in this case is not only governed by this quantum mechanical oscillation, but contains also the scattering probability of the projectile by the target atom, and the neutralization of the projectile along the incoming and the outgoing trajectory at distances where B–RN is not active anymore. (see above, and Ref. [1] for a general discussion).

The experiments of Helbig and Adelman [59,28] have confirmed that the oscillatory structures for scattering of the helium-3 and helium-4 isotopes are the same when they are plotted as a function of the inverse velocity.

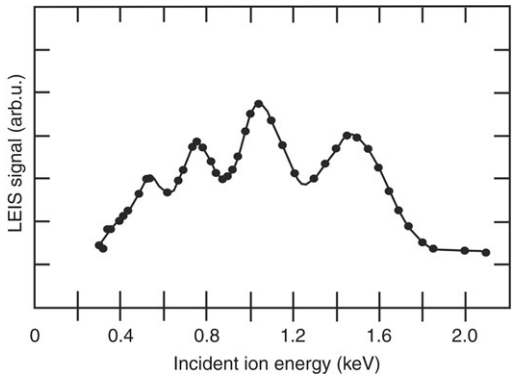

Fig. 3.11. LEIS signal as a function of the primary energy for He^+ scattered from Ge [7].

In B–RN, the core electrons that are involved in the charge transfer are well-defined in energy, notwithstanding the fact that they belong to an atom that is part of a solid. This minimizes damping effects. Chemical effects are also small, although they have been observed [23,26].

(d) *Collision induced processes*

Common to collision induced processes is that they work only at internuclear distances smaller than a critical value $R_M : r < R_M$. For a given scattering angle θ this minimum distance of closest approach corresponds to a certain threshold energy, $E_{\text{th}}(\theta)$. This makes clear that the probabilities for collision induced processes to occur (P_{CIN} for neutralization and P_{CIR} for reionization) depend on the *projectile energy* (not on the velocity), on the impact parameter, and on the scattering angle.

Collision induced ionization has two major consequences: firstly, at energies $E > E_{\text{th}}$, the LEIS spectrum (scattered ions) contains a background which involves reionization and increases from E_{th} to the maximum energy, kE_0 (see also Section 6.3). Secondly, the interplay of collision induced processes and of Auger neutralization leads to a more complex dependence of the intensity of scattered ions on the projectile parameters (see Section 4).

3.2. Classification of ion yield curves as a function of energy

In Table 3.1(a)–(c) a classification of the shapes of the scattered ion yields are given for the presently known ion–solid combinations:

(i) for class I ("classical") elements (bold frame, e.g. Al), the ion yield is given by the scattering cross section and the ion fraction from Eq. (3.7),
(ii) for class II elements (light grey background, e.g. Pb), the ion yield shows oscillations as a function of energy (neutralization due to B–RN),
(iii) for class III elements (light dark background, e.g. S) the scattered ion yields are clearly structured, but not a single neutralization model (neither (i) nor (ii)) is applicable.

An early version of this table was given by Rusch and Erickson [27], but their classes III and IV are now combined with more recently discovered structures in our category III.

3.3. Implications to related subjects

3.3.1. H and alkali ions as projectiles

In many experiments noble gas projectiles are used, because of their superb surface sensitivity. To complement our discussion of neutralization of noble gas ions, let us allude to another class of projectiles, i.e. H^+ and alkali ions. In the seventies, Eckstein and Verbeek performed many experiments to study charge states, angular and energy spectra of H^+ projectiles, see, e.g., their reviews [60,61]. More recently, MacDonald et al. have reported on the advantage of using H^+ ions for surface studies [62]. From these investigations one can deduce how scattering and neutralization of low energy H^+ and of He^+ ions are related:

(i) In general, the energy spectra of H^+ ions do not exhibit a pronounced surface peak, but consist of a continuum that extends up to a maximum energy, like a Rutherford backscattering spectrum (RBS) spectrum. There are, however, exceptions to this rule, e.g. $H^+ \rightarrow Cs$ [63].
(ii) For ionic crystals, even multiple surface peaks have been found for H^+ ions as well as for other projectiles, and have been interpreted in terms of inelastic energy loss processes (electron–hole pair excitation) (see, e.g. [38]).
(iii) The dependence of the ion fraction on the reciprocal velocity is for H^+ ions – similar as for He^+ ions – rather well described by a single exponential.

From these observations, the following conclusions can be drawn:

(i) There is one neutralization process that dominates in the interesting range of velocities. Due to the lower binding energy of the hydrogen ground state, this should be RN.
(ii) There is no noticeable difference in neutralization between scattering from the surface and from deeper layers. This may indicate a too poor resolution in those experiments to resolve surface effects. If there are indeed no surface effects, this means that the projectiles are either in charge equilibrium or they forget their history along the outgoing path. Since resonance processes are fast, they may fix the final charge state on the outgoing path, whatever the charge state of the ion is when leaving the surface.

3.3.2. LEIS versus grazing surface scattering

Surface scattering under grazing incidence conditions is a powerful technique to study the interaction of ions with surfaces of metals and insulators. The main difference to the LEIS regime is that for grazing scattering the perpendicular velocity is extremely small, even if the total energy is high. E.g., for 100 keV He^+ ions, impinging under 3° relative to the surface, $v_\perp = 2.3 \cdot 10^5$ m/s, i.e. the same as for 250 eV He^+ ions at perpendicular incidence. Under these conditions, the projectiles are specularly reflected by multiple scattering from surface atoms. For a given target–projectile combination, the minimum distance to the surface plane is closely related to the angle of incidence deciding which are the relevant interaction processes of the projectile with the electrons. Concerning interaction of projectiles with electrons at the surface in grazing

Table 3.1
Neutralization behavior of projectile–target combinations for (a) He^+, (b) Ne^+ and (c) Ar^+ projectiles

(a) He^+ projectiles:

Li	Be											B	C	N	O	F	Ne
Na	Mg											Al	Si	P	S	Cl	Ar
K	Ca	Sc	Ti	V	Cr	Mn	Fe	Co	Ni	Cu	Zn	Ga	Ge	As	Se	Br	Kr
Rb	Sr	Y	Zr	Nb	Mo	Tc	Ru	Rh	Pd	Ag	Cd	In	Sn	Sb	Te	I	Xe
Cs	Ba	La	Hf	Ta	W	Re	Os	Ir	Pt	Au	Hg	Tl	Pb	Bi	Po	At	Rn
Fr	Ra	Ac															

Rare earths:

Ce	Pr	Nd	Pm	Sm	Eu	Gd	Tb	Dy	Ho	Er	Tm	Yb	Lu

(b) Ne^+ projectiles:

Na												Al	Si	P	S	Cl	Ar
K	Ca	Sc	Ti	V	Cr	Mn	Fe	Co	Ni	Cu	Zn	Ga	Ge	As	Se	Br	Kr
Rb	Sr	Y	Zr	Nb	Mo	Tc	Ru	Rh	Pd	Ag	Cd	In	Sn	Sb	Te	I	Xe
Cs	Ba	La	Hf	Ta	W	Re	Os	Ir	Pt	Au	Hg	Tl	Pb	Bi	Po	At	Rn

Rare earths:

Ce	Pr	Nd	Pm	Sm	Eu	Gd	Tb	Dy	Ho	Er	Tm	Yb	Lu

(c) Ar^+ projectiles:

K	Ca	Sc	Ti	V	Cr	Mn	Fe	Co	Ni	Cu	Zn	Ga	Ge	As	Se	Br	Kr
Rb	Sr	Y	Zr	Nb	Mo	Tc	Ru	Rh	Pd	Ag	Cd	In	Sn	Sb	Te	I	Xe
Cs	Ba	La	Hf	Ta	W	Re	Os	Ir	Pt	Au	Hg	Tl	Pb	Bi	Po	At	Rn

Rare earths:

Ce	Pr	Nd	Pm	Sm	Eu	Gd	Tb	Dy	Ho	Er	Tm	Yb	Lu

The following characterization codes are used (see Section 3.2): (i) Class I ("classical"): frame around elemental symbol (ii) Class II ("oscillations"): light grey background (iii) Class III ("structure"): dark grey background.

surface collisions, the present status of knowledge is thoroughly summarized in [64].

It becomes clear from this that the physical situation is quite different in grazing surface collisions, as compared to LEIS. Firstly, in the former case the trajectories are due to multiple scattering, while in the latter case the relevant trajectories are due to binary collisions. Secondly, in grazing surface scattering the electronic properties of the *surface* are relevant to understand the physics involved, while in LEIS the interaction of the projectile with a single atom is relevant.

4. Interplay of different mechanisms

4.1. Scaling laws

4.1.1. One dominating neutralization mechanism (AN or RN)

In Section 3, we have discussed the individual neutralization processes and their energy dependences, and have given arguments whether the velocity, v, or the perpendicular component, $v_\perp$, or the energy is the relevant parameter. What is common to AN and RN is that, whenever only one process dominates, i.e. as long as B–RN and collision induced processes (CIN, CIR) are absent, the ion yield is given by the survival probabilities along the incoming and the outgoing trajectories. This leads to the following formalism for the total survival probability that applies similarly for atomic and for nonlocal processes (see Eq. (3.7)). For atomic processes the ion fraction is obtained from:

$$P^+ = \exp\left[-u_c\left(\frac{1}{v_0}+\frac{1}{v_f}\right)\right]. \tag{4.1a}$$

Here, the characteristic velocity u_c is a measure for the neutralization probability. The indices 0 and f refer to the ingoing and outgoing trajectory, respectively. While for atomic processes the velocity is the relevant quantity, for nonlocal neutralization, it is the perpendicular velocity $v_\perp$ which counts. In this case P^+ is obtained from

$$P^+ = \exp\left[-v_c\left(\frac{1}{v_{0,\perp}}+\frac{1}{v_{f,\perp}}\right)\right] = \exp\left[-v_c\left(\frac{1}{v_0\cos\alpha}+\frac{1}{v_f\cos\beta}\right)\right]. \tag{4.1b}$$

For this case (class I in Section 3.2), the characteristic velocity is denoted v_c, and the angle of incidence α, and the exit angle β, are both measured relative to the surface normal. Note that at fixed scattering geometry it is hardly possible to distinguish between v and $v_\perp$ scaling, since neither v_c nor u_c are known sufficiently precisely a priori. To be able to discern v and $v_\perp$ scaling one has to vary not only the energy but also the angles of incidence and exit over a wide range.

4.1.2. Two neutralization mechanisms

(a) *Surfaces with high work function*

In the case of more than one process contributing, the situation is more complex. In the presence of collision induced processes, the ion fraction of the backscattered projectiles is not anymore given by the survival probability of the incoming charge state, but is composed of two contributions: survivals and reionized projectiles:

$$P^+ = P^+_{\text{in}}\cdot(1-P_{\text{CIN}})\cdot P^+_{\text{out}} + (1-P^+_{\text{in}})\cdot P_{\text{CIR}}\cdot P^+_{\text{out}}. \tag{4.2}$$

Here, P^+_{in} and P^+_{out} denote the survival probability on the ingoing and outgoing trajectory, respectively, and may be calculated from Eq. (3.6). The first term in Eq. (4.2) describes the survivals. At $E < E_{\text{th}}$, $P_{\text{CIN}} = P_{\text{CIR}} = 0$. Consequently, assuming nonlocal neutralization, Eq. (4.2) simplifies for metals to $P^+ = P^+_{\text{in}}\cdot P^+_{\text{out}} = \exp[-v_c(1/v_{i\perp}+1/v_{f\perp})] = \exp[-v_c(1/v_\perp)]$ with $1/v_\perp \equiv 1/v_{i\perp}+1/v_{f\perp}$ (see Eq. (4.1b)). As mentioned above, measurements in which only the ion energy is varied cannot distinguish between total and normal velocity scaling.

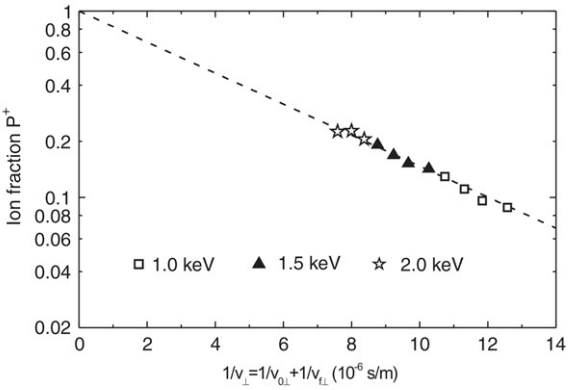

Fig. 4.1. Ion fraction of He after scattering by Cu as a function of the inverse perpendicular velocity component. Measurements are done for 3 incident ion energies. All three energies are below the threshold energy for collision induced processes for different geometries. The linear behavior shows the exponential dependence of the ion fraction $P^+ = \exp(-v_c/v_\perp)$ on the reciprocal perpendicular velocity with $v_c = 1.9\cdot 10^5$ m/s [49].

Energies $E < E_{\text{th}}$ correspond to (relatively) large values of $1/v$. In this regime, all P^+ data are expected to be described by Eq. (4.1). Therefore, in a semilog plot of P^+ as a function of $1/v_\perp$ all data should follow a single straight line, independent of the actual scattering geometry (α, β) and the actual primary energy [65]. As shown in Fig. 4.1, this is the case for He^+ scattered from polycrystalline Cu [43] ($E_{\text{th}} = 2.1$ keV [66]). Thus, P^+ is a unique function of $1/v_\perp$, proving experimentally that only the non-local neutralization mechanism (Auger neutralization) is active in this energy regime.

At energies $E > E_{\text{th}}$, for metallic surfaces P^+ depends on the scattering geometry (α, β) leading to a boomerang-shaped $P^+(\alpha)$ curve. If the measurements are performed at constant energy, a given value of $1/v_\perp$ can be obtained in two ways, by choosing either a large value for α or for β (see Fig. 4.2) In terms of neutralization, these two geometries are not equivalent, since a large value of α corresponds to a large neutralization probability on the way in and a good chance for reionized projectiles to survive the way out as an ion (large value for $P^+ = P^+_{\text{in}}\cdot P^+_{\text{out}}$), while for a large value of β neutralization on the way out is very likely (low value of P^+). This can also be seen in Fig. 4.3, which shows P^+ data for He^+ and polycrystalline Cu [65], obtained for different angles

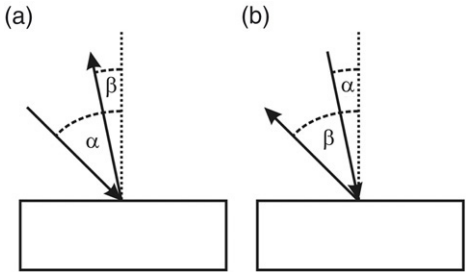

Fig. 4.2. Visualization of how to obtain the same value of $1/v_\perp = 1/v_{0\perp} + 1/v_{f\perp}$ by choosing either large α (a) or large β (b).

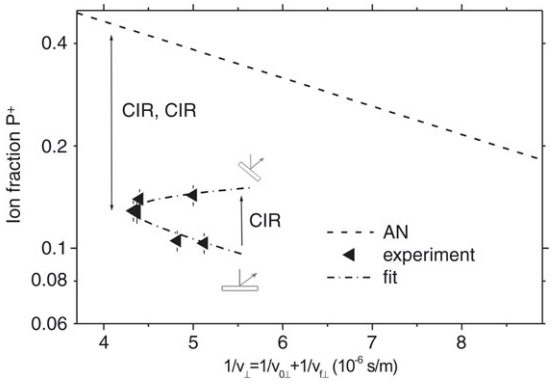

Fig. 4.3. Ion fraction as a function of the inverse perpendicular velocity component for primary energies of He^+ of 6 keV and polycrystalline Cu for different geometries including model fits. This energy is well above the threshold energy E_{th} for collision induced processes. The deviation from Auger Neutralization (AN) caused by Collision Induced Neutralization (CIN) and Reionization (CIR) is clearly visible [49].

of incidence at fixed primary energy ($E_0 = 6$ keV) and at a fixed scattering angle ($\theta = 129°$). These data exhibit the following features: first, the data are lower compared to the case of exclusive Auger neutralization. This is related to $P_{CIN} > P_{CIR}$ (if the opposite was true, the data would be found above the Auger line (in agreement with Ref. [5] that $P_{CIN} > P_{CIR}$ holds in general). Second, the width of the $P^+(\alpha, \beta)|_{E_0}$ curve is entirely due to $P_{CIR} > 0$ (for $P_{CIR} = 0$ one would obtain $P^+ = P^+_{in} \cdot (1 - P_{CIN}) \cdot P^+_{out}$, which is a line parallel to the Auger line). Third, there is an apex at the minimum value of $1/v_\perp$, with a unique P^+ value. The position of this apex would have been at $\alpha = \beta$, if the projectile would not lose energy in the backscattering collision. As long as the recoil energy of the target atom is small, the apex still corresponds to a scattering geometry close to the symmetric case, $\alpha = \beta$.

If the projectile energy is varied, the energy dependences of P_{CIN} and P_{CIR} determine the position and the shape of the individual $P^+(\alpha, \beta)$ curves. Fig. 4.4 shows the results, again for He^+ and polycrystalline Cu, for primary energies in the range 2.25–7 keV [65].

The discussion about the system He^+ and Cu is expected to hold quite generally, but usually the variation of P^+ with the scattering geometry is not seen, since in a conventional experiment only the primary energy is varied. In such a set-up, a single exponential dependence of P^+ on the inverse velocity has been observed for many elements by the Eindhoven group

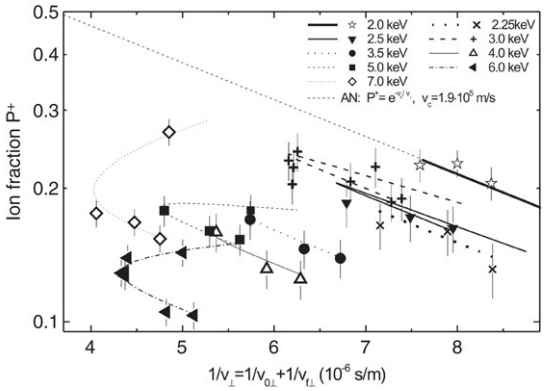

Fig. 4.4. Ion fraction as a function of the inverse perpendicular velocity component for primary energies of He^+ of 2–7 keV for different geometries. The curves are calculated P^+ values (obtained from Eq. (4.2)) [43].

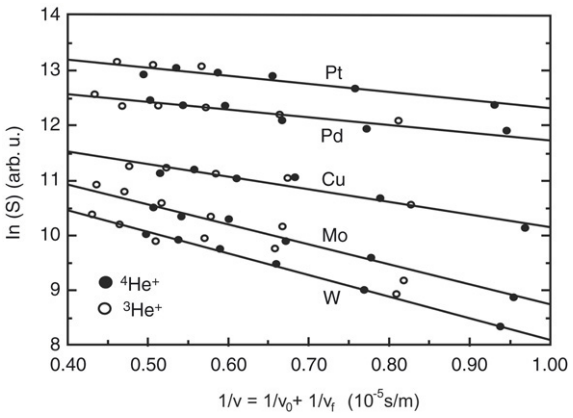

Fig. 4.5. Reduced LEIS signal S (corrected for the differential scattering cross section and the instrumental factor) as a function of the reciprocal velocity $1/v = 1/v_0 + 1/v_f$ for scattering of $^3He^+$ and $^4He^+$ ions from clean surfaces of Cu, Pd, Mo, W and Pt. For clarity the lines have been shifted vertically [5].

(see Fig. 4.5). Note that in Fig. 4.5 the quantity $S/(I \cdot \sigma \cdot E_f)$ is proportional to the ion fraction P^+. There are, however, also exceptions from such a simple velocity dependence of P^+, as shown in Fig. 4.6, where a change in the slope is shown for He^+ on Si and Al, and a nonmonotonic velocity dependence is shown for He^+ on Zn, qualitatively supporting the observations for He^+ on Cu.

(b) *Surfaces with small work function*

What was said above about neutralization effects applies only to the case where the work function of the sample is large enough to prevent RN to excited levels of the projectile. If such an RN to an excited level is possible, it can be much more efficient than AN and can strongly decrease the ion yield. The first report on neutralization from low work function materials was given by Brongersma et al. [67]. The work by Souda et al. [36,68] has provided important indications on the neutralization mechanisms at low work function. Cortenraad et al. have studied in detail the influence of the work function on the neutralization of noble gas ions backscattered from Ba atoms adsorbed on a W surface [69]. Adsorption of Ba up to a coverage of 0.4 ML lowers the work function of W(110) from 5.3 eV down to 1.8 eV. The Ne^+ signal was measured

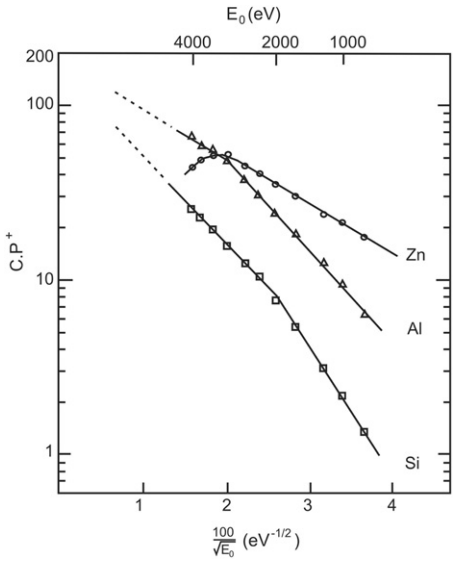

Fig. 4.6. Product of the ion fraction P^+ and an experimental constant C for $^4He^+$ ions scattered from clean surfaces of Al, Si and Zn as a function of the inverse square root of the reciprocal incident energy, which is proportional to $1/v_0 + 1/v_f$ [76].

for scattering by Ba as a function of the Ba coverage. At low coverages, just AN is possible and the Ne^+ yield increases proportional to the Ba coverage. At a critical coverage, RN to excited Ne level sets in thereby even reducing the Ne^+ yield with increasing coverage (see Fig. 4.7(a)). The resulting dependence of the characteristic velocity on the work function is shown in Fig. 4.7(b), where work functions greater than 4 eV correspond to the AN regime, while below 4 eV the probability for RN to Ne* increases with decreasing work function. From Fig. 4.7(b) it becomes clear that this feature depends on the magnitude of the work function only, since it can be reproduced quantitatively by different ways to reduce the work function (coadsorption of O and Ba on Re as a substrate). In the following, however, we will concentrate on standard situations of work functions >4 eV, for which neutralization will occur to the ground state of the projectile (see Section 9.2.2 for a more detailed description of low work function neutralization).

In the literature, various attempts have been undertaken to extend the model for P^+ to go beyond Eq. (3.7). For instance, in [70] the neutralization was studied as a function of the exit angle for constant incident and scattering angle (90°) and constant energy. As a result, an approximate proportionality of v_c to the final velocity v_f was found, but no explanation for this finding could be given. More recently, the introduction of a preexponential factor was suggested [71] to account for additional electron transitions occurring between the surface and different electronic states of the projectile along the trajectory, but without proper justification. This indicates that the subject of neutralization is still a topic of discussion.

4.2. Quantification of surface composition

4.2.1. General trends

These findings are highly relevant for applications. From the foregoing it is clear that the neutralization process is not

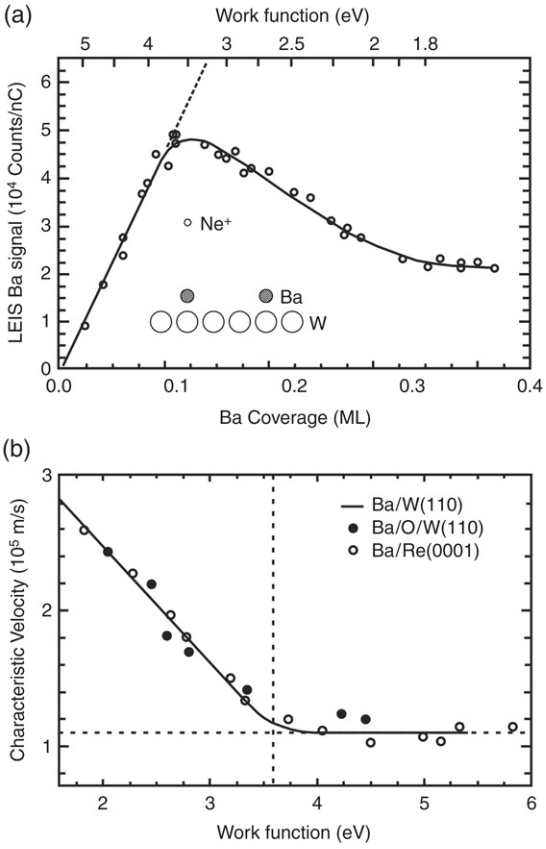

Fig. 4.7. The figure demonstrates that the increase in neutralization is due to the work function and not to the specific surface composition [69]. (a) LEIS signal of 2 keV Ne^+ ions scattered from the Ba adatoms on W(110) as a function of Ba coverage. The dashed line represents the extrapolation of linear behavior observed at low coverages. (b) Characteristic velocities for Ne^+ ions scattered from the Ba adatoms as a function of the work function. The open circles correspond to Ba adsorption on W(110), the solid squares to Ba and O coadsorbed on the W(110) surface, and the solid triangles to Ba adsorbed on the Re(0001) surface. The vertical dashed line represents the onset of the low work function mechanism.

a simple one, and the ion fraction is expected to be a rather complex quantity. This seems to be in contrast to the empirical finding, that as a common rule in LEIS the ion yield for one atomic species does not depend on the matrix (see Section 9), i.e. on the other atomic species present in the surface (absence of "matrix effects"). A detailed understanding of the observed absence of matrix effects would be highly desirable, but is not yet available. Thus, at the moment only more or less educated guesses are possible:

- Collision induced processes depend more on the atomic levels of the target atom while the Auger process is possibly more sensitive to the band structure of the target (if in a compound or an alloy the electronic density of states around atomic sites differs significantly from that of the monatomic material).
- At energies above E_{th}, the ion fraction – and the characteristic velocity – depends on the scattering geometry, i.e. on α and β; it is therefore not straightforward to compare the ion yields obtained in different experimental set-ups.

- For applications, the use of energies above the threshold may be more suitable, because there neutralization is more an atomic property.
- For materials with very low values of E_{th} the question arises how large the values of P_{CIN} and P_{CIR} will be at typical energies used for analytical purposes.

4.2.2. Experimental checks on matrix effects

In the following, we summarize the possibilities available to decide experimentally upon the absence of matrix effects. For a quantitative analysis of the surface composition one can relate the signal S_i, i.e. the measured number of scattered ions detected for a primary ion current I_p, to the surface concentration N_i of element i (atoms per surface area) via (see Eq. (2.2)):

$$S_i = \frac{I_p}{e} \cdot t \cdot \xi \cdot StF_i \cdot \eta_i \cdot N_i \tag{4.3}$$

with e the elementary charge and ξ the instrumental factor. StF_i is a steric factor taking into account the shielding by neighboring atoms ($StF_i = 1$ for atoms in the outer surface). The elemental sensitivity η_i is given by

$$\eta_i = P_i^+ \cdot \frac{d\sigma_i}{d\Omega}. \tag{4.4}$$

For rough surfaces, such as encountered for powders, also a roughness factor should be included (see Section 8.3).

In the case that the sensitivity η_i for a given element does not depend on the presence and identity of its neighboring atoms ("the matrix"), quantification of the surface composition is possible by using a reference sample of known surface density N_i^{ref} via

$$S_i = S_i^{ref} \cdot \frac{N_i}{N_i^{ref}}. \tag{4.5}$$

The usefulness of reference samples in the quantification of LEIS is illustrated by various tables that have been published [72,6, Section 9.1.3], and naturally relies on the absence of matrix effects. Therefore, in the following, experimental approaches to check on the absence of matrix effects are presented.

4.2.3. Use of the total signal

The fraction ζ_i of the surface covered by atoms i is given by

$$\zeta_i = \frac{N_i}{N_i^{ref}}. \tag{4.6}$$

When pure elemental samples are used as reference materials, $\zeta_i^{ref} = 1$. For binary compounds consisting of elements i and j, the applicability of Eq. (4.5) can easily be checked by studying the signals of the elements for targets of differing atomic compositions. The elements i and j should cover the full surface:

$$\zeta_i + \zeta_j = 1. \tag{4.7}$$

This equation implicitly assumes that there is no net change in the total number of atoms per unit area when elements i and j are mixed. In fact, this assumption for surfaces is analogous to Vegard's law for the volume of an alloy. Combination of Eqs. (4.5) and (4.7) gives

$$S_i = S_i^{ref} - S_i \cdot \frac{S_i^{ref}}{S_j^{ref}}. \tag{4.8}$$

Thus, if matrix effects are absent and Vegard's law holds for the surface, one expects a linear decrease of the signal for element i with increasing content of element j.

The surface atomic fraction x_i^{surf} of a binary alloy consisting of elements i and j is

$$x_i^{surf} = \frac{N_i}{N_i + N_j} = \frac{\frac{S_i}{S_j}}{\frac{S_i}{S_j} + \frac{N_j^{ref} \cdot S_i^{ref}}{N_i^{ref} \cdot S_j^{ref}}}. \tag{4.9}$$

Thus, to determine the surface atomic fractions we need to know the ratio of the surface densities of the reference samples as well as the LEIS signal ratios of the elements i and j in the binary target and in the reference targets. Analogous to Eq. (4.9) for binary compounds, one can write an equation for multicomponent samples containing j_{max} elements in the surface:

$$x_i^{surf} = \left[\sum_{j=1}^{j_{max}} \frac{S_j}{S_i} \frac{S_i^{ref}}{S_j^{ref}} \frac{N_j^{ref}}{N_i^{ref}} \right]^{-1}. \tag{4.10}$$

4.2.4. Semilog plots of the ion fraction

As long as Auger neutralization is the dominant neutralization mechanism, the ion fraction P^+ depends exponentially on the ratio $v_c/v_\perp$, where v_c is a characteristic velocity and $1/v_\perp = 1/v_{i\perp} + 1/v_{f\perp}$, i.e. the sum of the inverse reciprocal velocities, according to Eq. (3.7). Consequently, at least for energies below the reionization threshold, a straight line is expected, if $\log P^+$ is plotted as a function of $1/v_\perp$. Since usually not all the constants are known quantitatively, the intersect for the extrapolation $1/v_\perp \to 0$ is not relevant, but the slope in this plot is given by $-v_c$. Thus, the absence of matrix effects corresponds to the observation of identical slopes in the $\log P^+(1/v_\perp)$ plot for a given chemical element and different matrices. This has been observed for numerous alloys and compounds (even oxides!) by the Eindhoven group [73] (see Fig. 4.5). The observation of identical slopes for the element in the pure sample and in the compound is quite a convincing proof of identical neutralization behavior in both environments; equivalently, the ratio of the scattered yields should in this case be independent of the primary energy (see Fig. 4.8). An important consequence is that it permits the determination of the concentration from the ratio of the signals in the compound and in the pure reference sample (see Eqs. (4.9) and (4.10)), independent of the primary energy used. This also holds for elements which exhibit a more complex neutralization behavior (class III elements, see Table 3.1 and Fig. 4.6), as long as the shapes of the ion fractions over $1/v$ are identical.

Up to now, no theory has been developed to decide how in a compound the neutralization by Auger processes depends on the band structure and on surface effects. It is not clear a priori what one should expect since one has to take into account the

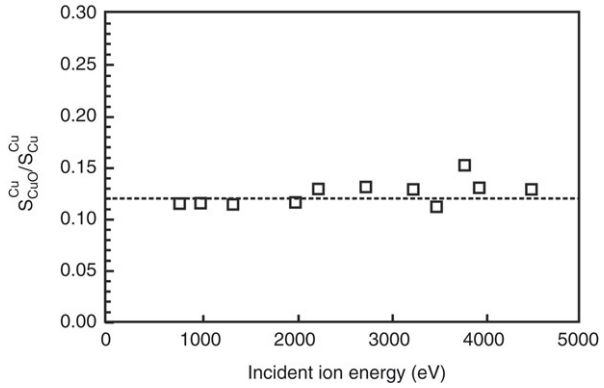

Fig. 4.8. Ratio of the He^+ signal after scattering from clean Cu (S^{Cu}_{Cu}) and from Cu in CuO (S^{Cu}_{CuO}) as a function of the incident ion energy [73].

– very strong – perturbation of the conduction electrons by the presence of the ion.

If for a given element the usual range of primary energies ($E_0 = 1$–3 keV) is above the reionization threshold E_{th}, Eq. (4.1) is not sufficient to describe P^+; no straight line is expected in the semilog plot $P^+(v_\perp)$. In this regime, collision induced neutralization, which is an atomic property, is expected to be important and it should be still possible to determine surface concentrations by comparing the sample of interest to a reference sample (calibration standard).

4.2.5. Energy dependence of sample to standard yield

A relatively easy method to find out whether matrix effects are present or not has been described by Jacobs et al. [74]. For a number of different incident energies the LEIS signals for a given element in the sample are compared with those of the pure element. In this way, only ions that pass through the analyzing and detection system with the same energy are compared. Therefore, the ratios do not have to be corrected for experimental factors such as the transmission of the analyzer or the efficiency of the detector.

Since the ion fraction, and thus the LEIS signal, is strongly dependent on the ion energy, small differences in neutralization behavior will have a major effect on the energy dependence of P^+. If there are no matrix effects, the ratio should be a constant and equal to the ratio of the surface concentrations of the element in the sample and in its pure state. Jacobs et al. checked this for 1–3.5 keV He^+ scattering by Al in some compounds (NiAl, $Ag_{80}Al_{20}$ and aluminum oxides). While a clear matrix effect was found for Al in NiAl, the ratio was constant for the aluminum oxide and for the AgAl alloy (see Fig. 4.9).

A major advantage of this method is that it can be carried out with any LEIS set-up, without any calibration of its sensitivity. A condition is, of course, that significantly different primary energies can be used.

4.2.6. Energy dependence of yield ratios

For compounds, such as oxides, it has been found by McCune [75] that the energy dependence of the cation/anion ratio is very characteristic for the compound. While for compounds such as SiO_2 and Al_2O_3 this ratio increases

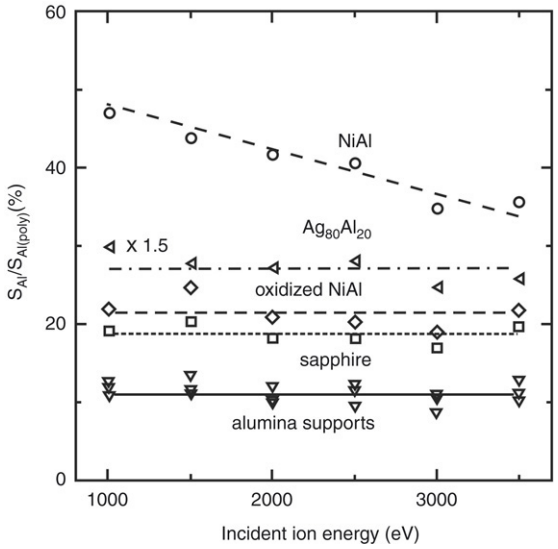

Fig. 4.9. Ratios of LEIS signals of aluminum in alloys (NiAl, $Ag_{80}Al_{20}$) and compounds (oxidized NiAl, sapphire, alumina supports) and in polycrystalline Al, as a function of the primary energy [74]. The energy independence demonstrates the absence of a matrix effect for these materials. For the Al signal in NiAl a clear matrix effect is observed (Section 4.2.5).

strongly with energy, no increase or even a decrease was observed for compounds like MgO, ZnO and $CaCO_3$. Originally this difference was ascribed to a difference in screening of the cations by the anions. Later it was demonstrated, however, that the energy dependence of the signal ratio is an intrinsic property of the elements involved [76]. The ratios were found to be the same for the compounds and for the constituting elements. This independence of the environment (matrix) also shows that matrix effects are absent in these cases. The composition, as determined by LEIS, is thus independent of the precise incident energy that has been used for the analysis.

4.2.7. Angular dependence

Usually, surface analysis by LEIS is made at a constant primary energy (which depends on the lab) and at constant geometry (angles of incidence, exit). As has been pointed out in [70], the variation of the exit angle for a given angle of incidence, scattering angle and a given primary energy permits the study of the influence of the outgoing path on the ion fraction. Due to the rather complex dependence of P^+ on the survival probabilities and on the collision induced charge exchange probabilities, angular dependent measurements at $E_0 > E_{th}$ do not easily yield information on the absence of matrix effects, even if the scattering angle is kept constant. From Eq. (4.2) one learns that the most direct information one can deduce from measurements at different exit angles (β, β') is the ratio $P^+(\beta)/P^+(\beta') = P^+_{out}(\beta)/P^+_{out}(\beta')$.

4.2.8. Instructive examples

Ne^+ *and* CuPd

One of the many cases where it has been found that matrix effects are absent has been presented by Ackermans et al. [77] for the scattering of Ne^+ ions by CuPd alloys. For these

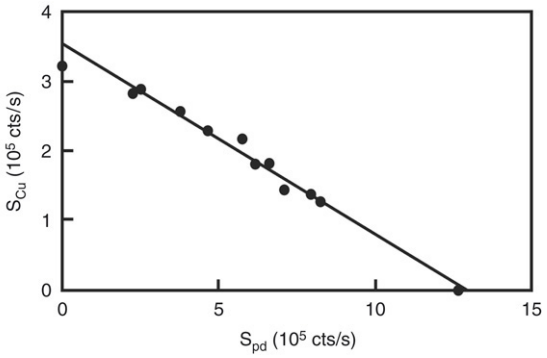

Fig. 4.10. For CuPd alloys of different compositions the Cu signals are plotted against the Pd signals. The data were measured using 3 keV Ne^+ ions. The linear relationship indicates the absence of matrix effects [77].

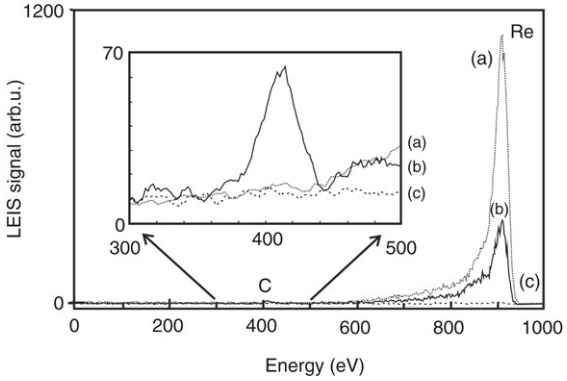

Fig. 4.11. Energy spectra for 1 keV $^3He^+$ scattered by (a) pure Re, (b) carbidic carbon ($1 \cdot 10^{15}$ at/cm^2) on Re and (c) graphitic carbon ($3.8 \cdot 10^{15}$ at/cm^2) on Re [66].

alloys Vegard's law is valid. In their study 7 polycrystalline targets having different bulk compositions (including the pure elements) were investigated. By subjecting these targets to (preferential) sputtering and annealing (surface segregation), a great variety of surface compositions was prepared. In Fig. 4.10 the LEIS results for 3 keV Ne^+ scattering (normal incidence and a scattering angle of 136°) are given. Similar results were obtained for 2 keV Ne^+ ions. The plot shows a linear dependence as predicted by Eq. (4.8). The fact that the signal for pure Cu is a little too low was attributed to the fact that the surface of this target still contained some impurities. Similar linear dependencies have been found for many other alloys, mixed oxides, mixed polymers, etc. (see Section 9.1). The results show that in these cases the elemental sensitivities are independent of the matrix. This is in sharp contrast to techniques such as Secondary Ion Mass Spectrometry (SIMS), where strong matrix effects are very common [78].

He^+ *on* C/Re *and graphite*

Probably the most extreme deviation from Eq. (4.8) was found for LEIS studies of carbon on rhenium by Mikhailov et al. [66]. In their studies they used a carbon doped polycrystalline Re target where the carbon content of the surface could be accurately adjusted (from absent till a monolayer and even more) by raising or lowering the temperature, which determined the dissolution and surface segregation. The carbon concentration was quantified by Auger electron spectroscopy. In Fig. 4.11 the results for 1 keV He^+ scattering are given (normal incidence and 136° scattering angle). For low carbon concentrations the carbon signal increases with carbon coverage, while the Re signal decreases. From Auger spectroscopy it was known that at these carbon concentrations the carbon is still carbidic, and Eq. (4.8) is believed to hold. However, when the carbon concentration is further increased, not only the Re signal decreases strongly but also that for carbon (see inset of Fig. 4.11). For these carbon concentrations the carbon is present in a graphitic state. When a graphitic monolayer is reached the Re signal has disappeared and at the same time the carbon signal has dropped by several orders of magnitude in comparison to that for carbidic carbon! In fact, the carbon signal had become so low that it was only detectable at primary energies of 3.5 keV and higher. The carbon signal of such a monolayer was the same as that of highly oriented pyrolytic graphite (HOPG). Energy dependent measurements showed that the ion fraction of the scattered ions was indeed much lower for graphitic than for carbidic carbon.

The C/Re example demonstrates a case where the use of a carbidic reference target for the quantification of the LEIS results would have led to the conclusion that "there was no target", which was obviously incorrect. If one wants to use LEIS as a quantitative tool to determine the surface composition, one has to understand the processes that determine the scattered ion signals. Also, one must know where and when the use of reference targets will be applicable. In general, it is important to be able to recognize situations where it is not valid and a more sophisticated interpretation is required.

In Section 9 an overview is given of the cases where matrix effects have been found and where it has been established that they are absent in LEIS.

5. Experimental details

Vital in obtaining reliable and reproducible data is a thorough understanding of the characteristics of the equipment used. There are many different kinds of LEIS instruments available. For a detailed review of experimental set-ups the reader is referred to, for example, Ref. [79]. Each set-up has the same basic components. A schematic of a LEIS set-up containing all these components is given in Fig. 5.1. In the next sections characteristics of each individual part

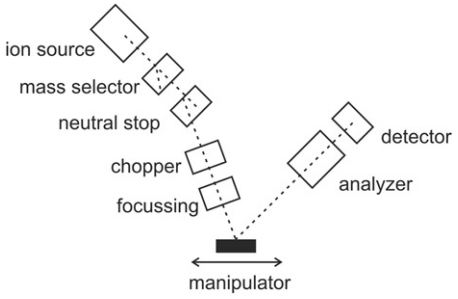

Fig. 5.1. Schematic of the different components of a standard LEIS set-up. The chopper is only needed in TOF measurements.

will be described in view of their influence on the LEIS measurement. For backscattered ions either their energy is analyzed by use of an electrostatic analyzer (ESA) or their velocity is determined by use of a Time-of-Flight (TOF) analyzer. Therefore, characteristic aspects of both types of set-ups are reviewed.

5.1. Ion source

The energy range of LEIS extends from 0.5 to 10 keV. An ion beam with a low energy spread is preferred, since a spread in the primary energy is directly related to a spread in the final energy according to Eq. (2.1) and thus contributes to the width of the binary collision peak in the LEIS spectrum. In view of the rather large typical peak widths in LEIS, an energy spread below 0.5% of the primary energy is adequate.

Surface analysis is often facilitated if measurements using different primary energies, i.e. 1–5 keV, are feasible. Since the LEIS signal is energy dependent, a change of the primary energy can give a higher sensitivity for a certain element. The use of several energies (velocities) is also important for the determination of neutralization effects (Sections 3 and 4). For a given projectile–target combination, the required ion current depends on the elemental sensitivity and experimental parameters like the acquisition time, the analyzer transmission and the detector efficiency. Typical ion currents range from 0.1 to 50 nA.

5.2. Mass filter

The primary ion beam should preferably be made up of only one type of noble gas (He, Ne or Ar), and in the case of Ne of only one isotope. The easiest way to achieve this is the use of isotopically pure gases. Another way is the use of a mass filter. Impurities that are present in the ion beam due to residual gas in the ion source or due to impurities in the gas feed do not only lead to significant contamination of the sample, but will also affect the LEIS spectra: when, for example, impurity ions such as H^+ hit the sample, they can be scattered back with a wide range of energies and thus give an unwanted background. Therefore, the mass filter should have a resolution of $\Delta M/M \leq 0.1$, which is sufficient to remove most of the non-noble gas impurities. In the case one would like to separate the Ne isotopes a mass resolution of $\leq$0.05 is required.

5.3. Neutral stop

At high pressures, i.e. in or near the ion source, there is a significant probability for neutralization of primary ions via a resonant charge exchange process [58]. A primary beam (used for analysis) will thus contain neutrals with the same energy and direction as the primary ions. These neutrals will contribute to the LEIS signal, but not to the current measurement and must therefore be filtered out by use of a neutral stop. The neutral stop deflects ions by several degrees onto an aperture.

5.4. Chopper

In order to perform TOF measurements a pulsed ion beam is needed. By either scanning the incident ion beam over an aperture or by deflecting the beam onto the aperture with deflection (chopper) plates ion pulses with duration $\delta\tau$ down to a few ns can be created [80,81]. By easy means, $\delta\tau$ can be varied: by choosing $\delta\tau$ very small ultimate energy resolution for scattered projectiles can be obtained; choosing $\delta\tau$ very large leads to improved sensitivity.

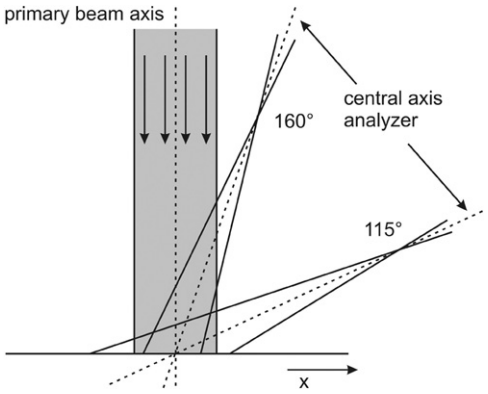

Fig. 5.2. Width of the acceptance area of an analyzer with a fixed acceptance angle for 2 scattering angles. For this spot size of the ion beam and a scattering angle of 160° only a fraction of the backscattered projectiles can be detected. For 115° scattering proper positioning of the sample is important.

5.5. Focusing

Lenses and collimators are required to limit the divergence of the ion beam. The spot size at the target should be smaller than the acceptance pupil of the analyzer (Fig. 5.2). For most analyzers, a spot size of 1 mm is sufficient. Spot sizes $\ll$1 mm are often not desired, since static analysis (Section 8.2.3) becomes impossible. Furthermore, the spread in the angle of incidence α (see Fig. 2.1) may become too large if the focusing of the beam is too strong. This would lead to a large spread in the scattering angle and consequently to a broadening of the binary collision peaks.

5.6. Manipulator

The requirements for the sample manipulator used in composition analysis are less strict than in structure analysis, where more degrees of freedom (usually at least the angle of incidence and the azimuthal angle) and greater accuracy are required (typically 1° for angular orientation).

In composition analysis, measurements are usually carried out in a fixed geometry. The target surface must be positioned at the intersection of the primary beam axis and the axis of the analyzer (Fig. 5.2) within an accuracy of typically 0.1, 0.5 and 1 mm for a cylindrical mirror analyzer (CMA), for a TOF-based analyzer and for a double toroidal analyzer (DTA), respectively. The accuracy and stability of the manipulator in x direction should be better than typically 1 mm (see Section 5.5).

Scanning of the target is not a requirement, but will reduce the ion fluence at a given spot (and thus reduce surface damage) and may also be useful in the case of depth profiling.

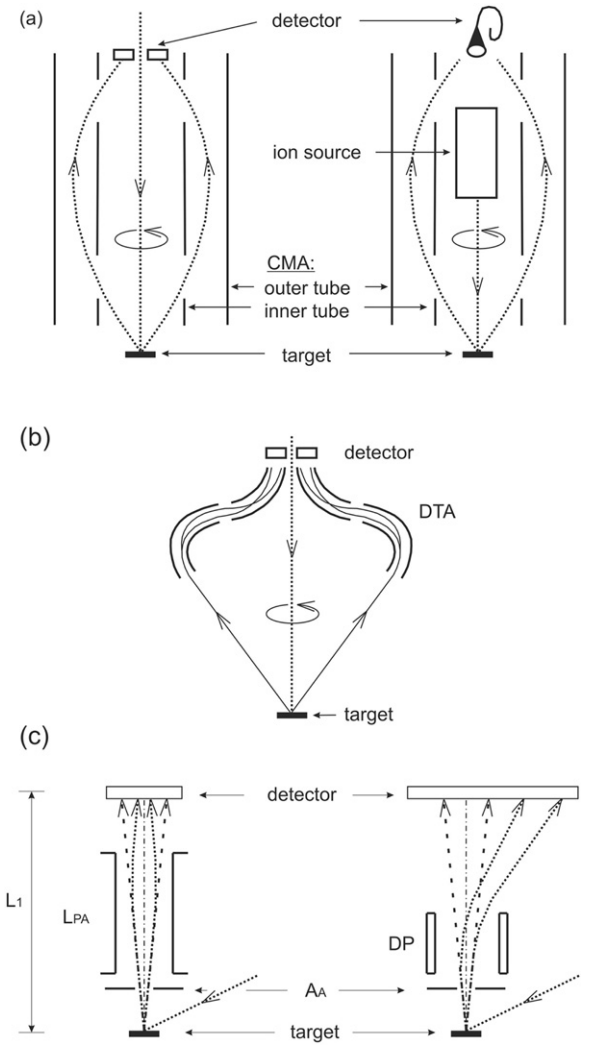

Fig. 5.3. Illustrations of electrostatic analyzers dedicated to LEIS. (a) Cylindrical Mirror Analyzer (CMA) with a ring-shaped detector and external coaxial ion source (left) and one with a built-in ion source (right). (b) Double Toroidal Analyzer (DTA). The ion trajectories are shown for 2 energies, illustrating the parallel energy detection. (c) Time-of-Flight (TOF) analyzer. Dashed lines represent trajectories of neutral particles; dotted lines represent trajectories of charged particles. L_1 denotes the flight path, L_{PA} a post-acceleration lens, DP deflection plates and A_A an aperture defining the same solid angle for all projectiles entering the TOF line.

5.7. Analyzer

There are many ESAs available, but not many of them are specifically designed for LEIS. An analyzer that is dedicated to LEIS spectroscopy is characterized both by a well-defined scattering angle (θ well above 90°, $\Delta\theta \sim 1°$–$2°$) and a large azimuthal acceptance angle (ideally 360°). The choice of $\Delta\theta$ always represents a compromise between sensitivity and energy resolution: large $\Delta\theta$ yields a high sensitivity, but at the expense of the energy (mass) resolution.

Schematics of ESAs dedicated to LEIS are shown in Fig. 5.3. Most commonly used are CMAs, shown in Fig. 5.3(a). There are two basic designs for CMA-based analyzers: one with a disc-shaped detector with a hole in the centre for the primary ions to pass through on their way to the target [82], and one with the ion source integrated in the CMA [83]. Energy selection is done by varying the bias on the outer tube. Only energies in a small window $\Delta E \propto E$ are analyzed simultaneously. This is different for the DTA ([84], Fig. 5.3(b)) where a large energy window is imaged onto a position sensitive detector. The energy image of the DTA enables parallel detection and, therefore, increases the sensitivity by about 3 orders of magnitude in comparison to CMA and hemispherical analyzers. The acceptance angle of the DTA is 1°–4°, which gives a high mass resolution. A drawback of the DTA being, of course, the more complicated detector read-out and signal storage. In some CMA-based set-ups the primary ion source is not placed at the axis of the analyzer but under a small angle with the target surface. To avoid a great variation in scattering angles the analyzer accepts only a small azimuthal window.

Hemispherical analyzers, which are primarily dedicated to photoelectron spectroscopy, have limited sensitivity and resolution for LEIS. First of all, backscattered ions in only a narrow azimuthal range are accepted (low sensitivity). Secondly, the acceptance angle ($\Delta\theta$) is of the order of 10°, which causes the binary collision peaks to broaden enormously (low mass resolution).

A TOF analyzer (see Fig. 5.3(c)) measures the flight time of projectiles, which leave the sample at a well-defined instance (within the time resolution $\delta\tau$) with a characteristic energy E_f. For a quantitative analysis, the TOF analyzer has to fulfill the following requirements: (i) the aperture A_A defines the same solid angle for all projectiles (ions and neutrals) scattered into the TOF-line; (ii) ions and neutrals have to be separated, either by a post-acceleration lens (L_{PA}) along the flight path L_1, or by deflection plates (DP) in front of the detector. If post-acceleration is used, the lens L_{PA} must be properly designed in order not to lose ions due to defocusing.

For ESAs, the width of the energy transmission window ΔE scales with the pass energy E, i.e. $\Delta E/E =$ constant. At energies lower than 1 keV special attention should be drawn to stray magnetic fields as they can cause a deviation from this general rule. The correction of the LEIS spectrum for the influence of the transmission window is different for each analyzer. For CMA-based analyzers normalization to a single pass energy is applied [85]. For DTA based analyzers no correction is needed. All backscattered ions are accelerated/decelerated by an addlens to approximately the same energy before they enter the analyzer [86,84,87]. The design of this addlens ensures that for the whole range of acceleration/deceleration potentials no ions are lost on the way to the analyzer. For typical TOF analyzers such corrections are hardly relevant.

5.8. Detector

Most LEIS set-ups use an electron multiplier, like a channeltron or a microchannelplate, as detector. In order to be detected, a projectile has to cause emission of at least one electron when hitting the surface of the detector. The emitted electrons have to be multiplied (10^6–10^7 times) so that the signal can be processed electronically. However, the efficiency

of multipliers decreases with time. This loss in performance can to some extent be compensated by use of an increased bias voltage.

The probability of electron emission due to ion impact onto the detector plate varies by at least a factor 2 for impact energies in the range of 0.5–3 keV [85]. A set-up with a DTA based analyzer minimizes this effect, because only ions with an energy within 10% of the pass energy reach the detector. The detector efficiency becomes almost constant within this small energy window. When the energy difference between backscattered ion and pass energy is larger the ions are accelerated before they enter the analyzer. Set-ups with a CMA based or a TOF analyzer usually (post-)accelerate the ions before they hit the detector, because at impact energies >3 keV the differences in detection efficiencies become small. However, any side effects from the post-acceleration due to e.g. focusing or deflection of the ions by the post-acceleration voltage have to be avoided.

Besides the impact energy also type and charge state of the projectile and the angle at which it hits the detector surface influence the detector efficiency [85,88,89]. Since usually ions are accelerated into the detector, the main uncertainty concerns the detection efficiency for neutrals, which requires calibration. A convenient way to do so is to determine P^+ as described in Section 7.1 for a well known system.

6. Features of LEIS spectra

Composition analysis in LEIS is based on the principle that only ions that have been backscattered by a single binary collision (single scattering: SS) contribute to the peaks in the spectrum (Section 2). The actual position of the surface peak and the reason for its width are discussed in Section 6.1. Since noble gas ions are used for the analysis, effective neutralization (Section 3) strongly reduces the contributions from double (DS) and multiple (MS) scattering processes. However, depending on the scattering conditions, DS and MS can still be important and even dominate a LEIS spectrum. In general, the scattered ion energies for DS and MS differ significantly from that of SS. The typical features of a LEIS spectrum were already shown in Fig. 2.3. For a reliable composition analysis it is thus important to recognize the DS and MS contributions and preferably select conditions where these processes are negligible. An important feature of LEIS is its surface sensitivity. Section 6.2 discusses how far the 2nd and deeper layers may contribute to the LEIS signal and what is really meant by the "outer" atomic layer. Section 6.3 discusses how DS and MS help to understand the morphology of the surface better.

6.1. Position and shape of the binary collision peak

In Section 2, Eq. (2.1), it is shown how the kinematic factor k depends on the scattering angle θ and the masses of the projectile and target atom. In a LEIS experiment a number of parameters will contribute to the width of the SS peak. According to Eq. (2.1) both the spread in the energy E_0 of the primary ions and in the scattering angle (angular spread in the primary beam and in the acceptance of the analyzer) will contribute.

Since the target atom is not a free atom and inelastic processes may occur, some deviations from Eq. (2.1) are observed. The coupling of the target atom with the lattice of the sample will have some effect. For the energies used in LEIS the actual scattering process, during which the momentum and energy of the projectile change significantly, is much shorter than a characteristic vibration time. At primary energies of 100 eV or more the effective mass of the target atom is, therefore, still that of a free atom. A non-zero motion of the target atom will induce, however, a Doppler broadening in the final energy of the scattered ion [90]. The broadening is of the order of $\sqrt{(E_0 \cdot E_\nu)}$, where E_ν is the vibrational energy of the target atom. Thus for a 1 keV He^+ ion scattered by an Al atom with a vibrational energy of only 25 meV, the Doppler broadening is already of the order of 5 eV. The increase of the Doppler broadening with temperature has been confirmed for 90° scattering of Ne^+ by Br atoms adsorbed on Ni [90].

While the parameters discussed above will lead to a symmetric broadening of the SS peak, inelastic processes will give a shift to lower energies. At very low energies discrete energy losses have been reported. A loss of about 20 eV has been reported [68] by Souda and Aono for 389 eV scattering of He^+ by Ta and was related to the reionization of He. In another study with 100 and 200 eV He^+ ions Souda et al. [48] could also identify discrete energy losses related to the excitation of valence electrons in KBr.

At higher energies various inelastic processes may take place, which leads to an increase in the widths of the LEIS peaks. This makes it impossible to separate elastic and inelastic processes. The SS peak in LEIS will thus contain both processes. The shift of the maximum of the peak is a good indication of the importance of inelastic effects. Mikhailov et al. [5] reported for 1 keV He^+ scattering by different elements that the maximum of the SS peak was 19–35 eV lower than expected on the basis of a binary collision (Eq. (2.1)). The shift was largest for elements where reionization is important. For even higher energies and other noble gas ions the contribution of inelastic processes can become even larger.

As a result of the peak shift, some authors prefer the use of the high-energy onset, while others take the maximum of the SS peak to determine the mass of the target atom. While neither procedure is fully correct, the experimental conditions will determine which is closest to SS.

Although the peak shift can be considerable, the differences in the kinematic factors for the various elements are generally much larger than this uncertainty of the peak position. It will thus not stand in the way of a proper identification of the target atom involved. In case of doubt, the use of a heavier projectile, Ne^+ or Ar^+ instead of He^+, will solve the problem. Using a low-energy spread ion source and a well-defined scattering angle (145°) it was possible [91], for instance, to distinguish elements like Pd and Ag with 5 keV Ar^+. This notwithstanding the overlap in the masses of their isotopes and the close proximity of their average masses (106.4 and 107.9, respectively).

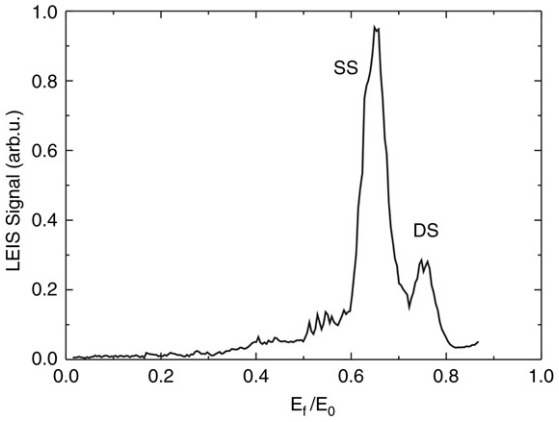

Fig. 6.1. LEIS spectrum [92] for 600 eV Ne^+ scattering by Ni(110). Both a single (SS) and double (DS) scattering peak are observed (see Section 6.2.1). The scattering angle is $\theta = 68°$, angle of incidence $\alpha = 30°$, the azimuth is oriented in [110] direction.

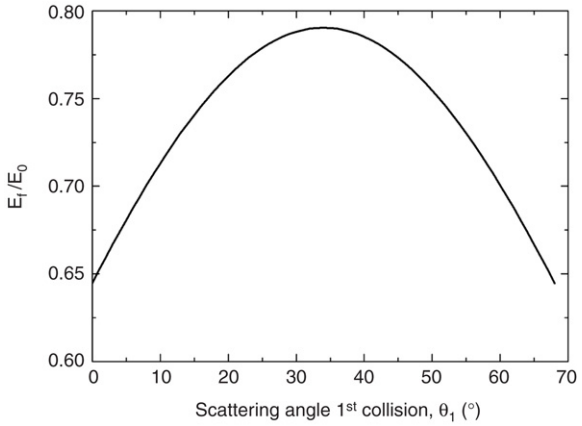

Fig. 6.2. The final energy E_f after two collisions of a Ne^+ ion with Ni atoms. E_f/E_0 is plotted as a function of the scattering angle θ_1 for the 1st collision. The total scattering angle (68°) is the same as in the experiment of Fig. 6.1.

6.2. Double and multiple scattering

6.2.1. Kinematics of DS and MS

When an ion collides with more than 1 atom, its final energy can be calculated by using Eq. (2.1) for each interaction. The energy after the first collision (scattering angle θ_1) is the incident energy for the next collision (scattering angle θ_2), etc.

For in-plane scattering of an ion by 2 atoms, the final energy E_f after the second collision is always higher than that for scattering by only one atom over an angle θ, where $\theta = \theta_1 + \theta_2$. The maximum E_f (smallest energy loss) in DS by atoms of the same mass is reached for the symmetric scattering: $\theta_1 = \theta_2 = \theta/2$.

The importance of DS is illustrated in Fig. 6.1 [92] where 600 eV Ne^+ ions have been scattered in the [110] azimuth by Ni over 68°. Using Eq. (2.1) the theoretical energy ratio for SS is $E_f/E_0 = 0.645$. In Fig. 6.2 the E_f/E_0 ratio for in-plane scattering is given for a total scattering angle of 68° as a function of the θ_1. The maximum energy ratio of DS (0.790) is reached when the 1st and 2nd scattering angles are equal. If one had not realized that the peak at $E_f/E_0 = 0.75$ (Fig. 6.1) was due to DS, it would have been erroneously assigned to SS by a much heavier atom such as Mo or Ag.

The final energy E_f for in-plane scattering by more than 2 atoms will lead to values of E_f that are even higher than for the symmetric DS. For grazing angles this situation is quite common and can lead to complex collisions and multiple peaks in the energy spectrum. Such conditions have been used to study surface vacancies [93,94] and to obtain detailed information on surface structures [95]. For larger scattering angles (>90°), that are preferred for composition analysis, such a series of significant in-plane collisions is geometrically much less probable. Thus, if neutralization does not prevent the detection of DS, the high-energy onset will be determined by the symmetric DS.

The low-energy tail in a LEIS spectrum (Section 6.3) is the result of ions that penetrated several nm into the sample and underwent multiple collisions involving many atoms before being scattered back into the analyzer. The scattering will not be in-plane anymore (thus the sum of the individual scattering angles is much larger than the SS angle to reach the detector) and the final energy can become much lower than E_f for a SS event. Also, during the long trajectories in the solid inelastic processes contribute significantly to the energy loss.

6.2.2. Relevance of multiple scattering

Relative probabilities of SS, DS and MS depend on the scattering conditions. DS and MS are especially important for small scattering angles, low-energies, low-index directions (short distance nearest neighbors) and ions of higher atomic number. The relatively intense DS peak in Fig. 6.1 is thus due to the use of Ne^+ ions, the low-energy (600 eV) and the low-index [110] direction. In Fig. 6.3 it is illustrated how MS can be suppressed. He^+ and Ne^+ ions of 3 keV have been scattered over 145°. Since a DTA (Section 5) was used, the scattered ions were collected for all azimuths. The insets show the expanded high-energy parts of the spectra. The energy values for the symmetric DS (2514 and 1214 eV for He and Ne, respectively) are indicated by the arrows. As discussed above, they are the maximum energies that are observed. The contribution of the DS to the signal is now reduced to less than 1%. Although this fraction is very small, it can still be used in the analysis of supported catalysts to distinguish islands/clusters from atomically dispersed systems. In special cases it can also be used to verify the absence or presence of atomic mixing in alloys.

6.2.3. Information depth

Many of the applications of LEIS relate to its ability to selectively analyze the outer atomic layer of a surface. This was first shown by Smith in 1971 [96]. The extreme surface sensitivity of LEIS has been demonstrated in studies of the polar faces of non centrosymmetric crystals. It was confirmed that the outer surfaces of the ZnS and CdS polar faces contained only Zn (Cd) or S, which was the proof of the absolute configuration assignment of these crystals [97]. In adsorption experiments of bromine on a Si(111) surface, only Br atoms were detected once the adsorption layer was

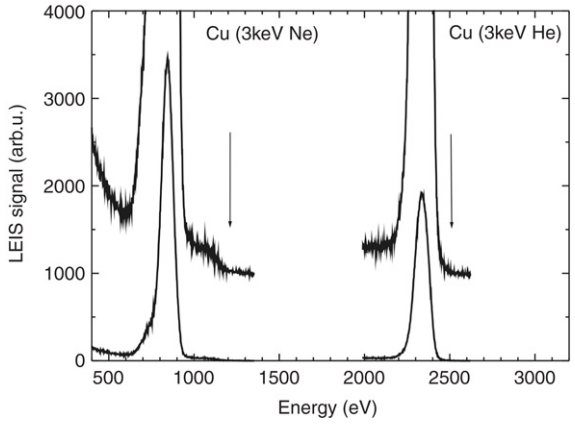

Fig. 6.3. 3 keV He^+ and Ne^+ scattering by Cu for perpendicular incidence and a scattering angle of 145° [112]. The energy values for the symmetric DS collisions (2514 and 1214 eV for He and Ne, resp.) are indicated by the arrows. The signal was integrated over all azimuths.

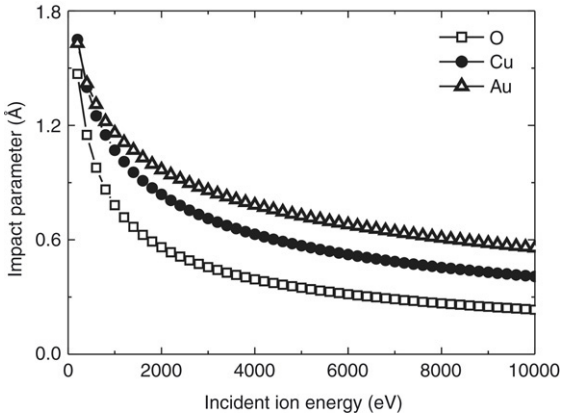

Fig. 6.4. Simulation of the dependence of the impact parameter on the incident ion energy for He^+ ion scattering over 3° by O, Cu and Au using the ZBL potential and screening length [3].

completed [98]. While these experiments were carried out under specular conditions at scattering angles of 90° or less, recent experiments at higher energies and large angles of the projectile with the sample surface have confirmed the very small information depth of LEIS. Moest et al. [99] concluded from the azimuthal dependence of the LEIS signal in 3 keV Ne^+ scattering (normal incidence, 145° scattering angle) that for a Rh(100) crystal with fcc structure, the contribution of the 2nd plane is approximately 4%. For the more open (110) plane, Bergmans et al. [100] found for 2 keV Ne^+ scattering that about 10% of the signal comes from the 2nd and deeper planes for the more open (110) fcc surface. Cortenraad et al. [101] concluded for the close packed W(110) bcc that the LEIS signal originates fully from the 1st atomic plane, while a small contribution (about 2%) was found for the 2nd atomic plane of the (100) surface. For a very open structure, such as the W(211) surface, about 1/3 of the signal comes from the 2nd and deeper planes. These results for the W crystals were found to be more or less independent of the energy (1–5 keV) and the ion (He^+, Ne^+, Ar^+) used (normal incidence, 136° scattering angle).

The openness of a surface structure can be quantified by considering whether the ions that are backscattered in the 2nd or deeper layers have suffered small angle scattering along the incident or outgoing trajectories. A deflection of a few degrees (e.g. 3°) still gives hardly any energy loss. During the scattering process, however, the core of the atom is not fully screened and the ions penetrate into the electron cloud of the atom. The impact parameter (which is equal to the distance of closest approach for these small angles) for scattering over a couple of degrees is thus a measure for the distance at which neutralization becomes significant. In Fig. 6.4 impact parameters are given as a function of the incident energy for He^+ ion scattering over 3° by O, Cu and Au. In the LEIS regime these impact parameters are of the order of 1 Å. For scattering from the 2nd or 3rd atomic plane in a close packed W(110) structure, the ions will pass an atom in the 1st atomic layer within this distance, while this is much less likely for W(211). The effective outer surface in W(110) is thus the 1st atomic plane, while in W(211) it partially includes deeper layers.

6.2.4. *Preferred conditions for composition analysis*

Studies of the azimuthal dependence of LEIS signals can provide a good criterion for the selection of reliable scattering conditions for a composition analysis by LEIS.

Souda et al. [55] have studied the scattering of 1 keV He^+ ions by a NaCl (001) surface. The ions were incident along the surface normal, while the azimuthal dependence of the scattered ion signal was investigated. As shown in Fig. 3.9, the intensity of scattering by Na^+ ions varies with the azimuth. The presence of the neighboring Cl^- ions clearly reduces the signal in those azimuths. This reduction is significant for low angles and disappears more or less for angles of 50°–60° with the surface plane. Although integration over all azimuths reduces the influence of the presence of the Cl^- ions, it is better to avoid it altogether by using large angles (and thus large scattering angles) with the surface. At higher incident energies the blocking of the backscattered ions is further reduced. For this, and other reasons (Section 8), scattering angles of at least 140° and energies of e.g. 3 keV are preferred for a quantitative surface composition analysis.

6.3. *Tails in LEIS spectra*

The tail in a LEIS spectrum is the background signal at energies that start just below the elastic binary collision peak and extends to a low-energy threshold (see also Fig. 2.3). In Table 6.1 the values for the thresholds are presented for He^+, Ne^+, Ar^+ ion scattering by various elements.

The tail is generally ascribed to primary ions that penetrated into the solid, suffered multiple collisions (nuclear stopping) and inelastic losses (electronic stopping) and were finally emitted from the target into the direction of the analyzer. Due to the statistical nature of these processes, the tails have a very smooth structure. On average, the larger the energy loss the longer the path through the solid. To be analyzed and detected in an ESA the scattered particle must be in an ionized state. This could either mean that the ion has survived neutralization during its passage through the solid or that after neutralization the noble gas atom is reionized. Different models have been presented to describe the physics that determines

the ion fraction after passage through the solid and thus the intensity and shape of the tail. This subject is still a matter of debate.

6.3.1. Models for the tails

Garrison [102] described the tail by assuming that during passage through the solid the fraction of the particles that are still ionized decreases exponentially with the residence time in the solid. Buck and Van der Weg et al. [103,104] investigated the tails at energies of 2–30 keV. They found that for Ne^+ ion scattering by Au the tails were fully determined by the energy of the backscattered ion. They ascribed this to a very fast charge equilibration of the ions in the solid. For Ar^+ ions the tails did not only depend on the energy but also on the history of the ions.

In many studies it has been observed that the presence of certain elements, in particular oxygen, leads to intense tails. Hoflund and coworkers observed in studies of the oxidation of Ni/Cr alloys [105] that the intensity of the tail increased with increasing oxygen content. They suggested, therefore, that the intensity of the tail is related to the low conductivity of the oxide. For materials having such a low conductivity one could imagine that the ion neutralization is less which would give a high ion fraction and thus an intense tail. Analogous to the oxidation also for the reaction of fluorine with a silver substrate a strong increase of the tail was observed. The intensity of the tail was, therefore, taken as a measure for the low conductivity of the fluoride [106].

In He^+ studies of oxidized tantalum Baun [107] found that the presence of oxygen increased the intensity of the tail. Since the probability for neutralization is already very high for a single collision, he assumed that most of the helium passes the solid as a neutral species and that it is reionized in a hard collision at the surface before entering the vacuum.

Recently, Beikler and Taglauer [108] showed that one can simulate the shape of the tails by combining trajectory calculations with the assumption that upon each collision with a target atom a fixed fraction of the ions is neutralized. This description is similar to the residence time model by Garrison [102]. Although it proved quite useful in the interpretation of LEIS spectra for supported catalysts [109], it fails to explain various details (Sections 6.3.2 and 6.3.3). Also the elemental dependence of the neutralization, that is required in the model, is just the opposite to what is observed. For instance, in the case of 1.85 keV He^+ scattering by Al and Ni one needs in the model per collision a survival probability of 0.9 and 0.2, respectively. However, Mikhailov et al. [5] and Sasaki et al. [110] found for 1–2 keV He^+ scattering a high ion fraction and no tail for Cu and Ni, while Al gives an intense tail and a low ion fraction.

6.3.2. "Decisive" experiments

In Fig. 6.5 the LEIS spectra of Sasaki et al. [110] are given for He^+ ion scattering by pure aluminum for a number of incident energies. It is clear that the tails have the same shape. Apparently the final energy fully determines the ion fraction. This could be, as suggested by Van der Weg et al. [104] for Ne^+ ion scattering, due to the fact that the ions reach a charge equilibrium within a very short distance. The alternative

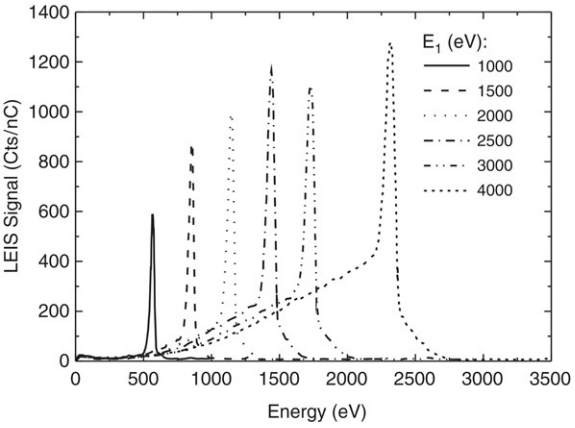

Fig. 6.5. LEIS spectra for several incident energies of He^+ ions scattered by Al. The scattering angle is 136° [110].

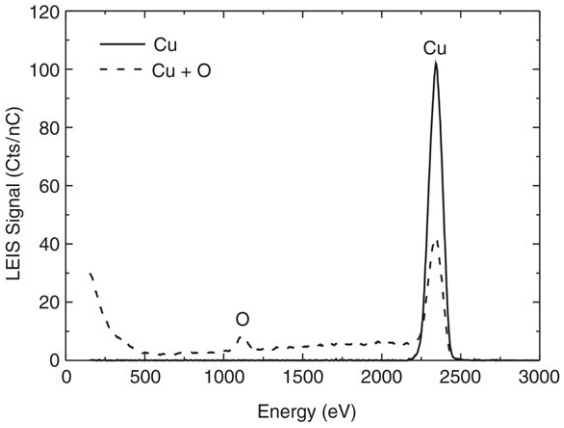

Fig. 6.6. Energy spectra for 3 keV He^+ scattered by pure Cu and by Cu on top of which a submonolayer of oxygen has been adsorbed. The presence of oxygen enables the reionization of the backscattered helium, which results in an intense tail [112]. The increased background below 500 eV is due to sputtered ions (O^+, Cu^+).

explanation by Baun [107] will, however, give similar spectra if one assumes that the probability for reionization is determined by the energy of the noble gas atom leaving the surface. This is not unreasonable, since the reionization process has a well-defined threshold energy. It is known that aluminum can reionize He atoms with energies above the threshold of about 300 eV (Table 6.1).

A particularly interesting experiment is that by Souda et al. [111] where they compared the energy spectra of He^+ ions scattered from Al(111) by impact of 2 keV He^+ and He^0 beams. The spectra were normalized relative to each other through the intensities of the secondary ions at energies close to zero. Both the shapes of the spectra and the signal intensities were essentially the same. Thus in this case ion survival can even be ruled out. The signals are completely due to reionization.

To investigate whether the charge equilibrium in the solid or the reionization in the last collision is responsible for the tails, a Cu sample has been investigated [112]. As shown in Fig. 6.6, pure Cu has no tail at energies below its reionization threshold (about 2300 eV). However, as soon as a sub-monolayer of oxygen is adsorbed on top of the Cu sample, a tail is observed.

Thus, the tail finds its origin in the reionization at the outer surface and not in ion survival, dynamic equilibrium in the bulk or ion conductivity (only a fraction of a monolayer of oxygen is adsorbed on the Cu). The onset (500 eV) of the oxygen induced tail gives an upper limit for the threshold value for reionization of He by an oxygen atom (Section 6.3.3). These experiments thus demonstrate that Baun's explanation [107] was correct. The increased signal at energies below 500 eV is not due to scattered He^+, but to sputtered ions (O^+, Cu^+).

6.3.3. Intensity and shape of the tail

The intensity and shape of the tail is determined by backscattering in the deeper layers, the straggling through these layers and the ion fraction of the backscattered particles. Whenever the scattering and reionization probabilities are high and neutralization unlikely, the tails can dominate the LEIS spectrum. The main contribution to a high ion fraction is due to reionization. The threshold energy for reionization is determined by the energy of the projectile and the scattering angle, being lowest for 180° scattering. At the threshold the distance of closest approach between projectile and target atom just reaches the internuclear distance (R_M) of the (avoided) crossing (see Fig. 3.4). At projectile energies greater than the threshold energy, also for collisions with smaller scattering angles reionization is possible. This leads to the observation that usually the intensity of the tail increases with increasing energy.

In Table 6.1 the threshold energies for reionization are given. Souda et al. [68,113,114] determined these values by studying the energy at which the impact of neutral noble gas atoms (He, Ne, Ar) led to reionization (method 1). Thomas et al. [37] used both neutral and He^+ ion impact and determined the ratios in the ion signal which results in upper limits for the reionization thresholds. Since the ratios were only determined for a few discrete energies (500, 1000, 1500 and 2000 eV) these threshold values can be as much as 500 eV too high. As stated by the authors, it was not always easy to obtain 100% clean surfaces. Especially for the reactive surfaces this is far from trivial. Somewhat arbitrarily, we have therefore only included their reionization thresholds if the ratio of the ion fractions exceeded 0.1%.

As discussed above, the reionization threshold can also be derived from the tail (method 3). Unlike the reionization observed in the experiments by Souda et al. and Thomas et al., the ions contributing to the tail cannot have been formed in a head-on collision, since in that case they would have been scattered back into the solid. The threshold energy of the tail must thus correspond to noble gas atoms that scattered back in deeper layers and had upon leaving the solid still just enough energy to enable a strong enough interaction with a surface atom (approach within R_M) to be reionized. Van Leerdam et al. [115] showed for He^+ scattering by silicon that the intensity ratio of the elastic peak height and the maximum of the tail increase linearly with energy above the threshold. This enables a simple extrapolation to determine the threshold energy of the tail. The threshold energy for the tail should be higher than the values of Souda et al. and Thomas et al. Although the shape of the tail does not make it easy to determine an accurate onset, the experimental data support that the onset is indeed somewhat higher than the values derived from a head-on value. For low-energy thresholds its determination is hampered by the presence of sputtered ions (Fig. 6.6).

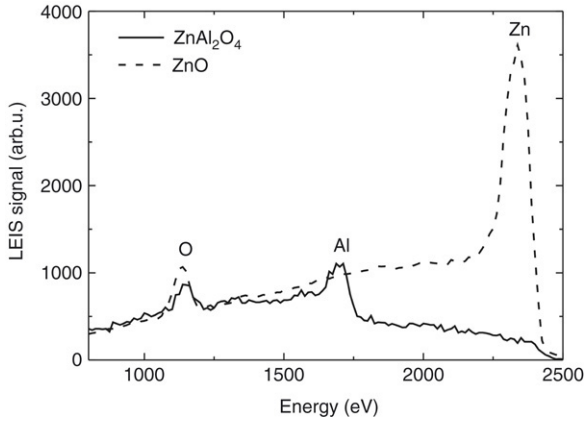

Fig. 6.7. Energy spectra of 3 keV He^+ backscattered from $ZnAl_2O_4$ (solid line) and ZnO (dashed line). In $ZnAl_2O_4$ there is no surface peak for Zn, since the Zn cations are below the surface. The onset of the tail agrees with ZnO, indicating that Zn is present in the 2nd and deeper layers [136].

For example, for Si a threshold energy of 350 eV was found by Souda et al. for the head-on situation. The distance of closest approach is then 0.030 nm. The threshold energy for the tail in LEIS is 500 eV. At this energy the same distance of closest approach is reached for 75° scattering, which is a reasonable threshold value for ions coming from deeper layers to be scattered into the analyzer positioned at 55° with respect to the surface.

Since many LEIS instruments do not have a facility to produce well-defined neutral beams, the tails in ion scattering provide a simple alternative to determine the reionization thresholds. In this way, for instance, a threshold value of 500 eV was determined for oxygen (Fig. 6.6, [112]).

Table 6.1 shows that reionization only occurs for certain ion–atom combinations, which result in a low-energy tail in LEIS spectra. A pure element like Cu will thus not have a tail below 2 keV, while W does.

As discussed in Section 3.1.3 and illustrated in Fig. 3.8, the elements that show reionization have a low intensity elastic peak (high characteristic velocity v_c), due to the much stronger collision induced neutralization for these elements. The influence of collision induced neutralization/reionization is thus twofold: on the one hand it reduces the intensity of the elastic peak and on the other hand it produces an intense tail.

Although there is no low-energy tail for a pure copper target, the presence of impurities such as oxygen or silicon in the outer surface will produce the tail. For complex systems high intensity tails are thus quite common, since it is likely that one of the surface components will provide the reionization. Fig. 6.7 [116] gives the LEIS spectrum for $ZnAl_2O4$ as a characteristic example of a mixed oxide. Since only the surface peaks of Al and O show up, the Zn atoms must be located below the outer surface. The fact that there is a background in the spectrum extending from low energies up to the expected

Table 6.1
Table for reionization thresholds (see Section 6.3.3(b))

Element	He			Ne	Ar
	Method 1	Method 2	Method 3		
Ag	>2000 [113]	≤1500 [37]		700 [113]	
Al	300 [113]	≤500 [37]	400 [110]		
Au		≤1000 [37]		900 [114]	
Ba	600 [114]			600 [114]	100 [114]
C	200 [113]				
Ca	≤200 [113]		290 [110]		
Cd	>2000 [113]	≤2000 [37]		700 [113]	
Cl	>2000 [113]				
Co	>2000 [113]	≤1000 [37]			
Cr		≤1000 [37]			
Cu	>2000 [113]	>2000 [37]			
F	>2000 [68]				
Fe		≤1000 [37]			
Ge	>2000 [113]			600 [113]	
I	>2000 [68]				
In	>2000 [113]	≤1000 [37]		600 [113]	1400 [113]
Ir			700 [91]	1600 [91]	
K	≤200 [113]				
La	≤400 [113]				
Mg	≤200 [113]				
Mn	500 [113]				
Mo	400 [113]	≤1000 [37]	900 [5]	1000 [91]	
Na	≤200 [113]				
Ni	>2000 [113]	≤1500 [37]	2300 [6]		
O			700 [91]		
Pb	>2000 [113]			600 [113]	>2000 [113]
Pd		≤1000 [37]	1100 [115]		
Pt			1000 [91]		1300 [91]
Rh			800 [91]	700 [91]	
Ru			600 [91]	900 [91]	
Sb	1100 [113]			1100 [113]	
Sc					
Si	300 [113]	≤500 [37]	400 [91]		
Sn	600 [113]	≤1000 [37]	800 [114]	600 [113]	1800 [113]
Sr	≤200 [113]			500 [113]	
Ta	300 [113]	≤500 [37]		>2000 [113]	<400 [113]
Te	1200 [113]			1000 [113]	
Ti	≤200 [113]				
W		≤500 [37]			
Y	300 [113]			700 [113]	
Zn	>2000 [113]				
Zr	300 [113]			1000 [113]	

The values for He impact were obtained by three different methods. Method 1: neutral impact gave reionization. Method 2: from ratios in the scattered ion fractions for He^0 and He^+ impact for fixed energies (because of possible surface impurities, only values are included where the reionization is at least 0.1% of the survival. Since the data were obtained for 500, 1000, 1500 and 2000 eV, the thresholds can be as much as 500 eV too high). Method 3: from low-energy tails. For Ne and Ar impact the thresholds were determined by method 1 (Souda et al.) and method 3 (Ridder et al.).

energy for Zn shows that the presence of Zn extends from deeper layers to just below the surface. The helium ions that are detected in LEIS were first neutralized when entering the solid, backscattered by a Zn atom below the surface and made "visible" in LEIS by reionization during an interaction with an oxygen atom when leaving the solid.

This example illustrates the strength of the LEIS technique: the peaks can be used to selectively analyze atomic composition of the outer surface. These are the atoms that can be chemically active. The shapes of the tails provide information on the in-depth distribution of the elements. This has been used, for instance, to follow the formation of palladium silicide on a silicon wafer for thicknesses up to 6 nm [115]. Nowadays, investigation of the tails in LEIS is used as a tool for high-resolution non-destructive in-depth composition analysis of ultra-thin layers [117] and shallow interfaces [118].

Note that the tail intensity observed in an experiment depends on the primary energy and the type of analyzer used. The tails should not be included in the signal used for the surface composition analysis. This means that in quantitative analysis background subtraction is important [119–121].

7. Determination of the ion fraction from experiment

In Sections 3 and 4 the various mechanisms have been treated that determine the ion fraction of the backscattered particles. In the absence of a general theory, the absolute value of the ion fraction P^+ can only be determined experimentally. Two methods are described. The most straightforward way is to measure both the charged and the neutral fraction of the scattered particles using a TOF analyzer. However it is far from trivial to ensure that the neutrals and ions have the same detection efficiencies (Section 7.1). ESAs do not have the possibility to measure the scattered neutral fraction. However, if there exists at least one element for which the ion fraction depends exponentially on the ratio of characteristic and ion velocities, the absolute ion fraction of all other elements can be determined (Section 7.2). In Section 7.3 an evaluation of the two methods is given.

7.1. TOF experiments

In a TOF–LEIS experiment both ions and neutrals are measured (Section 5.7). As already described in Section 2, the LEIS signal of backscattered ions is given by Eq. (2.2). The spectrum of scattered neutrals is broad in energy, it has a rather well defined high-energy onset at kE_0 (corresponding to scattering at the surface), a considerable contribution due to plural scattering at energies $> kE_0$ and extends to lower energies (corresponding to scattering from deeper layers). In RBS the scattering processes can easily be described using the single scattering model. In LEIS the scattering cross section is orders of magnitude larger. The single scattering model only holds for the surface and thin films [122].

As long as the single scattering model is valid, i.e. for sufficiently thin films, the thickness Δx is related to the energy width ΔE_{LEIS} of the LEIS spectrum via the (electronic) stopping power $S = \mathrm{d}E/\mathrm{d}x$ or, equivalently, the stopping cross section $\varepsilon = (1/n) \cdot S$ [123] of the material for the probing ions:

$$\Delta E_{\mathrm{LEIS}} = \Delta x \cdot \left[\frac{k \cdot \left.\frac{\mathrm{d}E}{\mathrm{d}x}\right|_{E_0}}{\cos\alpha} + \frac{\left.\frac{\mathrm{d}E}{\mathrm{d}x}\right|_{k\cdot E_0}}{\cos\beta} \right] \equiv [S(E_0, k, \alpha, \beta)] \cdot \Delta x = [\varepsilon] \cdot n\Delta x \tag{7.1}$$

with n the atom density in the target. Here, the surface energy approximation has been applied, and the stopping power factor $[S]$ – or, equivalently, the stopping cross section factor $[\varepsilon]$ – has been defined [124].

Similarly as for scattered ions (Eq. (2.2)), the yield of scattered neutrals Si^0 due to backscattering from a layer of thickness Δx that contains n atoms (of identical species) per unit volume is given by

$$S_i^0 = I_p \cdot t \cdot \xi^0 \cdot \frac{\mathrm{d}\sigma_i}{\mathrm{d}\Omega}(1 - P_i^+) \cdot \epsilon \cdot \frac{n\Delta x}{\cos\alpha} \tag{7.2}$$

where ϵ is the energy width of one channel of the experimental spectrum and ξ^0 is the instrumental factor (including the detector efficiency) for scattered neutrals. Note that Eq. (7.2) is based on the assumption that only two charge states (+ and 0) are relevant. From Eqs. (7.1) and (7.2), the height H^0 of the spectrum of the neutrals follows as

$$H^0 = \frac{S_i^0}{\Delta E_{\mathrm{LEIS}}} = I_p \cdot t \cdot \xi^0 \cdot \frac{\mathrm{d}\sigma_i}{\mathrm{d}\Omega} \cdot \frac{n_\epsilon}{\cos\alpha} \cdot (1 - P_i^+) \tag{7.3}$$

where n_ϵ is defined by $\epsilon = n_\epsilon[\varepsilon]$, in close analogy to the usual procedure in RBS [125]. Note that Eq. (7.3) applies only to the contribution from the outermost layer, since only there $P^+ > 0$; neglecting reionization. For scattering contributions from deeper layers, the ion fraction $P^+ \approx 0$. Consequently, if $n\Delta x \gg 1$ monolayer, the factor $1 - P^+ \approx 1$.

From the knowledge of S_i^+ and H^0 the ion fraction P_i^+ can be obtained from the ratio S_i^+/H^0 as [126]:

$$P_i^+ = \frac{S_i^+}{H^0} \cdot \frac{\epsilon}{n\Delta x \cdot [\varepsilon]} \cdot \frac{\xi^0}{\xi^+}. \tag{7.4}$$

The most trustworthy procedure to measure absolute ion fractions is to use a single crystal in channeling geometry and to measure the yields of ions and neutrals backscattered from the outermost atomic layer. In this case, Eq. (7.2) reduces to

$$S_i^0 = I_p \cdot t \cdot \xi^0 \cdot \frac{\mathrm{d}\sigma_i}{\mathrm{d}\Omega}(1 - P_i^+) \cdot \frac{N_{hkl}}{\cos\alpha}, \tag{7.5}$$

and P^+ follows directly from the ratio

$$\frac{S^+}{S^0} = \frac{\xi^+}{\xi^0} \cdot \frac{P^+}{(1 - P^+)}. \tag{7.6}$$

In a TOF analyzer, the ratio ξ^+/ξ^0 reduces to the ratio of the detector efficiencies, which can be determined with good precision. The most convenient way to calibrate the detector efficiency for neutrals is to apply Eq. (7.6) to a system, where P^+ as a function of energy is known to a good precision.

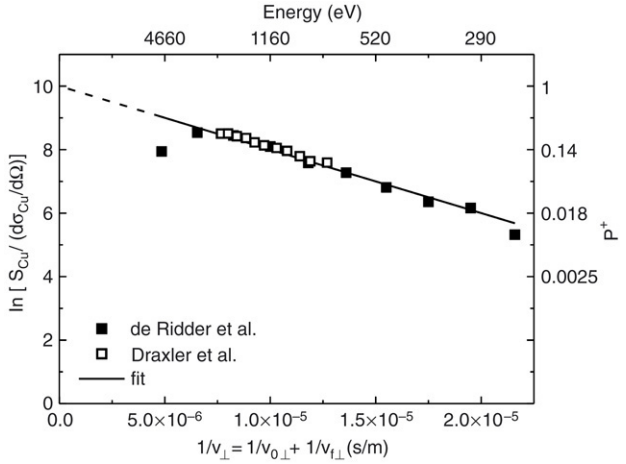

Fig. 7.1. Determination of the ion fraction by de Ridder et al. [112]. Measurements are done with $^4He^+$ ions on polycrystalline Cu. Primary energies between 250 eV and 5 keV are used. Only the velocity components perpendicular to the surface are taken for the reciprocal value. The incident ion beam is perpendicular to the surface. The values for the absolute ion fractions for ^4He on Cu are reproduced from Draxler et al. [43]. Both set-ups used for obtaining the data have similar geometry.

7.2. ESA experiment

With ESAs only backscattered ions are detected. If all other factors in Eqs. (2.2) and (2.3) are known, the absolute ion fraction can be calculated, using:

$$P_i^+ = \frac{S_i}{I_p \cdot t \cdot \xi \cdot R \cdot \frac{d\sigma_i}{d\Omega} \cdot N_i}. \tag{7.7}$$

Mostly the instrumental factor is not fully known. In order to determine the absolute ion fraction it is convenient to use an approach different from Eq. (7.7) [127]. It relies on the assumption that one can find at least one element for which the relation $P^+ = \exp(-v_c/v_\perp)$ is valid for a reasonable energy range. Here, v_c is a constant that is characteristic for the neutralization and $v_\perp$ is the perpendicular component of the velocity (see Section 3). A simple mathematical rearrangement of Eq. (2.2) results in

$$\ln\left(\frac{S_i}{\frac{d\sigma_i}{d\Omega} \cdot C}\right) = \ln(P_i^+) + \ln(N_i) = \frac{v_c}{v_\perp} + \ln(N_i) \tag{7.8}$$

with $C = I_p \cdot t \cdot \xi \cdot R$. This gives a linear dependence of the logarithmic value of the term on the left hand side on the reciprocal value of the perpendicular ion velocity $v_\perp$.

Most factors in Eq. (7.8) can simply be measured (the LEIS signal S_i^+ for a given ion fluence), calculated (differential scattering cross section $d\sigma/d\Omega$) or simply chosen (a flat single crystal has a known elemental surface density (N_i)). While it is very difficult to determine the absolute value of the instrumental factor ξ, its energy dependence is the only information needed to determine the ion fraction. For instance, for a DTA the instrumental factor ξ is independent of energy ($\xi = c$), while for a CMA it is proportional to energy ($\xi = c \cdot E$).

In Fig. 7.1 it is illustrated how P^+ can be determined from energy dependent measurements of the ion fraction for $^4He^+$ and Cu. The measurements have been done with a DTA which has got a constant instrumental factor. The logarithmic value of the LEIS signal, corrected for the differential cross section (see left vertical axis) shows a linear dependence on the reciprocal value of the perpendicular ion velocity, in agreement with Eq. (7.8). The slope of the linear fit represents the characteristic velocity v_c and is determined as $2.0 \cdot 10^5$ m/s. The results show good agreement with the data of Draxler et al. [43] who determined the absolute ion fraction between 1 and 2 keV on a set-up with similar scattering geometry. Above 2 keV a large deviation between measurement and linear extrapolation is observed, which shows that an additional neutralization channel becomes possible at these energies.

For "infinite velocity" the ion fraction extrapolates to 1 (see also Eq. (4.1a) and extrapolation of the absolute ion fraction data of Draxler in Fig. 7.1), which reduces Eq. (7.8) to

$$\ln\left(\frac{S_i}{\frac{d\sigma_i}{d\Omega}}\right) = \ln(N_i \cdot \xi) \quad v_\perp \to \infty. \tag{7.9}$$

The value for $\ln(N_i \cdot \xi)$, determined after extrapolating the linear fit in Fig. 7.1 (see dashed line), equals 10. With N_{Cu} known (e.g. $1.8 \cdot 10^{15}$ atoms/cm^2 for a (111) surface) the instrumental factor ξ can be calculated. Once this response function has been determined, one can determine the ion fraction for any other material for the used energies and given experimental geometry using Eqs. (2.2) and (2.3).

When two isotopes of the same noble gas ion having the same incident energy are scattered from the same target, the signal for the lighter isotope is generally significantly larger. This is particularly true when comparing the signals for scattering of $^3He^+$ and $^4He^+$. The higher velocity of $^3He^+$ for a given incident energy and the lower kinematic energy loss in the collision lead to a shorter dwell time in the electron density in front of the surface, and thus to less neutralization (Section 3). Ackermans et al. [128] have shown that when Eq. (4.1) holds, one can determine the ion fraction P^+ by comparing the signals for the two isotopes. If the measurements are carried out consecutively, or even better simultaneously by using a ^3He–^4He gas mixture of known composition, the results pertain to the same target with the same roughness and composition. If a mass filter is used for the primary ion beam, this requires regular switching between $^3He^+$ and $^4He^+$. Especially for samples where good reference samples are not easily available, this Dual Isotope for Surface Composition (DISC) analysis is quite helpful to determine the ion fractions for all elements involved [129]. From this information, the surface composition can be calculated. The accuracy is, however, poorer than what can be obtained by calibration against standards.

7.3. Validity of experimental determination of P^+

Both evaluation procedures to determine P^+ (Eqs. (7.4) and (7.7)) can have severe systematic errors which can exceed the statistical errors of the experiment considerably, typically 20%–30% [49]. But if one compares these two procedures, it becomes obvious that the possible systematic errors have very

different origins. If the resulting P^+ values coincide within statistics, one may trust that the result obtained is reliable. The most reliable cross check is to compare the P^+ values obtained via Eqs. (7.4) and (7.7) to the ion fraction obtained for a single crystal in channeling geometry under identical conditions. In this case, not even the scattering cross section must be known.

8. Analysis of "real" surfaces

Some knowledge about the target before measuring certainly will be helpful. The analysis is drastically distorted when the target is an insulator, but no charge compensation is used. In Section 8.1 strategies will be discussed how to choose primary energy and type of projectile used for surface analysis. How the target itself may influence the choice of the 7 experimental conditions is discussed in Section 8.2. Section 8.3 deals with the quantification of the composition of rough surfaces.

8.1. Choice of projectile and primary energy

The choice of which type of noble gas ions at which primary energy are used as projectiles influences mass separation and elemental sensitivity.

The analysis of low mass elements requires the use of He^+ ions. To obtain a higher elemental sensitivity for the lowest masses, such as C, the use of the $^3He^+$ isotope is generally preferred for the analysis, since it has a higher velocity (higher P^+) for a given primary energy than the $^4He^+$ isotope. With increasing mass one may have to switch from He^+ to Ne^+ or even Ar^+ ions (Section 2.1). Fig. 8.1 illustrates how different types of incident ions, i.e. He^+, Ne^+ and Ar^+, may be chosen to resolve LEIS peaks of different elements in the surface. The spectra were taken for a thermionic dispenser cathode with an Os/Ru top layer at 1030 °C [130]. In the He^+ spectrum the peaks due to scattering from Ru, Ba, W and Os, having average atomic masses of 101, 137, 184 and 190, respectively, all overlap. The insert shows a peak for the low-mass element O, obtained for a cathode after exposure to 20 Langmuir (L) of O_2 at room temperature. With Ne^+ the Ru and Ba peaks are well separated and only the W/Os peaks are still not resolved. With Ar^+ even these elements are separated.

Eq. (2.1) shows that for different masses the corresponding peaks are separated in energy by an amount $\Delta E = \Delta k E_0$ that increases linearly with the primary energy E_0. However, the peak width also broadens with increasing energy due to elastic and inelastic effects. The choice of energy is of minor importance if the broadening due to elastic effects dominates. Then, peak separation and elastic effects both scale linearly with energy. If, however, inelastic effects are dominant, the peak also broadens with velocity, i.e. the square root of the energy. In this case a higher energy results in a higher resolving power.

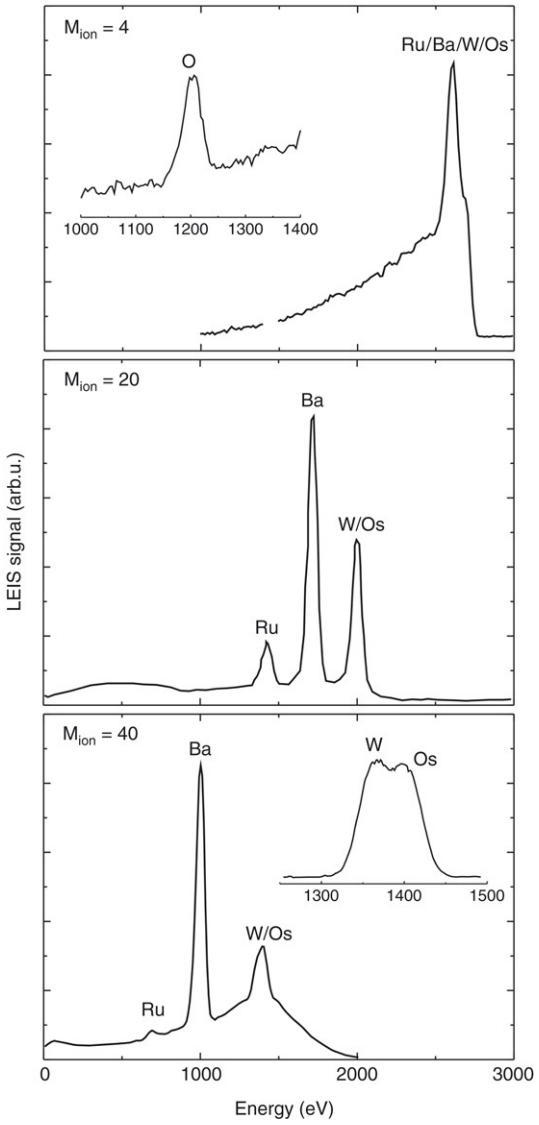

Fig. 8.1. Example of the use of different ions to resolve LEIS peaks. Spectra obtained from a dispenser cathode with an Os/Ru top layer using 3 keV He^+, Ne^+ and Ar^+ beams [130].

8.2. Targets

One of the main advantages of LEIS is that analysis is possible for a great diversity of materials, from metals, oxides and polymers to even liquid surfaces (Section 9). The only restriction concerns the vapor pressure of the studied material, which should be low enough to keep the vacuum below 10^{-5} mbar as required for safe operation of channeltrons and microchannelplates and to prevent significant neutralization along the path from the sample to the detector.

8.2.1. Sample charging

Most oxides and polymers are insulators. To prevent them from charging by the incident ion beam the surfaces have to be flooded with low-energy electrons. In the case of inhomogeneous charging (extremely rough surfaces) LEIS peaks are broadened. Proper charge compensation can avoid this. However, when using charge compensation, one also has to consider the possible modification of the surface due to the electron impact. Especially in the case of halides this can be a serious problem.

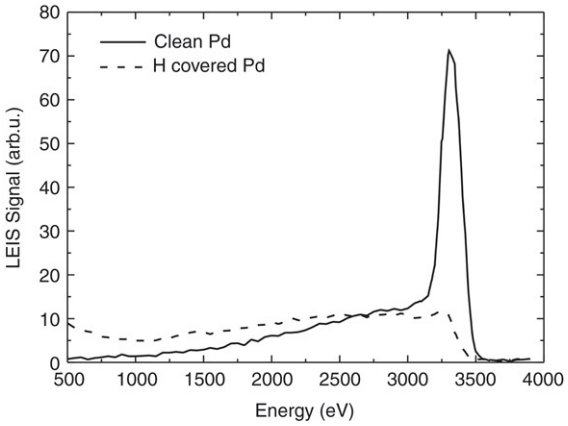

Fig. 8.2. LEIS spectra (4 keV He^+) measured on Pd demonstrating the influence of H on LEIS signals. When the Pd is clean a high-intensity Pd peak is observed in the LEIS spectrum. When the Pd is covered by H the Pd peak has disappeared. The increased background below 1000 eV is due to sputtered H^+ ions [289].

Catalysts are generally very good insulators, especially when they are highly dispersed and (inhomogeneous) charging of the surface is difficult to avoid.

Insufficient neutralization, due to a too low electron current causes a positive charging voltage, and consequently an energy dependent shift of the LEIS spectrum towards higher energies. In the extreme case this charging prevents the ions from reaching the sample and they are reflected with their primary energy E_0. This was especially difficult in the past, when the ion currents used in the analysis were much higher than in modern times. Nowadays ion currents used for analysis are much lower.

There are several ways to measure the ion current. The most reliable way is to use a Faraday cup. A simpler approach is to measure the current on a conducting part of the manipulator. However, when ions hit the manipulator, (secondary) electrons are emitted. These electrons contribute to the current measurements. Biasing of the sample to approximately +50 V is generally sufficient to avoid electron emission and measure the actual ion current.

8.2.2. *"Real" surfaces*

An important feature of LEIS is its sensitivity for the outermost layer. Thus, a monolayer of impurities will have a dramatic effect on the result. For example, H cannot be detected directly when analyzing energy spectra of backscattered projectiles (see Fig. 2.2). If detection of hydrogen is required, the energy spectra of recoiling particles emitted in a forward direction have to be investigated. This type of spectroscopy is well known as "Scattering and Recoiling Spectrometry" (SARS) [131,132]. The effect of H in LEIS is demonstrated [289] in Fig. 8.2. The solid curve in the LEIS spectrum is obtained for a clean Pd surface, whereas the dashed curve shows the LEIS spectrum for a Pd surface that is saturated with H. Obviously, the Pd surface peak has completely disappeared due to the presence of H. The ions that scatter from Pd atoms are neutralized when they pass close to a H atom, thereby completely suppressing the binary collision peak.

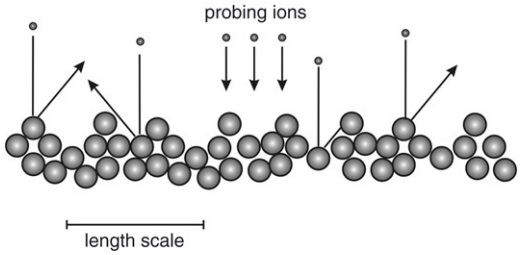

Fig. 8.3. Illustration how shadowing and blocking reduce the LEIS signal for a rough surface consisting of spherical particles. For 3 trajectories a particle shields the presence of the underlying atoms (shadowing), while in one trajectory a deeper lying particle is reached, but the scattered ion is blocked on the way out. As long as the ion beam probes a distance at the sample that is much larger than the length scale, the signal reduction is independent of the value of the length scale.

When a sample is introduced from the ambient atmosphere into the analysis chamber, it is generally contaminated to some degree by water or organic molecules. As one is mostly interested in the underlying surface, cleaning procedures have become an essential part of LEIS measurements. Commonly used cleaning procedures include sputtering, heating and chemical treatment. For example H atoms on a Pd surface (Fig. 8.2) are very efficiently removed by ion bombardment due to their enhanced desorption efficiency. One can even use this property to selectively remove H from e.g. an oxide or alloy without doing any noticeable damage to the sample.

8.2.3. *"Non-destructive" or "static" analysis*

Composition analysis by ions damages the surface. The extent to which this damage occurs depends on the fluence used and sputter yield of the target elements. Parameters like acquisition time, beam current, beam spot size, primary energy and ion type should be chosen appropriately. For example, even for He^+ projectiles and polymer surfaces the large sputter yield limits the fluence for static analysis to about $1 \cdot 10^{13}$ ions/cm^2 [133]. For He^+ projectiles and a metal surface the allowed fluence may be up to 100 times higher [134]. The ion fluence required to gain sufficiently large scattered intensity depends on the system under investigation and on experimental details. Nevertheless, using a detector with sufficiently large solid angle and/or measuring a large energy window simultaneously usually warrants that a spectrum is acquired for a fluence of typically 10^{10}–10^{12} ions/cm^2.

8.3. *Quantification of the composition of rough surfaces*

Surface roughness is often considered as one of the important parameters that influences the LEIS signal. This is especially relevant, when samples with different roughnesses are used for quantification.

In Fig. 8.3 it is illustrated how roughness affects the scattered ion signal. Shadowing will prevent part of the incoming ions to reach all atoms from which they could be scattered, while blocking along the outgoing trajectory can prevent them from reaching the analyzer. This shielding (shadowing + blocking) results not only from scattering but also from neutralization. These effects both reduce the number of backscattered particles

into the analyzer. Surface roughness can also lead to a higher effective density of the surface atoms and thus to an increase in the LEIS signal. Due to the monolayer sensitivity of LEIS, the influence of shielding will be more severe in a surface analysis by LEIS than in an analysis using surface techniques that probe deeper.

In fact, many applications involve extreme surface roughness. In heterogeneous catalysis, for instance, where the important chemical conversions are restricted to the surface, specific surface areas of 100–1000 m^2/g are quite normal. The relevance of surface roughness is not restricted, however, to such surfaces. Processes such as chemical etching and sputtering may lead to roughness at an atomic scale, which also reduces the scattered ion signal significantly. An adequate strategy for dealing with surface roughness is thus essential.

In Eq. (2.1) the factor R corrects for signal changes due to surface roughness [135,136]. The influence of surface roughness on the LEIS signals was already investigated by Nelson [137] in 1976. He used angles of incidence and scattering of 45° and 90°, respectively. His samples consisted of 3 μm thick evaporated and 1 μm thick sputtered Au films on ceramic Al_2O_3 and sapphire substrates. The gold on sapphire was considered to be smooth in comparison to the gold on the ceramic. Using a Talystep it was verified that the roughness had a normal distribution. Similar to the study of Ebel et al. [138] for X-ray photoelectron spectroscopy, Nelson used a 2D model of tilted cubes to describe the rough surface. For the distribution of tilt angles a normal distribution was taken. The model gave a good description of the experimental data. Although it may seem surprising at first sight, it was found that the surface with the highest rms roughness (1.06 μm for the Au on sapphire) gave the smallest signal reduction (6%). For Au on the ceramic surface (0.25 μm rms roughness) the reduction was 22%. As pointed out by the author, however, the reduction (shadowing by neighboring atoms) is determined by the rms slope (4.8° and 21°, respectively) of the surface rather than the roughness itself. Thus the local tilt of the surface is important for the signal reduction.

Margraf et al. [139] found in studies of α- and γ-Al_2O_3 that the signals for the γ-Al_2O_3 were up to a factor 5 to 6 smaller than those for α-Al_2O_3 surface. The effect was ascribed to a difference in roughness of the aluminas. Jacobs et al. [74] also studied the α- and γ-modifications (5.5 m^2/g and 269 m^2/g, respectively, being roughly the same specific surface areas as those in the study of Margraf et al.). After some sputtering (to eliminate structural effects) the α- and γ-modifications gave the same Al/O ratio and roughly the same signal intensities. The signals were only 1.7 times lower than that of sputter cleaned sapphire (a flat α-Al_2O_3 reference).

Recently Jansen et al. [140] carried out a comprehensive study of the influence of surface roughness on the LEIS signals. They circumvented the problem of the different surface modifications by using silicas instead of aluminas. In Sections 8.3.1–8.3.4 the approach of Jansen et al. is followed.

8.3.1. Compaction

Similar to the study of Jacobs et al. [74], Jansen et al. [140] pressed the silica powders to pellets. This is believed to be important to obtain reliable and reproducible results. Jansen et al. obtained the same Si and O signals for pressures between 2 and 2000 MPa (20–20 000 kg/cm^2). One could expect that the influence of compaction is more pronounced for inhomogeneous samples. Therefore, the influence of compaction was also studied for highly dispersed silica that had been impregnated with a sub-monolayer of Ta_2O_5. It was found that up to 300 MPa the compaction had no influence on the Si, O and Ta signals [140].

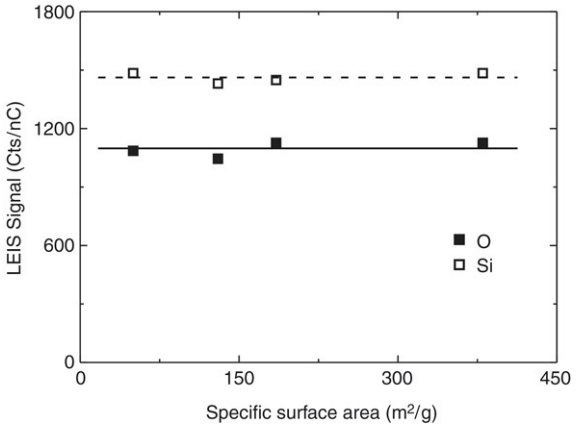

Fig. 8.4. Si and O LEIS signals are shown for silica powders having specific surface areas varying from 50 to 380 m^2/g [140]. The results show that the LEIS signal is not influenced by the surface roughness.

The insensitivity of the silicas to compaction can be understood by realizing that the structure of silica powders resembles that of a bunch of grapes: spheres connected by weak links. Upon pressing the spheres stay intact, but many weak links are broken. It has been verified using Scanning Electron Microscopy (SEM) that the pressing did not affect the spheres themselves, only their packing. In the ideal case compaction will lead to a close-packed array of equally sized spheres. Although the precise value of the compaction was not important, a minimum value (<1 MPa) is required to ensure that the characteristic length scale of the roughness of the powder is smaller than the diameter of the ion beam.

While the insensitivity to compaction has been observed for many materials, this is not a general rule. For $MgCl_2$ powders, for instance, the Mg/Cl ratio is affected when higher compaction pressures are used.

8.3.2. Dispersion and packing density

In Fig. 8.4 the Si and O LEIS signals are shown for silica powders having specific surface areas varying from 50 to 380 m^2/g. All samples were compacted with the same pressure (300 MPa). Also a flat quartz substrate was included in the study [140]. All samples had the same Si/O ratio, confirming that the surface compositions were indeed the same. Moreover, the powders gave the same absolute values for the LEIS signals within experimental errors, despite the large differences in the surface areas. This value was 17% lower (roughness factor $R = 0.83$) than that of the flat quartz sample.

From fractal theory one can understand that for normal experimental conditions the LEIS signal does not depend on the size of the spheres (and thus not on the specific surface area)

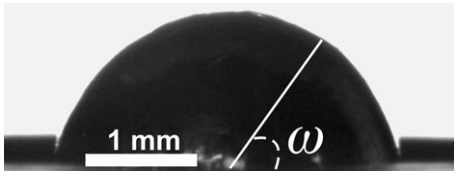

Fig. 8.5. Photograph of the upper half of an analyzed Ga droplet.

nor on the "unit cell" (length scale in Fig. 8.3), irrespective whether the length scale is of the order of 1 nm (for a very high specific surface area) or as large as 0.1 mm (for a very low specific surface area). The lower limit results from the fact that the ions are scattered by the cores of the atoms (Section 8.3.4). The upper limit is determined by the beam size, which should be large enough to probe at least one characteristic pattern. This is the reason why a minimum compaction pressure is required: it removes the macroscopic roughness of the sample.

If we assume that the compacted surface of silica clusters consists of a close-packed array of equally sized spheres, the theoretical surface packing density is 0.907. This value is independent of the size of the spheres. The experimental R value (0.83) for silica is only somewhat lower. The origin of this difference is discussed in Section 8.3.3.

8.3.3. Modeling surface roughness in LEIS

The 2D models of Nelson [137] and of Jacobs et al. [74] overestimate the influence of roughness as encountered in supported catalysts. Jansen et al. [140] have developed a 3D model taking into account physical shielding, density of scattering centers and neutralization. This was applied to ion scattering by a close-packed array of equally sized spheres. For scattering angles of 135° and 145° the signal reduction due to the shielding and neutralization is almost completely due to that by the other atoms of the same sphere and not by the neighboring spheres. For these very rough surfaces the 2D models a signal reduction $R = 0.5$ is found [137], which is a clear over-estimation. This over-estimation is caused by the assumption that in the scattering plane the neighboring spheres touch the sphere from which the ions are scattered. This only occurs for a few azimuthal directions and is thus an unlikely event in a 3D model.

The density of the scattering centers is also an important factor. When a surface is tilted, the number density of the scattering centers in the outer surface increases. For an ion beam hitting a sphere, this density increases as $1/\sin(\omega)$, with ω the tilt angle (Fig. 8.5). Thus the probability to be scattered increases when ω is lowered (more grazing angles). For very grazing angles the surface atoms start to shield each other. Depending on the packing density and perfectness of the surface, the effective number of centers for backscattering drops to zero for angles below 10° or 20°.

In order to verify and better understand the influence of spherical particles and of packing density on the LEIS signal, Jansen et al. [140] have investigated the LEIS signal of a single spherical particle and of inclined surfaces. A 3 keV Ne^+ microbeam was scanned over the surface of a gallium droplet (diameter about 3 mm) while accepting the full cone

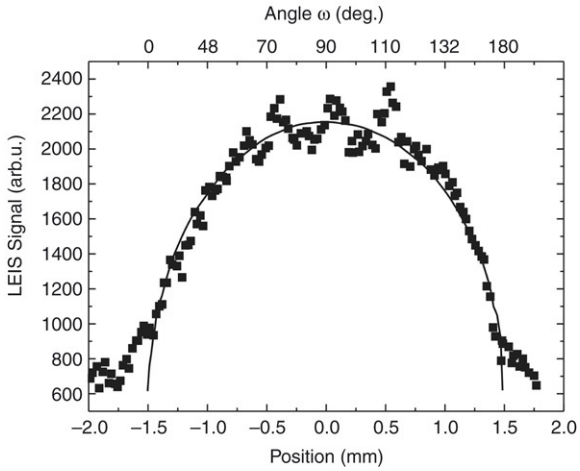

Fig. 8.6. Angular dependence of the LEIS signal of a Ga droplet of 3.04 mm diameter [140]. The solid line represents a fit of the LEIS signal with $\sin(\omega)$ (see also Fig. 8.5).

of ions scattered over 145°. The high surface tension of the Ga produces a very nice spherical surface. The LEIS signal as a function of the position of the impact of the ion beam is given in Fig. 8.6 (Fig. 8.5 shows a photograph of the Ga droplet). The signal is found to be proportional to the sine of the tilt angle ω. Similar results were obtained for Au by tilting the surface over various angles. When the LEIS signal is integrated over the surface of the droplet, one finds that for a scattering angle of 140° a spherical particle yields a signal that is 2/3 of that of its projected area. Assuming that this result is more general for metals, this finding greatly simplifies the quantification of LEIS for such particles. It has found already important applications in the quantification of the size of (hemi) spherical nanoparticles by LEIS [141].

The signal reduction for powders, as compared to flat surfaces, will have a different value than obtained for the silicas. For the aluminas, for instance, the structure is more plate like. This will be the reason why Jacobs et al. [74] found a much stronger signal reduction (factor of 1.7) when comparing a flat sapphire surface with that of 5 m^2/g α-Al_2O_3.

In the literature, signal reductions by an order of magnitude have been ascribed to surface roughness [139]. We know now, however, that under characteristic experimental conditions the influence of surface roughness is relatively small (R = 0.6–0.9, depending on the material) [140]. The relatively small differences result from the fact that one averages the result over many conditions (angles of incidence and azimuth).

8.3.4. Atomic scale roughness

As discussed in Section 8.3.3, it is not the specific surface area (roughness) but the surface slopes that determine the shielding/blocking. This is of particular relevance to roughness at an atomic scale. For this extreme roughness the model of Jansen et al., that was discussed above, is no longer applicable. Cortenraad et al. [101] investigated both well-annealed and freshly sputtered tungsten surfaces. It was found that the W signal was reduced significantly by sputtering. The sputtering will lead to surface damage, in particular to atomic vacancies.

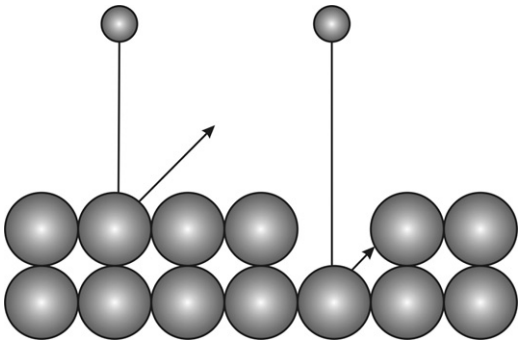

Fig. 8.7. Schematics on the influence of a monolayer vacancy on the LEIS signal. After scattering by an atom in the outer surface, the ion is able to reach the analyzer. However, when scattered by an atom in the 2nd layer (as a consequence of a vacancy) the He^+ ion is blocked by the atom of the outer layer, which results in signal loss.

In Fig. 8.7 it is illustrated that a mono-atomic vacancy will reduce the LEIS signal. Ions that are scattered at the bottom of the vacancy cannot escape without another interaction with a surface atom. The signal reduction is thus a measure for the surface roughness at an atomic scale. Especially for refractory metals, where the self-annealing of vacancies during the collision cascade or afterwards at room temperature will be small, the concentration of mono-atomic vacancies can be high. The signal reduction by this type of roughness will be largest when a close-packed surface is sputtered. For the W(110) a reduction of 28 ± 3% was found. For other crystal faces the atomic density is already lower and the effect of sputtering is less [101]. Ermolov et al. [142] found similar results for Mo surfaces. For materials having lower melting points annealing will be more efficient thus reducing the atomic roughness. Since surfaces are generally prepared under conditions where some kind of (local) thermodynamic equilibrium exists, reduction of the surface energy will make atomic roughness less likely. This will also reduce the influence of atomic surface roughness.

Reductions in the LEIS signals similar to the ones observed by Cortenraad et al. have been found for oxidic glasses from which part of the cations had been leached in an alkaline or acidic solution [143].

The observed signal reduction will depend on the scattering geometry. If one would assume that the signal reduction only originates from shadowing and blocking by scattering, there should be no signal reduction for 180° scattering. Neutralization will, of course, lead to signal loss. Comparing 180° with smaller angle scattering may, however, be a useful tool in the understanding of atomic roughness.

Since the adsorption energy for atomic vacancies is much higher than that for a flat surface, such vacancies are believed to play an important role in the surface chemistry and in diffusion of adsorbates. While a surface technique such as Scanning Tunneling Microscopy gives very detailed information on the surface topography of single crystals, LEIS is useful to obtain statistically relevant information on surface vacancies on microscopically rough surfaces.

9. Survey of surface composition analyses

In the early days of LEIS there were many disputes about the possible use of LEIS for composition analysis of the surface. Studies of secondary ion mass spectrometry (SIMS), in which the sputtered ions are detected, had shown that this technique suffers from strong matrix effects. The similarity between LEIS and SIMS suggested that LEIS studies might also be hampered by these effects. Although a few well-documented studies demonstrated already the quantitativeness of LEIS [144, 98,145], skepticism remained. As will be shown below, in the overwhelming majority of the reported LEIS studies no matrix effects occur and quantification is straightforward. There are, however, also a number of well-established cases where the chemical environment of an atom does influence its LEIS signal. It is thus important to recognize these situations and know how to cope with them.

In Section 2 it has been described how the surface composition of a sample can be determined with LEIS. The equations in Section 2.2 are based on the assumption that matrix effects are absent, i.e. the ion fraction P^+ for scattering by a certain type of atom in the outer surface is for all incident ion energies of interest independent of the target in which the atom is present. In Section 4 methods have been described to verify the absence or existence of matrix effects. In Section 9.1 the cases are described where the absence of matrix effects has been claimed and the procedures are discussed how to quantify the surface composition. Section 9.2 treats the cases where matrix effects are observed. Although this complicates the analysis, it is shown how these matrix effects can be avoided or minimized and how it is still possible to obtain a quantitative analysis of the outer surface.

9.1. Known cases without matrix effects

If matrix effects (Section 4.2) are absent, the quantification of the surface composition is straightforward (Eq. (4.5)). In Table 9.1 an overview is given of cases that have been reported since 1994, where the absence of matrix effects is claimed. Compilations of earlier cases can be found in previous reviews [146,136].

Table 9.1 illustrates the great variety of cases where the authors quantified the surface composition by LEIS and claimed the absence of matrix effects. This means that elemental sensitivity factors can be determined. The examples include single crystals, polycrystalline materials, many amorphous samples and highly dispersed catalysts. Metals, semiconductors and insulators have been investigated. In many cases they are alloys or compounds (including oxides and halogenides). In recent years the development of high-sensitivity LEIS has stimulated studies of sensitive polymers, self-assembled monolayers and other organic materials, but the number of quantitative studies is here still limited.

The use of reference samples (pure elements or compounds) is generally preferred above the use of tabulated sensitivity factors from the literature, the main reason being that the experimental conditions (type of ion, primary energy, and scattering angle) are far from standardized in LEIS. It is

Table 9.1
A compilation of ion–solid combinations where the absence of matrix effects has been reported (papers since 1994)

		Projectile	Quantification method	Reference
(a) Elements				
Aluminum	FeAl(100)	^{4}He	2	[171]
	$Ni_{90}Al_{10}(111)$	^{4}He	1	[172]
	$Cu_{82}Al_{18}(100)$	^{4}He, Ne	1	[173]
	$Al_{70}Pd_{21}Mn_9$	^{3}He	1, 4	[174,2]
	Al/Pd(001)	^{4}He	4	[175,176]
	Al/Ru(0001)	^{4}He	1	[177]
	Al/Fe(100)	^{4}He	4	[178]
	Pd(001)-(2 × 2)p4g-Al	^{4}He	1	[179]
	Ni_3Al/Ni(100)	^{4}He	4	[180,181]
	$Ag_{80}Al_{20}$	^{4}He	1	[74]
	Fe_xAl_{1-x}	^{4}He	1	[182]
	p-Al	^{3}He, ^{4}He	3	[5]
	VO_x/Al_2O_3	^{4}He	4	[183]
	Ni/Al_2O_3	^{4}He	1	[74]
Antimony	GaSb	Ne	1	[184]
	InSb	Ne	1	[184]
Barium	$BaZrO_3$	^{4}He, Ne	2	[185]
	$LiBaF_3$	^{4}He, Ne	2	[185]
Cadmium	CdSe	Ne	1	[184]
Calcium	CaO/NiO	^{4}He	2	[186,154]
	CaO/YSZ	^{4}He	2	[187,117]
Cerium	$CeGdO_x$	Ar	2	[188]
Chromium	Cr/Pt(111)	^{4}He	1	[189]
	p-Cr	^{3}He, ^{4}He	3	[5]
Cobalt	$Pt_{90}Co_{10}(110)$	^{4}He	1	[190]
	Pt_3Co	Ne	1	[191]
Copper	CuAu(100)	^{4}He	1, 4	[192,193]
	$Cu_3Pt(111)$	^{4}He	1	[194]
	$Cu_3Pt(001)$	^{4}He	1	[195]
	$Cu_{82}Al_{18}(100)$	^{4}He, Ne	1	[173]
	$Cu_{85}Pd_{15}(110)$-(2 × 1)	Ne	1	[100]
	Cu/Ru(0001)	^{4}He	1	[196]
	Cu/ZnO(0001)	^{4}He	2	[197]
	Cu/Ir(100)-(5 × 1)	^{4}He	1	[198]
	$Fe/Cu_3Au(001)$	Ne	4	[199]
	Pd/Cu(110)	^{4}He	3	[200]
	Ir/Cu(100)	^{4}He	1	[201]
	Cu(001)-(2 × 2)p4g-Pd	^{4}He	1	[202]
	$Cu_{55}Pd_{45}$	^{4}He	1	[6]
	$Cu_{81}Pt_{19}$	Ne	1	[203]
	CuZr	^{4}He	1	[204]
	CuTi	^{4}He	1	[205]
	CuNi	Ne	1	[206]
	CuPt	^{4}He	1	[207]
	p-Cu	^{3}He, ^{4}He	3	[5]
	CuO/ZnO	^{4}He	1	[73]
Fluorine	$LiBaF_3$	^{4}He, Ne	2	[185]
	p-LiF	^{4}He	4	[208,260]
Gadolinium	$CeGdO_x$	Ar	2	[188]
Gallium	GaP(100)	Ne	1	[209]
	GaAs(100)	Ne	1	[209]
	GaSb	Ne	1	[184]
Germanium	$Si_{1-x}Ge_x$	^{4}He	1	[210,211]
Gold	$Au_3Pd(110)$	^{4}He	3	[212]

Table 9.1 (*continued*)

		Projectile	Quantification method	Reference
	CuAu(100)	^{4}He	1, 4	[192,193]
	Au/TiO_2	^{4}He	1, 2	[213,214]
	Au/Si(100)	^{4}He	1	[215,216]
	Pd/Au(110)-(1 × 2)	^{4}He	1	[217]
	Fe/Cu_3Au(001)	Ne	4	[199]
Indium	InP(100)	Ne	1	[209]
	InAs(100)	Ne	1	[209]
	InSb	Ne	1	[184]
Iridium	Ir/Cu(100)	^{4}He	1	[201]
	p-Ir	^{3}He, ^{4}He	3	[5]
	Cu/Ir(100)-(5 × 1)	^{4}He	1	[198]
Iron	FeAl(100)	^{4}He	2	[171]
	FeSi(100)	^{4}He	3	[218]
	$Pt_{80}Fe_{20}$(111)	^{4}He, Ne	1	[219]
	Fe/Cu_3Au(001)	Ne	4	[199]
	Fe/Ag(100)	Ne	1	[220]
	Fe_xSi_y	^{4}He	2	[221]
	Fe_xAl_{1-x}	^{4}He	1	[182]
	$Fe_{99}Pd_1$	^{4}He, Ne	1	[222]
	Al/Fe(100)	^{4}He	4	[178]
	FeO_x/SiO_2	^{4}He	2	[223]
Lithium	$LiBaF_3$	^{4}He, Ne	2	[185]
	p-LiF	^{4}He	4	[208]
Magnesium	MgO/NiO	^{4}He	2	[186,154]
Manganese	Mn/Ag(001)	^{4}He	1	[224]
	Mn/Ag(100)	^{4}He	1	[225]
	$Al_{70}Pd_{21}Mn_9$	^{3}He	1, 4	[174,2]
Mercury	Hg/CeO_2	Ne	2	[226]
Molybdenum	Mo(100)-Mo(110)	Ne	3	[142]
	$Pt_{70}Mo_{30}$	^{4}He	1	[227]
	MoO_x/SiO_2	^{4}He	4	[116]
Nickel	Ni(100)	^{3}He, ^{4}He	3	[5]
	$Ni_{90}Al_{10}$(111)	^{4}He	1	[172]
	Pd_8Ni_{92}(111)	^{4}He	1	[228]
	Pd_8Ni_{92}(110)	^{4}He	1	[228]
	$Pt_{25}Ni_{75}$(100)	^{4}He	1	[229]
	$Pt_{25}Ni_{75}$(110)	^{4}He	1	[229]
	Pt_xNi_{1-x}(100)	^{4}He	1	[230]
	$Pt_{50}Ni_{50}$(111)	^{4}He	1	[231]
	Ni/Pt(111)	^{4}He	1, 3	[232]
	Ni/W(111)	^{4}He	1	[233]
	Ni/Al_2O_3	^{4}He	1	[74]
	Pd/Ni(110)	^{4}He	3	[234]
	Ni_3Al/Ni(100)	^{4}He	4	[180,181]
	$Ni_{80}Pt_{20}$	^{4}He	1	[74]
	$Ni_{50}Zr_{50}$	Ar	4	[235]
	Pd_1Ni_{99}, Pd_5Ni_{95}	^{4}He	1	[236]
	CuNi	Ne	1	[206]
	Pt_3N_i	Ne	1	[191]
	MgO/NiO	^{4}He	2	[186,154]
	CaO/NiO	^{4}He	2	[186,154]
Niobium	Nb_xTa_{1-x}(110)	^{4}He	4	[237]
	O/Nb	^{4}He	4	[136]
Oxygen	O_2/Ag(111)	^{4}He	4	[238]
	O_2/Si(100)	^{4}He	2	[239]

(*continued on next page*)

Table 9.1 (*continued*)

		Projectile	Quantification method	Reference
	O/Nb	^{4}He	4	[136]
	O/Ta	^{4}He	4	[136]
	$BaZrO_3$	^{4}He, Ne	2	[185]
	$CeGdO_x$	Ar	2	[188]
	YSZ	^{4}He, ^{20}Ne	2	[240]
	V/YSZ	^{4}He	2	[241]
	W/YSZ	^{4}He	2	[241]
	CaO/YSZ	^{4}He	2	[187,117]
	CaO/NiO	^{4}He	2	[186,154]
	MgO/NiO	^{4}He	2	[186,154]
	ZrO_2/SiO_2	^{4}He	2	[242]
	MoO_x/SiO_2	^{4}He	4	[116]
	FeO_x/SiO_2	^{4}He	2	[223]
	VO_x/Al_2O_3	^{4}He	4	[183]
	CuO/ZnO	^{4}He	1	[73]
	Cu/ZnO(0001)	^{4}He	2	[197]
	$Pt/TiO_2(110)$	^{4}He	4	[243]
	Au/TiO_2	^{4}He	1, 2	[213,214]
	Hg/CeO_2	Ne	2	[226]
	Ni/Al_2O_3	^{4}He	1	[74]
Palladium	$Pd_8Ni_{92}(111)$	^{4}He	1	[228]
	$Pd_8Ni_{92}(110)$	^{4}He	1	[228]
	$Au_3Pd(110)$	^{4}He	3	[212]
	$Cu_{85}Pd_{15}(110)$-(2 × 1)	Ne	1	[100]
	Pd/Au(110)-(1 × 2)	^{4}He	1	[217]
	Pd/Cu(110)	^{4}He	3	[200]
	Pd/Ni(110)	^{4}He	3	[234]
	Pd/Pt(111)	^{4}He	1, 3	[244]
	Pd/W(111)	^{4}He	1	[233]
	Cu(001)-(2 × 2)p4g-Pd	^{4}He	1	[202]
	Pd(001)-(2 × 2)p4g-Al	^{4}He	1	[179]
	Al/Pd(001)	^{4}He	4	[175,176]
	V/Pd(111)	^{4}He	1	[150]
	$Al_{70}Pd_{21}Mn_9$	^{3}He	1, 4	[174,2]
	Pd_1Ni_{99}, Pd_5Ni_{95}	^{4}He	1	[236]
	PdPt	^{4}He	1	[205]
	$Cu_{55}Pd_{45}$	^{4}He	1	[6]
	$Fe_{99}Pd_1$	^{4}He, Ne	1	[222]
	p-Pd	^{3}He, ^{4}He	3	[5]
Platinum	$Pt_{90}Co_{10}(110)$	^{4}He	1	[190]
	$Pt_{80}Fe_{20}(111)$	^{4}He, Ne	1	[219]
	$Pt_xNi_{1-x}(100)$	^{4}He	1	[230]
	$Pt_{50}Ni_{50}(111)$	^{4}He	1	[231]
	$Pt_{25}Ni_{75}(100)$	^{4}He	1	[229]
	$Pt_{25}Ni_{75}(110)$	^{4}He	1	[229]
	$Pt_{50}Rh_{50}(100)$	^{4}He	1	[245]
	$Pt_{50}Rh_{50}(511)$	^{4}He, Ne	4	[246]
	$Pt_{25}Rh_{75}(111)$	^{4}He	1	[247,248]
	$Pt_{25}Rh_{75}(110)$	^{4}He	1	[247,248]
	$Pt_{25}Rh_{75}(100)$	^{4}He	1	[247,248]
	$Pt_3Sn(111)$	Ne	1	[249]
	$Pt_3Sn(110)$-(3 × 1)	Ne	4	[250,251]
	$Pt_3Sn(111)$-p(2 × 2)	Ne	4	[250,252]
	$Cu_3Pt(111)$	^{4}He	1	[194]
	$Pt/TiO_2(110)$	^{4}He	4	[243]
	Cr/Pt(111)	^{4}He	1	[189]
	Ni/Pt(111)	^{4}He	1, 3	[232]
	Pd/Pt(111)	^{4}He	1, 3	[244]
	Si/Pt(111)	^{4}He	1	[253]

Table 9.1 (*continued*)

		Projectile	Quantification method	Reference
	Pt_3Ni	Ne	1	[191]
	Pt_3Co	Ne	1	[191]
	$Pt_{70}Mo_{30}$	^{4}He	1	[227]
	CuPt	^{4}He	1	[207]
	$Cu_{81}Pt_{19}$	Ne	1	[203]
	$Ni_{80}Pt_{20}$	^{4}He	1	[74]
	PdPt	^{4}He	1	[205]
	p-Pt	^{3}He, ^{4}He	3	[5]
Rhenium	p-Re	^{3}He, ^{4}He	3	[5]
Rhodium	$Pt_{25}Rh_{75}(111)$	^{4}He	1	[247,248]
	$Pt_{25}Rh_{75}(110)$	^{4}He	1	[247,248]
	$Pt_{25}Rh_{75}(100)$	^{4}He	1	[247,248]
	$Pt_{50}Rh_{50}(100)$	^{4}He	1	[245]
	$Pt_{50}Rh_{50}(511)$	^{4}He, Ne	4	[246]
	p-Rh	^{3}He, ^{4}He	3	[5]
Ruthenium	Cu/Ru(0001)	^{4}He	1	[196]
	Al/Ru(0001)	^{4}He	1	[177]
Scandium	Sc/W(100)	^{4}He	4	[254]
Selenium	CdSe	Ne	1	[184]
Silicon	Si(100)	^{3}He, ^{4}He	3	[5]
	FeSi(100)	^{4}He	3	[218]
	Si/Pt(111)	^{4}He	1	[253]
	Au/Si(100)	^{4}He	1	[215,216]
	O_2/Si(100)	^{4}He	2	[239]
	$Si_{1-x}Ge_x$	^{4}He	1	[210,211]
	Fe_xSi_y	^{4}He	2	[221]
	FeO_x/SiO_2	^{4}He	2	[223]
	ZrO_2/SiO_2	^{4}He	2	[242]
	MoO_x/SiO_2	^{4}He	4	[116]
Silver	Mn/Ag(001)	^{4}He	1	[224]
	Mn/Ag(100)	^{4}He	1	[225]
	O_2/Ag(111)	^{4}He	4	[238]
	Fe/Ag(100)	Ne	1	[220]
	$Ag_{80}Al_{20}$	^{4}He	1	[74]
Tantalum	$Nb_xTa_{1-x}(110)$	^{4}He	4	[237]
	p-Ta	^{3}He,^{4}He	3	[5]
	O/Ta	^{4}He	4	[136]
Tin	$Pt_3Sn(111)$	Ne	1	[249]
	$Pt_3Sn(110)$-(3×1)	Ne	4	[250,251]
	$Pt_3Sn(111)$-$p(2 \times 2)$	Ne	4	[250,252]
Titanium	CuTi	^{4}He	1	[205]
	Au/TiO_2	^{4}He	1, 2	[213,214]
	$Pt/TiO_2(110)$	^{4}He	4	[243]
Tungsten	W(110), W(211)	^{4}He	4	[255]
	W(211), W(111)	^{4}He, Ne, Ar	1	[101]
	W(100), W(110)	^{4}He, Ne, Ar	1	[101]
	Sc/W(100)	^{4}He	4	[254]
	Zr/W(111)	^{4}He	1	[256]
	Pd/W(111)	^{4}He	1	[233]
	Ni/W(111)	^{4}He	1	[233]
	W/YSZ	^{4}He	2	[241]
	p-W	^{4}He, Ne, Ar	1, 3	[101,5]
Vanadium	V/Pd(111)	^{4}He	1	[150]
	V/YSZ	^{4}He	2	[241]
	VO_x/Al_2O_3	^{4}He	4	[183]

(*continued on next page*)

Table 9.1 (*continued*)

		Projectile	Quantification method	Reference
Yttrium	YSZ	^{4}He, ^{20}Ne	2	[240]
	V/YSZ	^{4}He	2	[241]
	W/YSZ	^{4}He	2	[241]
	CaO/YSZ	^{4}He	2	[187,117]
Zinc	Cu/ZnO(0001)	^{4}He	2	[197]
	CuO/ZnO	^{4}He	1	[73]
Zirconium	Zr/W(111)	^{4}He	1	[256]
	CuZr	^{4}He	1	[204]
	$Ni_{50}Zr_{50}$	Ar	4	[235]
	$BaZrO_3$	^{4}He, Ne	2	[185]
	YSZ	^{4}He, ^{20}Ne	2	[240]
	ZrO_2/SiO_2	^{4}He	2	[242]
	V/YSZ	^{4}He	2	[241]
	W/YSZ	^{4}He	2	[241]
	CaO/YSZ	^{4}He	2	[187,117]
(b) Organics, polymers:				
Ni	C_2H_5I/Ni(100)	^{4}He, Ne	1, 2	[166]
	2-C_3H_7I/Ni(100)	^{4}He, Ne	1, 2	[166]
	2-C_3H_7I/O/Ni(100)	^{4}He, Ne	2, 4	[257]
Cu	Cu/CH_3, $Cu/COOCH_3$	^{4}He	1	[258]
Mo	$H_4PMo_{11}VO_{40}/SiO_2$	^{4}He	2	[259]
F	F_8-thiol/Au(111)	^{3}He	2	[152]
	F_6-thiol/Au(111)	^{3}He	2	[152,117,260]
	PTFE	^{3}He	2	[152,117,260]
	P(MMA–co–F_nMA) $n = 1, 6, 10$	^{3}He	2	[261]
Si	Siloxane/OC_1C_{10}-PPV	^{4}He	2	[262]
	Siloxane/P3HT/SiO_2/Si(100)	^{3}He,^{4}He	2	[263]
(c) Catalysts				
	Pt/Rh/CeO_2/γ-Al_2O_3	^{4}He	1	[264,260]
	Pt/MoO_x/Al_2O_3	^{4}He	3	[265]
	Re/Al_2O_3	^{4}He	4	[201]
	Re/Al_2O_3	^{4}He	4	[266]
	W/Al_2O_3	^{4}He	4	[147]
	Mo/Al_2O_3	^{4}He	4	[267]
	$(VO)_2P_2O_7$	^{4}He	1, 2	[268]
	$(VO)_2P_2O_7$	^{4}He	2	[269]
	$(VO)_2P_2O_7$	^{3}He, ^{4}He	4	[129]
	Cu/ZnO, Cu/ZnO/SiO_2	Ne	1, 2	[270]
	$Pt_xNi_{1-x}SiO_2$	^{4}He	1	[271]
	PdNi/SiO_2	^{4}He	1	[272]
	Mo/TiO_2	^{4}He	4	[148]
	Rh/TiO_2	^{4}He	4	[273]
	W/TiO_2	^{4}He	2, 4	[274]
	WO_3/ZrO_2	^{4}He	2	[275]
	$Mo_xV_yTe_z$	^{4}He, Ne	3	[276]
(d) Others				
Nanoclusters	$Pd_{80}Pt_{20}$, $Pd_{20}Pt_{80}/Al_2O_3$	Ne	1	[277]
	$Pd_{17}Pt_{83}$, $Pd_{65}Pt_{35}$/a-C	^{4}He	1	[278,279]
	$(Ni_{50}Ag_{50})_n$	^{4}He	3	[280]
	$(Ni_{50}Au_{50})_n$	^{4}He	3	[280]
Liquids	NaCl(H_2O)/Ag	^{4}He	2, 3	[281]
Artifacts	Medieval Venetian coin	^{4}He, Ne	1	[282]

Table 9.1 (*continued*)

	Projectile	Quantification method	Reference
(CuAgAu)			

(a)–(d) treat elements, organics/polymers, catalysts and others. The surface composition was quantified by using references (method 1 for pure elements and method 2 for compounds), sensitivity factors (method 3) or by other ways (method 4). See also Section 9.1.
Explanation notations: a- — amorphous; p- — polycrystalline; YSZ — yttria stabilized zirconia (Y_2O_3 in ZrO_2); F_6-thiol — 1H,1H,2H,2H-Perfluorooctanethiol; F_8-thiol — 1H,1H,2H,2H-Perfluorodecanethiol; PTFE — poly(tetrafluoroethylene); P(MMA-co-F_nMA) — Partially fluorinated polymethacrylates, $n = 1, 6, 10$; OC_1C_{10}-PPV — poly-dialkoxy phenylenevinylene; PDMS — poly-dimethyl-siloxane; P3HT — poly(3-hexylthiophene).

thus preferred and more accurate to use reference values that have been determined in the same instrument under the same scattering conditions.

In Section 4.2 procedures are described how the absence of matrix effects can be checked. For binary and multi-component systems where Vegards law also holds, the validity of Eq. (4.8) or (4.10) is easily verified (see the example in Fig. 4.10). Since matrix effects are rare in LEIS, a non-constant behavior in plots as in Fig. 4.9 could be an indication of a matrix effect. However, it is generally due to the presence of surface impurities such as H, Li, B and C that are impossible or difficult to detect with LEIS.

In the absence of matrix effects the sum of the surface coverages of the various elements or constituents should add up to 100%. Even for ternary systems with elements that are chemically as different as W, Br and O, it has been verified that within experimental error (3%) the surface coverages added up to 100% [145]. The LEIS signals are, therefore, generally normalized to 100%. Since in-situ calibration is not always easy, relative sensitivities are often used for the analysis.

In cases where matrix effects have been observed, the deviation from the 100% coverage can be as small as a few %. In exceptional cases, however, they can be as large as a factor of 1000, which makes them very easy to recognize. In Section 9.2 remedies for such situations are described.

For the quantification of the surface compositions of supported catalysts a different normalization is popular. Hercules, Houalla and coworkers have shown that for different loadings of oxides on oxidic supports the O signal is almost independent of the loading [147,148]. The O signal is thus taken for normalization. A deviation from this independence of the O signal was reported by Peeters et al. [149] for overlayers of molybdenum oxide on γ-Al_2O_3 (an ammoxidation catalyst). By accurate determination of the O signal they could distinguish the formation of $Al_2(MoO_4)_3$ from separate Mo-oxide and Al_2O_3 phases.

A general disadvantage of normalization on the O signal is, of course, that one neglects possible differences in the presence of species such as H that are undetectable with LEIS, but can effectively shield the underlying atoms. When such species are preferentially adsorbed on certain elements, this will affect the surface composition but will go unnoticed. In addition, one would not detect deviations from Vegard's law (see Section 9.1.2).

In Table 9.1 the methods that are used in quantification (Eqs. (4.5)–(4.10)) are divided into 4 categories:

1. pure elements as references (Section 9.1.1),
2. compounds (oxides, etc.) as references (Section 9.1.2),
3. sensitivity factors (Section 9.1.3) and
4. other quantification procedures (Section 9.1.4).

9.1.1. Pure elements as references

In half of the cases pure elements are used as references to determine the surface composition. These references are often single crystalline surfaces with well-defined atomic surface densities (N_i^{ref}).

In cases where polycrystalline samples are used as reference, N_i^{ref} is sometimes estimated by assuming that the dominant surface termination is the close-packed surface plane (because it minimizes the surface free energy). Alternatively, it is approximated as $(\rho_i^*)^{2/3}$ with $\rho_i^* = \rho_i \cdot N_{\mathrm{Av}}/M_i$, where N_{Av} is Avogadro's number ($6.02 \cdot 10^{23}$ atoms/mol), ρ_i the mass density and M_i the molar mass of element i. Although the error in the 2nd approach can be about 20%, it is simpler and therefore often used.

9.1.2. Compounds (oxides, etc.) as references

In 25% of the cases in Table 9.1 compounds rather than the pure elements have been used, as references. An obvious reason for doing so is that a pure element such as O is a gas at room temperature.

In principle, the sensitivity of such an element can be (and has been) determined using well defined chemisorbed overlayers on single crystals [150,151], single crystals of stable compounds [152] or crushed glasses to minimize the influence of surface segregation and contamination [153]. For instance, the elemental sensitivity of fluorine was determined in this way using a LiF(001) crystal. This sensitivity factor was then used to determine the surface concentration of F in fluorinated acrylates and polytetrafluoroethylene ("Teflon") [152].

For materials such as mixed oxides, the constituting oxides are generally used as references. In analogy to Eqs. (4.8)–(4.10) for the elements, one uses these equations for the constituting compounds. Especially for mixed oxides and oxidic overlayers this works very well and is now common practice. Thus in a study of the growth of NiO on MgO, Xu et al. [154] used the pure oxides as reference compounds. From the ratio of the sensitivity factors of Ni and Mg in these oxides, the surface fractions of the oxides were determined. In principle, it would also have been possible to use the sensitivities of the elements Ni, Mg and O.

For multicomponent samples the signal for one component can be plotted as a function of the sum of the other components. This is analogous to Fig. 4.10 for a binary alloy. As expected from. Eq. (4.10), a linear relation is generally obtained. This

Table 9.2
Claimed matrix effects

	Element	Projectile	Reference
Oscillatory			
	In, InAs	^{4}He	[7]
	In, Ga and compounds	^{4}He	[27]
	Ga	^{3}He,^{4}He ^{20}Ne, ^{22}Ne	[28]
	Pb gas and Pb solid	^{4}He	[26]
	Pb, $PbCl_2$, $Pb(NO_3)_2$	^{4}He	[25]
	Bi, Bi_2O_3	^{4}He	[25]
	Carbidic and graphitic C/p-Re	^{4}He	[66,127]
	Au	Ne	[22]
Low work function			
	O/Al(100)	^{4}He	[167]
	O/W(100)	^{4}He	[283]
	Be/W(100)	^{4}He	[283]
	Na/Cu(110)	^{4}He	[284]
	K/Co(0001)	^{4}He	[161]
	K/Cu(110)	^{4}He	[284]
	K/V_6O_{13}	^{4}He	[162,163]
	Cs/Cu(110)	^{4}He	[284]
	Cs/Ni(110)	Ne	[285]
	Ba/W(110), Ba/Re(0001)	^{4}He, Ne, Ar	[69]
	Ba/p-W	^{4}He, Ne, Ar	[158,286]
	Ce/Rh(111)	^{4}He, Ne	[157]
	CeO_x/Pd(111)	^{4}He	[164]
Miscellaneous			
	$YBa_2Cu_{3-y}Al_yO_x$	Ar	[287]
	NiAl(110)	^{3}He, ^{4}He	[74]
	Ti–TiO_2(110)	^{4}He	[288]

See Section 9.2 for a detailed description.

shows that in these cases there are no matrix effects, and also Vegard's law is obeyed.

For many practical applications, such as wetting or dewetting of one oxide on another, it is also much easier to use pure oxides as references. If, for instance, one of the oxides is alumina (Al_2O_3), it would also be possible to take the elemental sensitivities of Al and O as reference. The observed Al/O ratio will depend on the crystallographic plane that is exposed. For the most stable surface (such as generally present for powders) the outer surface will be oxygen terminated and only part of the Al atoms in the second atomic layer are freely accessible for LEIS, the analysis will not reflect the bulk composition. It will thus give [74] an Al/O ratio that is significantly smaller than 2/3. The observed Al/O ratio is independent of the incident energy, thus confirming that the ratio results from partial shielding and not from a matrix effect (see Section 4.2). By using alumina as reference, one automatically corrects for the partial shielding of the Al by O.

9.1.3. Sensitivity factors

Compilations of elemental sensitivity factors have been reported by various authors [155,5,6]. For compounds such compilations do not exist and one is referred to the individual papers for such values. Even if sensitivity factors do exist, their use remains limited, since LEIS equipment is not yet standardized.

A round robin among groups suggests that, for a given primary energy, the factors are the same within a factor of 2 [6]. For accurate calibrations the sensitivity factors should be determined in the same or similar set-up as the actual LEIS analysis. This explains why in only 10% of the cases listed in Table 9.1 literature values were used for the sensitivity factors.

9.1.4. Other quantification procedures

A reliable determination of the surface composition should be independent of the type and energy of the incident ions (see also Section 4.2). Jacobs et al. [74] demonstrated for several alloys and oxides that this is indeed the case, but an exception (NiAl alloy; see Section 9.2) was also found.

9.2. Known cases of matrix effects

A compilation of the known cases of matrix effects is given in Table 9.2. The table is restricted to matrix effects that have been observed for experimental conditions that fall within the limits of this paper given in the introduction. Thus only non-grazing ($\geq$30° with the surface for both the in- and outgoing ions) scattering of noble gas ions having energies between 0.5 and 10 keV are considered. The observed matrix effects have been categorized in:

1. oscillatory (Section 9.2.1),
2. low work function (Section 9.2.2) and
3. miscellaneous (Section 9.2.3).

9.2.1. Oscillatory

In this category, all but one case (He–C) exhibit an oscillatory primary energy dependence of the LEIS signal. As described in Section 3.1.3(c), these oscillations result from quasiresonant quantum mechanical oscillations in the transition of bound electrons in the target to the projectile (B–RN). In the classification of Section 3.2 these cases all fall in class II. Table 3.1 gives an overview of the ion–atom combinations that are involved. In some cases (He–Pb, Bi; energies between 200 and 1000 eV) the scattered ion signal changes by as much as a factor of 5 over a small energy range. Erickson, Rusch and Smith and coworkers have shown in a number of studies [7,27, 25] that the precise shapes and intensities of these oscillations depend on the chemical environment. This was particularly true for He^+ ion scattering by Ga, In, Pb and Bi. Calibration against pure elements will then lead to significant errors.

Remedy

A simple remedy to avoid almost all of these matrix effects is to use Ne^+ instead of He^+ ions for the analysis. As can be seen in Table 3.1, only for Ga has oscillatory behavior been found for both ions, although the effect is not very pronounced for Ne^+. Since the oscillations become less pronounced for the higher energies, one can also (strongly) reduce the effect by performing LEIS at energies above 3 keV.

He^+–C

For He^+ scattering by C in organic molecules no or very weak matrix effects are present. Mikhailov et al. [66] found, however, a huge matrix effect for C on a polycrystalline Re target. When the carbon transformed from carbidic to graphitic carbon, the LEIS signal dropped by more than one order of magnitude (see also Section 4.2.8). The characteristic velocity increased from $0.47 \cdot 10^6$ to $1.1 \cdot 10^6$ m/s. This makes it difficult to detect graphitic carbon at incident energies below 2 keV.

This signal reduction was explained [127] in terms of a special, strongly damped, quasiresonant process in which electrons are very efficiently transferred from the sp^2 band in graphite to the 1s orbital in helium. Because of the strong damping, no oscillations are observed in the energy dependence.

Remedy

The matrix effect for graphitic carbon is so strong that the use of $^3He^+$ ions and higher incident energies improves the situation only marginally. It is, therefore necessary to measure the energy dependence of the carbon signal and determine the characteristic velocity and the ion fraction (Section 4.2.4). Here, a detailed knowledge of the properties of the analyzer/detector system is essential (Section 5).

9.2.2. Low work function (Φ)

For surfaces having work functions (Φ) below 3–4 eV neutralization of noble gas ions is also possible by resonant electron transfer to the first excited level of the ion (see Section 4.1.2(b)). This mechanism is similar to neutralization for alkali ions [156], where the energy of the ground state meets the resonant condition. Especially for very low work functions and low incident ion energies this process will seriously decrease the scattered ion intensities. Reductions by more than an order of magnitude have been observed [69,157].

In Table 9.2 there is a special section for matrix effects that are believed to be due to a low work function. Since the work function is strongly influenced by the precise structure and ionic charges of the atoms in the surface region, the extra neutralization to an excited projectile level is a clear matrix effect. Cortenraad et al. made a detailed study of this effect [69] and showed how LEIS can be used even for a quantitative analysis of the surface composition of activated thermionic cathodes with a work function of less than 2 eV [158–160].

Typically, low work functions are connected to surfaces containing alkali or earth alkali and some transition metals. For noble gas ion scattering at incident energies of a few keV it has been found that resonant neutralization due to low Φ is governed by the macroscopic work function and not by the local potential of the individual atom [69]. Thus it does not only lower the LEIS signal of that atom but also the signals for the other atoms in its vicinity. The signal reduction can be so strong that the LEIS signals are below the detection limit. It will thus seem that there is no target to scatter from. This clearly poses a challenge to LEIS for such surfaces.

There is a clear threshold in the work function below which the low Φ induced neutralization starts. Cortenraad et al. showed that the onsets are somewhat different for He, Ne and Ar ions, which correlates nicely with the differences in the binding energies of their first excited states [69]. The value of the onset also increases when the incident energy of the ion is lowered. Thus the influence of a low work function becomes more pronounced at lower ion energies. For Ne^+ ion scattering from a Ba covered W(110) surface with a work function of 2.8 eV, the resonant neutralization was very small at 5 keV, while it gave a significant signal decrease at lower energies. The increase in neutralization with decreasing energy is due to the increase of the freezing distance (where the scattered ion is so far from the surface that the charge exchange rate becomes negligible) for lower velocities. The absolute increase in the characteristic velocity with decreasing work function is identical for Ne^+ and Ar^+ ions, which is consistent with the additional neutralization mechanisms for noble gas ions at low work functions [69].

In many of the low Φ cases of Table 9.2 the LEIS signals were monitored as a function of deposited alkali, earth alkali or transition metal. When passing a certain surface coverage, all signals started to drop, even the signal of the element that was deposited (see for example Fig. 4.7 for Ba on W). Precisely at this coverage the work function dropped below the low Φ neutralization onset. This behavior is typical for low Φ matrix effects. Vaari et al. [161] observed this for the coadsorption of CO and K on Co(0001). In the studies of Vennik et al. [162, 163] on K doped V_6O_{13}(001) it was found that segregation of K first leads to an increase in the K signal, but decreases again when the K coverage is further increased.

Napetschnig et al. [157] observed a strong low Φ induced matrix effect when studying the growth of Ce on Rh(111). Since bulk Ce has a work function of 2.9 eV, such a matrix effect is to be expected at the low incident ion energy (1 keV) used in

this study. The LEIS signals depended sensitively on the Ce coverage.

Alexandrou and Nix [164] also reported a signal reduction in LEIS studies of the growth of ceria on Pd(111). Although its origin is less clear here, it may well be due to a low Φ effect. The effects observed by Andersen et al. [165] for scattering by Yb on Ni(100) may well have a similar origin.

Gleason and Zaera [166] have also held the work function responsible for a small matrix effect in the scattering of He^+ by an adsorbed layer of 2-propyliodide on oxygen covered Ni(100). They did not find a matrix effect for adsorbed layers of H_2, O_2 and 2-propyliodide on Ni(100).

Kravchuk et al. [167] claimed a low Φ effect in a LEIS study of the oxidation of Al(100). During oxidation the work function decreased from 4.4 to 3.4 eV. These Φ values are still rather high for a pronounced effect, although it may be due to the very low incident ion energies (350 and 1000 eV) used in their study. However, the observed effect may also be due to the use of sensitivity factors for Al and O that were obtained in a different set-up. It seems that when they had used a somewhat higher sensitivity ratio for Al/O, the effect would have disappeared.

Remedy for low Φ effects

Quantification of the LEIS signals for low Φ materials is complicated by the fact that there is no longer a single neutralization mechanism that dominates. Therefore, the characteristic velocity method (Section 4, Figs. 4.1 and 4.5) does not work. Cortenraad et al. [159] have illustrated with Ne^+ ion scattering from Ba on W(110) how this problem can be solved. By comparing the energy dependence of the Ba LEIS signal of the sample with that of a sample with a very low Ba coverage (having a work function well above the threshold of resonant neutralization), the two neutralization mechanisms can be separated. For resonant neutralization to an excited state theory predicts [168,169] for the ion fraction:

$$P^+_{RN} = \exp\{-C \cdot |\varepsilon_a - \varepsilon_F|/(\gamma \cdot v)\}. \quad (9.1)$$

Here C is a constant, ε_a the energy of the first excited state at the freezing distance and ε_F the Fermi level of the metal. The decay constant γ describes the decreasing width of the first excited level with increasing distance between the ion and the surface. When the ion fraction is first corrected for the velocity dependence of ε_a, it was found that the increase in the characteristic velocity by the resonant neutralization is then a constant (independent of the incident ion energy) for a given work function. Also, the determined surface concentrations are independent of the incident energy and the same for Ne^+ and Ar^+ scattering.

As shown above, the influence of a low work function on the LEIS signals is reasonably well understood. By using higher incident ion energies (3–5 keV) the influence of a low Φ is reduced significantly. If this is not enough, one can fully correct for the influence of low Φ induced neutralization by using the procedure as outlined by Cortenraad et al. [159].

This approach is, however, much more tedious and requires a good knowledge of the properties of the analyzer/detector system (see also Section 5).

9.2.3. Miscellaneous

While the matrix effects described above have a clear origin, a number of cases have been reported that are neither due to oscillatory effects nor to a low work function. Most of these cases date back to the early days of LEIS when the presence and important consequences of surface impurities such as H were not always realized. These cases and those that do not fall within the boundary conditions set for this review (see Section 1) have therefore been omitted in Table 9.2.

There is at least one clear exception. In a study of Al and Ni in various oxides and alloys the energy dependence of the Al and Ni was found to be independent of the chemical environment of these atoms. The results for the NiAl(110) alloy, however, showed that the calibrated (normalized against that of the pure element) Ni signal does not depend on the primary energy, while the calibrated Al signal decreases 25% with increasing incident energy from 1 to 3.5 keV [74]. Additional surface cleaning did not change this effect. Neither Al nor Ni falls in the oscillatory category. A low work function is also unlikely. Moreover, as discussed above, this should have affected both the Al and Ni atoms. The origin of this discrepancy is not understood at present. Perhaps it is due to an unusual influence of the band structure on the Auger processes involved.

10. Summary

Low energy ion scattering (LEIS) is a unique tool for surface composition analysis. It is nowadays applied to a great variety of materials, ranging from semiconductors to ceramics, polymers, highly dispersed catalysts and biomaterials. Many of these applications require quantitative analysis. To obtain this information in an absolute measurement would require the following information:

- Scattering cross sections
- Ion fractions
- Roughness factor R
- Experimental factors (ξ)
- Ion current (or ion fluence).

Although it is in principle possible to obtain these quantities, it would be demanding to do so. Especially the determination of absolute ion fractions is far from being trivial. In LEIS experiments the surface composition is, therefore, generally obtained in a relative measurement. This can be done by comparison of the LEIS signals of the elements in the sample of interest with those of reference samples. In this way most of the factors mentioned above cancel out, but is based on the following assumptions:

- neutralization is not subject to matrix effects, and
- surface roughness is similar for reference samples and the sample of interest.

When setting up the experiment one can choose the optimum type of ion, ion energy and angles of incidence and scattering. Fortunately it turns out that matrix effects are rare (Section 9) and the surface roughness (Section 8) is only of very minor

importance in LEIS (Section 9). This permits a quantitative surface composition analysis in almost any case — even if the neutralization process is not yet fully understood.

Nevertheless, it remains an important task to understand the origin of matrix effects. There are two main origins for these effects:

- An oscillatory dependence of the ion fraction as a function of energy (velocity) due to quasiresonant neutralization of the projectile by a bound target electron. This only occurs for a few well-known ion–atom combinations.
- A low work function of the target, enabling a resonant electron transfer to the first excited level of the ion.

Based on the physical concepts given in Sections 3 and 4, Section 9 contains a survey of the more recent literature of quantitative LEIS (1994–2006). Section 9 also describes procedures how to recognize matrix effects and how to obtain a quantitative analysis for such samples. This may require the use of another type of ion or other (generally higher) primary energies. It is discussed how experimental conditions can be chosen to minimize the influence of matrix effects and how to correct for them, if necessary.

Obituary

This report is dedicated to the memory of Arnoud Denier van der Gon, a dear friend and cherished colleague. Arnoud started his scientific career under the supervision of Friso van der Veen at the FOM-Institute AMOLF in Amsterdam. The phenomenon of surface melting had just been discovered and Arnoud conducted some very original MEIS experiments for his Ph.D. He received his doctor's degree from the University of Leiden in 1990. During his two years at the IBM Thomas J. Watson Research Center in Yorktown Heights, USA, he worked with Ruud Tromp, studying the growth of ultra-thin metal and semiconductor overlayers using low-energy electron microscopy (LEEM). In 1992 Arnoud joined the Surface and Interface Science group of Hidde Brongersma at the Eindhoven University of Technology as an assistant professor. He was responsible for the research with SPA-LEED and initiated a wide variety of low-energy ion scattering (LEIS) applications.

In his scientific career he performed and contributed to internationally highly renowned work, like the order-disorder transition at the Ge(111) surface and the discovery of the existence of a critical island size in epitaxial growth. Amongst his numerous studies he also investigated thermionic dispenser cathodes under operation using in-situ LEIS and thereby achieved a detailed microscopic understanding of the functionality of these highly complex devices. Arnoud also was a gifted experimentalist who very actively developed equipment, like a high-pressure LEIS instrument to study in-situ chemical reactions at surfaces. He was planning to form his own group to use techniques such as LEIS for biological and molecular applications when he was confronted with the fact that he was very ill.

Arnoud was a member of the board of the Dutch Vacuum Society (NEVAC) and a member of the international committee of the International Conferences on Atomic Collisions in Solids (ICACS). His lucid and enthusiastic talks at conferences and summer schools made him a popular speaker. It was Arnoud who convinced us that we should summarize our present knowledge about quantitative surface composition analysis using LEIS in a review paper. He was very active in setting up the outline and the scope of the review and it was his enthusiasm and encouragement that convinced us to do so despite a chronic lack of time.

Arnoud died on August 10, 2003, at the age of 39. We miss his passion, his strong motivation for excellence in science and especially his warm friendship.

Acknowledgements

We express our gratitude to A. Arnau, P. Echenique, R.C. Monreal, E. Taglauer, and P. Zeppenfeld for many inspiring discussions.

References

[1] H. Niehus, W. Heiland, E. Taglauer, Surf. Sci. Rep. 17 (1993) 213.
[2] R. Bastasz, J. Alloys Compd. 342 (2002) 427.
[3] J.F. Ziegler, J.P. Biersack, U. Littmark, The Stopping and Range of Ions in Solids, vol. 1, Pergamon, New York, 1985.
[4] H. Niehus, R. Spitzl, Surf. Interface Anal. 17 (1991) 287.
[5] S.N. Mikhailov, R.J.M. Elfrink, J.-P. Jacobs, L.C.A. van den Oetelaar, P.J. Scanlon, H.H. Brongersma, Nucl. Instrum. Methods Phys. Res. Sect. B 93 (1994) 149.
[6] H.H. Brongersma, et al., Nucl. Instrum. Methods Phys. Res. Sect. B 142 (1998) 377.
[7] R.L. Erickson, D.P. Smith, Phys. Rev. Lett. 34 (1975) 297.
[8] S.R. Kasi, H. Kang, C.S. Sass, J.W. Rabalais, Surf. Sci. Rep. 10 (1989) 1.
[9] A. Arnau, Nucl. Instrum. Methods Phys. Res. Sect. B 93 (1994) 195.
[10] F. Aumayr, AIP Conf. Proc. 360 (1995) 631.
[11] H. Winter, J. Phys.: Condens. Matter 8 (1996) 10183.
[12] W. More, J. Merino, R. Monreal, P. Pou, F. Flores, Phys. Rev. B 58 (1998) 7385.
[13] U. Fano, W. Lichten, Phys. Rev. Lett. 14 (1965) 627.
[14] M. Barat, W. Lichten, Phys. Rev. A 6 (1972) 211.
[15] S. Tsuneyuki, M. Tsukada, Phys. Rev. B 34 (1986) 5758.
[16] J.W. Gadzuk, Surf. Sci. 6 (1967) 133.
[17] J.W. Gadzuk, Surf. Sci. 6 (1967) 159.
[18] S.S. Shekhter, J. Exp. Theor. Phys. 7 (1937) 750.
[19] A. Cobas, W.E. Lamb Jr., Phys. Rev. 65 (1944) 327.
[20] H.D. Hagstrum, Phys. Rev. 96 (1954) 336.
[21] E.A. Garcia, E.C. Goldberg, M.C.G. Passegi, Surf. Sci. 325 (1995) 311.
[22] H.H. Brongersma, T.M. Buck, Surf. Sci. 53 (1975) 649.
[23] T.W. Rusch, R.L. Erickson, J. Vac. Sci. Technol. 13 (1976) 374.

[24] D. Christensen, V. Mosotti, T. Rusch, R. Erickson, Chem. Phys. Lett. 44 (1976) 8.
[25] D.L. Christensen, V.G. Mossotti, T.W. Rusch, R.L. Erickson, Nucl. Instrum. Methods 149 (1978) 587.
[26] A. Zartner, E. Taglauer, W. Heiland, Phys. Rev. Lett. 40 (1978) 1259.
[27] T.W. Rusch, R.L. Erickson, in: N.H. Tolk, J.C. Tully, W. Heiland, C.W. White (Eds.), Inelastic Ion–Surface Collisions, Academic Press, New York, 1977, p. 73.
[28] H.F. Helbig, K.J. Orvek, Nucl. Instrum. Methods 170 (1980) 505.
[29] P.M. Echenique, F. Flores, R.H. Ritchie, in: H. Ehrenreich (Ed.), Solid State Physics: Advances in Research and Applications, vol. 43, Academic Press, New York, 1990, p. 229.
[30] N. Lorente, R. Monreal, Phys. Rev. B 52 (1995) 4760.
[31] W. More, J. Merino, R. Monreal, P. Pou, F. Flores, Phys. Rev. B 58 (1998) 7385.
[32] N. Lorente, M.A. Cazalilla, J.-P. Gauyacq, D. Teillet-Billy, P.M. Echenique, Surf. Sci. 411 (1998) L888.
[33] M.A. Cazalilla, N. Lorente, R. Díez-Muiño, J.-P. Gauyacq, D. Teillet-Billy, P.M. Echenique, Phys. Rev. B 58 (1998) 13991.
[34] D. Valdés, E.C. Goldberg, J.M. Blanco, R.C. Monreal, Phys. Rev. B 71 (2005) 245417.
[35] S.B. Luitjens, A.J. Algra, E.P.T.M. Suurmeijer, A.L. Boers, Surf. Sci. 99 (1980) 652.
[36] R. Souda, M. Aono, C. Oshima, S. Otani, Y. Ishizawa, Surf. Sci. 150 (1985) L59.
[37] T.M. Thomas, H. Neumann, A.W. Czanderna, J.R. Pitts, Surf. Sci. 175 (1986) L737.
[38] R. Souda, K. Yamamoto, W. Hayami, T. Aizawa, Y. Ishizawa, Phys. Rev. B 51 (1995) 4463.
[39] M. Aono, R. Souda, Nucl. Instrum. Methods Phys. Res. Sect. B 27 (1987) 55.
[40] R. Souda, T. Aizawa, C. Oshima, S. Otani, Y. Ishizawa, Phys. Rev. B 40 (1989) 4119.
[41] E. Garcia, P.G. Bolcatto, E.C. Goldberg, Phys. Rev. B 52 (1995) 16924.
[42] E.C. Goldberg, R. Monreal, F. Flores, H.H. Brongersma, P. Bauer, Surf. Sci. 440 (1999) L875.
[43] M. Draxler, R. Gruber, H.H. Brongersma, P. Bauer, Phys. Rev. Lett. 89 (2002) 263201.
[44] W. Heiland, E. Taglauer, in: N.H. Tolk, W. Heiland, C.W. White (Eds.), Inelastic Ion–Surface Collisions, Academic Press, New York, 1977, p. 27.
[45] T. Li, R.J. Mac Donald, Phys. Rev. B 51 (1995) 17876.
[46] T.M. Buck, W.E. Wallace, R.A. Baragiola, G.H. Wheatley, J.B. Rothman, R.J. Gorte, J.G. Tittensor, Phys. Rev. B 48 (1993) 774.
[47] P. Kürpick, Phys. Rev. B 56 (1997) 6446.
[48] R. Souda, T. Aizawa, C. Oshima, Y. Ishizawa, Nucl. Instrum. Methods Phys. Res. Sect. B 45 (1990) 364.
[49] M. Draxler, J. Valdés, R. Beikler, P. Bauer, Nucl. Instrum. Methods Phys. Res. Sect. B 230 (2005) 290.
[50] D.J. Godfrey, D.P. Woodruff, Surf. Sci. 105 (1981) 438.
[51] D.J. Godfrey, D.P. Woodruff, Surf. Sci. 105 (1981) 459.
[52] G. Verbist, J.T. Devreese, H.H. Brongersma, Surf. Sci. 233 (1990) 323.
[53] G. Verbist, H.H. Brongersma, J.T. Devreese, Nucl. Instrum. Methods Phys. Res. Sect. B 64 (1992) 572.
[54] G. Verbist, C.A. Severijns, H.H. Brongersma, J.T. Devreese, Nucl. Instrum. Methods Phys. Res. Sect. B 73 (1993) 517.
[55] R. Souda, M. Aono, C. Oshima, S. Otani, Y. Ishizawa, Nucl. Instrum. Methods Phys. Res. Sect. B 15 (1986) 138.
[56] N. Rosen, C. Zener, Phys. Rev. 40 (1932) 502.
[57] N.F. Mott, H.W. Massey, The Theory of Atomic Collisions, Oxford Univ. Press, Oxford, 1975, p. 351.
[58] E.W. McDaniel, J.B.A. Mitchell, M.E. Rudd, Atomic Collisions, Wiley, New York, 1993, p. 381.
[59] H. Helbig, P. Adelman, J. Vac. Sci. Technol. 14 (1977) 488.
[60] W. Eckstein, H. Verbeek, Data on light ion reflection, Max-Planck-Institut für Plasmaphysik, Internal Report IPP 9/32, 1979.
[61] W. Eckstein, in: E. Taglauer, W. Heiland (Eds.), Inelastic Particle–Surface Collisions, vol. 17, Springer, Berlin, 1981, p. 157.
[62] R.J. MacDonald, D.J. O'Connor, B.V. King, Y. Shen, G. Xu, Nucl. Instrum. Methods Phys. Res. Sect. B 78 (1993) 56.
[63] W. Eckstein, H. Verbeek, R.S. Bhattacharya, Surf. Sci. 99 (1980) 356.
[64] H. Winter, Prog. Surf. Sci. 63 (2000) 177.
[65] M. Draxler, R. Beikler, E. Taglauer, P. Zeppenfeld, P. Bauer, Phys. Status Solidi B 241 (2004) 2380.
[66] S.N. Mikhailov, R.J.M. Elfrink, J.-P. Jacobs, L.C.A. van den Oetelaar, P.J. Scanlon, H.H. Brongersma, Nucl. Instrum. Methods Phys. Res. Sect. B 93 (1994) 210.
[67] H.H. Brongersma, W.J. Schouten, Acta Electron. 18 (1975) 47.
[68] R. Souda, M. Aono, Nucl. Instrum. Methods Phys. Res. Sect. B 15 (1986) 114.
[69] R. Cortenraad, A.W. Denier van der Gon, H.H. Brongersma, S.N. Ermolov, V.G. Glebovsky, Phys. Rev. B 65 (2002) 195414.
[70] R.J. McDonald, D.J. O'Connor, J. Wilson, Y.G. Shen, Nucl. Instrum. Methods Phys. Res. Sect. B 33 (1988) 446.
[71] A. Tolstogouzov, S. Daolio, C. Pagura, C.L. Greenwood, Surf. Sci. 466 (2000) 127.
[72] E. Taglauer, in: A.W. Czanderna, D.M. Hercules (Eds.), Ion Spectroscopies for Surface Analysis, vol. 2, Plenum Press, New York, 1991, p. 363.
[73] L.C.A. van den Oetelaar, H.E. van Benthem, J.H.J.M. Helwegen, P.J.A. Stapel, H.H. Brongersma, Surf. Interface Anal. 26 (1998) 537.
[74] J.P. Jacobs, S. Reijme, R.J.M. Elfrink, S.N. Mikhailov, M. Wuttig, H.H. Brongersma, J. Vac. Sci. Technol. A 12 (1994) 2308.
[75] R.C. McCune, J. Vac. Sci. Technol. 18 (1981) 700.
[76] G.C. van Leerdam, H.H. Brongersma, Surf. Sci. 254 (1991) 153.
[77] P.A.J. Ackermans, G.C.R. Krutzen, H.H. Brongersma, Nucl. Instrum. Methods Phys. Res. Sect. B 45 (1990) 384.
[78] H. Hutter, in: H. Bubert, H. Jenett (Eds.), Surface and Thin Film Analysis, Wiley-VCH, Weinheim, 2002, p. 106.
[79] J.W. Rabalais, in: D.M. Desiderio, N.M.M. Nibbering (Eds.), Principles and Applications of Ion Scattering Spectrometry, John Wiley & Sons, Inc., New York, 2003.
[80] Y.S. Chen, G.L. Miller, D.A.H. Robinson, G.H. Wheatley, T.M. Buck, Surf. Sci. 62 (1977) 133.
[81] D. Rathmann, N. Exeler, B. Willerding, J. Phys. E 18 (1985) 17.
[82] H.H. Brongersma, N. Hazewindus, J.M. van Nieuwland, A.M.M. Otten, A.J. Smets, Rev. Sci. Instrum. 49 (1978) 707.
[83] E. Gisler, E.B. Bas, Vacuum 36 (1986) 715.
[84] G.J.A. Hellings, H. Ottevanger, S.W. Boelens, C.L.C.M. Knibbler, H.H. Brongersma, Surf. Sci. 162 (1985) 913.
[85] R. Cortenraad, A.W. Denier van der Gon, H.H. Brongersma, Surf. Interface Anal. 29 (2000) 524.
[86] P.J. Hicks, S. Daviel, B. Wallbank, J. Corner, J. Phys. E 13 (1980) 713.
[87] C.L.C.M. Knibbler, G.J.A. Hellings, H.J. Maaskamp, H. Ottevanger, H.H. Brongersma, Rev. Sci. Instrum. 58 (1987) 125.
[88] R.S. Gao, P.S. Gibner, J.H. Newman, K.A. Smith, R.F. Stebbings, Rev. Sci. Instrum. 55 (1984) 1756.
[89] M. Barat, J.C. Brenot, J.A. Fayeton, Y.J. Picard, Rev. Sci. Instrum. 71 (2000) 2050.
[90] J.B. Theeten, H.H. Brongersma, Rev. Phys. Appl. 11 (1976) 57 (in French).
[91] M. de Ridder, H.H. Brongersma, 2006. Private communication.
[92] W. Heiland, E. Taglauer, Nucl. Instrum. Methods 132 (1976) 535.
[93] B. Poelsema, L.K. Verhey, A.L. Boers, Surf. Sci. 64 (1977) 537.
[94] H. Nakamatsu, A. Sudo, S. Kawai, Surf. Sci. 223 (1989) 193.
[95] W. Hetterich, C. Höfner, W. Heiland, Surf. Sci. 251–252 (1991) 731.
[96] D.P. Smith, Surf. Sci. 25 (1971) 171.
[97] H.H. Brongersma, P.M. Mul, Chem. Phys. Lett. 19 (1973) 217.
[98] H.H. Brongersma, P.M. Mul, Chem. Phys. Lett. 14 (1972) 380.
[99] B. Moest, P.T. Wouda, A.W. Denier van der Gon, M.C. Langelaar, B.E. Nieuwenhuys, D.O. Boerma, Surf. Sci. 473 (2001) 159.
[100] R.H. Bergmans, M. van de Grift, A.W. Denier van der Gon, H.H. Brongersma, Surf. Sci. 345 (1996) 303.
[101] R. Cortenraad, S.N. Ermolov, B. Moest, A.W. Denier van der Gon, V.G. Glebovsky, H.H. Brongersma, Nucl. Instrum. Methods Phys. Res. Sect. B 174 (2001) 173.

[102] B. Garrison, Surf. Sci. 87 (1979) 683.
[103] T.M. Buck, Y.S. Chen, G.H. Wheatly, W.F. Van der Weg, Surf. Sci. 47 (1975) 244.
[104] W.F. Van der Weg, T.M. Buck, G.M. Wheatley, Nucl. Instrum. Methods 132 (1976) 571.
[105] G.B. Hoflund, W.S. Epling, Thin Solid Films 307 (1997) 126.
[106] J.T. Wholan, G.B. Hoflund, Appl. Surf. Sci. 125 (1998) 251.
[107] W.L. Baun, Phys. Rev. A 17 (1978) 849.
[108] R. Beikler, E. Taglauer, Nucl. Instrum. Methods Phys. Res. Sect. B 182 (2001) 180.
[109] E. Taglauer, A. Kohl, W. Eckstein, R. Beikler, J. Mol. Catal. A 162 (2000) 97.
[110] M. Sasaki, P.J. Scanlon, S. Ermolov, H.H. Brongersma, Nucl. Instrum. Methods Phys. Res. Sect. B 190 (2002) 127.
[111] R. Souda, K. Yamamoto, W. Hayami, T. Aizawa, Y. Ishizawa, Surf. Sci. 363 (1996) 139.
[112] M. de Ridder, A. Knoester, H.H. Brongersma, Private communication.
[113] R. Souda, M. Aono, C. Oshima, S. Otani, Y. Ishizawa, Surf. Sci. 179 (1987) 199.
[114] R. Souda, T. Aizawa, C. Oshima, S. Otani, Y. Ishizawa, Surf. Sci. 195 (1988) L119.
[115] G.C. van Leerdam, K.M.H. Lenssen, H.H. Brongersma, Nucl. Instrum. Methods Phys. Res. Sect. B 45 (1990) 390.
[116] H.H. Brongersma, J.P. Jacobs, Appl. Surf. Sci. 75 (1994) 133.
[117] H.H. Brongersma, M. de Ridder, A. Gildenpfennig, M.M. Viitanen, J. Eur. Ceram. Soc. 23 (2003) 2761.
[118] F.J.J. Janssen, L.J. van IJzendoorn, A.W. Denier van der Gon, M.J.A. de Voigt, H.H. Brongersma, Phys. Rev. B 70 (2004) 165425.
[119] J.T. Grant, J. Vac. Sci. Technol. A 2 (1984) 1135.
[120] V.Y. Young, G.B. Hoflund, A.C. Miller, Surf. Sci. 235 (1990) 60.
[121] T.M. Buck, G.H. Wheatley, D.P. Jackson, Nucl. Instrum. Methods 218 (1983) 257.
[122] M. Draxler, R. Beikler, E. Taglauer, K. Schmid, R. Gruber, S.N. Ermolov, P. Bauer, Phys. Rev. A 68 (2003) 022901.
[123] E. Rauhala, in: J.R. Tesmer, M. Nastasi (Eds.), Handbook of Modern Ion Beam Materials Analysis, Materials Research Society, Pittsburgh, PA, 1995, p. 3.
[124] J.A. Leavitt, L.C. McIntyre Jr., in: J.R. Tesmer, M. Nastasi (Eds.), Handbook of Modern Ion Beam Materials Analysis, Materials Research Society, Pittsburgh, PA, 1995, p. 37.
[125] M. Draxler, R. Gruber, P. Bauer, J. Electron Spectrosc. Relat. Phenom. 129 (2003) 165.
[126] S.N. Markin, D. Primetzhofer, J.E. Valdes, E. Taglauer, P. Bauer, Nucl. Instrum. Methods Phys. Sect. B, in press (doi:10.1016/j.nimb.2006.12.081).
[127] L.C.A. van den Oetelaar, S.N. Mikhailov, H.H. Brongersma, Nucl. Instrum. Methods Phys. Res. Sect. B 85 (1994) 420.
[128] P.A.J. Ackermans, M.A.P. Creuwels, H.H. Brongersma, P.J. Scanlon, Surf. Sci. 227 (1990) 361.
[129] P. Delichere, K.E. Bere, M. Abon, Appl. Catal. A 172 (1998) 295.
[130] A.W. Denier van der Gon, R Cortenraad, W.P.A. Jansen, M.A. Reijme, H.H. Brongersma, Nucl. Instrum. Methods Phys. Res. Sect. B 161–163 (2000) 56.
[131] J.W. Rabalais, Science 250 (1990) 521.
[132] R. Bastasz, J.W. Medlin, J.A. Whaley, R. Beikler, E. Taglauer, Surf. Sci. 571 (2004) 31.
[133] A.J.H. Maas, M.M. Viitanen, H.H. Brongersma, Surf. Interface Anal. 30 (2000) 3.
[134] E. Taglauer, Appl. Phys. A 51 (1990) 238.
[135] E. Taglauer, Fundamental aspects of heterogeneous catalysis studied by particle beams, in: H.H. Brongersma, R.A. v. Santen (Eds.), NATO ASI B, vol. 265, Plenum Press, 1991, p. 301.
[136] H.H. Brongersma, P.A.C. Groenen, J.P. Jacobs, in: J. Nowotny (Ed.), Science of Ceramic Interfaces 2, in: Materials Science Monographs, vol. 81, Elsevier, 1994, p. 113.
[137] G.C. Nelson, J. Appl. Phys. 47 (1976) 1253.
[138] H. Ebel, M.F. Ebel, E. Hillbrand, J. Electron Spectrosc. Relat. Phenom. 2 (1973) 277.
[139] R. Margraf, H. Knözinger, E. Taglauer, Surf. Sci. 211–212 (1989) 1083.
[140] W.P.A. Jansen, A. Knoester, A.J.H. Maas, P. Schmit, A. Kytökivi, A.W. Denier van der Gon, H.H. Brongersma, Surf. Interface Anal. 36 (2004) 1469.
[141] W.P.A. Jansen, J.M.A. Harmsen, A.W. Denier van der Gon, J.H.B.J. Hoebink, J.C. Schouten, H.H. Brongersma, J. Catal. 204 (2001) 420.
[142] S.N. Ermolov, W.P.A. Jansen, S.N. Markin, V.G. Glebovsky, H.H. Brongersma, Surf. Sci. 512 (2002) 221.
[143] H.H. Brongersma. Private communication.
[144] E. Taglauer, W. Heiland, Surf. Sci. 47 (1975) 234.
[145] H.H. Brongersma, G.C.J. van der Ligt, G. Rouweler, Philips J. Res. 36 (1981) 1.
[146] H.H. Brongersma, H.J. van Daal, in: M. Grasserbauer, H.W. Werner (Eds.), Analysis of Microelectronic Materials and Devices, John Wiley & Sons, 1991, p. 389.
[147] C. Pfaff, M.J. Perez Zurita, C. Scott, P. Patino, M.R. Goldwasser, J. Goldwasser, F.M. Mulcahy, M. Houalla, D.M. Hercules, Catal. Lett. 49 (1997) 13.
[148] S. Rondon, M. Houalla, D.M. Hercules, Surf. Interface Anal. 26 (1998) 329.
[149] I. Peeters, A.W. Denier van der Gon, M.A. Reijme, P.J. Kooyman, A.M. de Jong, J. van Grondelle, H.H. Brongersma, R.A. van Santen, J. Catal. 173 (1998) 28.
[150] Ch. Konvicka, Y. Jeanvoine, E. Lundgren, G. Kresse, M. Schmid, J. Hafner, P. Varga, Surf. Sci. 463 (2000) 199.
[151] G. Gilarowski, H. Niehus, Phys. Status Solidi A 173 (1999) 159.
[152] R.D. van de Grampel, W. Ming, A. Gildenpfennig, J. Laven, H.H. Brongersma, G. de With, R. van der Linde, Langmuir 20 (2004) 145.
[153] F. Richter, H. Papp, G.U. Wolf, T. Gotze, B. Kubias, Fresenius J. Anal. Chem. 365 (1999) 150.
[154] C. Xu, W.S. Oh, Q. Guo, D.W. Goodman, J. Vac. Sci. Technol. A 14 (1996) 1395.
[155] E. Taglauer, Appl. Phys. A 38 (1985) 161.
[156] J. Los, J.J.C. Geerlings, Phys. Rep. 190 (1990) 133.
[157] E. Napetschnig, M. Schmid, P. Varga, Surf. Sci. 556 (2004) 1.
[158] A.W. Denier van der Gon, M.F.F.K. Jongen, H.H. Brongersma, U. van Slooten, A. Manenschijn, Appl. Surf. Sci. 111 (1997) 64.
[159] R. Cortenraad, A.W. Denier van der Gon, H.H. Brongersma, S.N. Ermolov, V.G. Glebovsky, Surf. Interface Anal. 31 (2001) 200.
[160] R. Cortenraad, A.W. Denier van der Gon, H.H. Brongersma, G. Gärtner, A. Manenschijn, Appl. Surf. Sci. 191 (2002) 153.
[161] J. Vaari, J. Lahtinen, T. Vaara, P. Hautojärvi, Surf. Sci. 346 (1996) 1.
[162] R. de Gryse, J. Landuyt, L. Vandenbroucke, J. Vennik, Surf. Interface Anal. 4 (1982) 168.
[163] J.P. Landuyt, L. Vandenbroucke, R. de Gryse, J. Vennik, Surf. Sci. 126 (1983) 598.
[164] M. Alexandrou, R.M. Nix, Surf. Sci. 321 (1994) 47.
[165] J.N. Andersen, J. Onsgaard, A. Nilsson, B. Erickson, N. Martensson, Surf. Sci. 202 (1988) 183.
[166] N.R. Gleason, F. Zaera, Surf. Sci. 385 (1997) 294.
[167] T. Kravchuk, R. Akhvlediani, V.V. Gridin, A. Hoffman, Surf. Sci. 562 (2004) 83.
[168] J.K. Norskov, B.L. Lundqvist, Phys. Rev. B 19 (1979) 5661.
[169] M.L. Yu, N.D. Lang, Nucl. Instrum. Methods Phys. Res. Sect. B 14 (1986) 403.
[170] N.P. Wang, E.A. Garcia, R. Monreal, F. Flores, E.C. Goldberg, H.H. Brongersma, P. Bauer, Phys. Rev. A 64 (2001) 012901.
[171] V. Blum, L. Hammer, W. Meier, K. Heinz, M. Schmid, E. Lundgren, P. Varga, Surf. Sci. 474 (2001) 81.
[172] T. Schulthess, E. Wetli, M. Erbudak, Surf. Sci. 320 (1994) L95.
[173] L. Zhu, E. Zur Muhlen, D.J. O'Connor, B.V. King, R.J. MacDonald, Surf. Sci. 359 (1996) 54.
[174] M. Gierer, M.A. van Hove, A.I. Goldman, Z. Shen, S.L. Chang, P.J. Pinhero, C.J. Jenks, J.W. Anderegg, C.M. Zhang, P.A. Thiel, Phys. Rev. B 57 (1998) 7628.
[175] D.J. O'Connor, Y.G. Shen, J. Yao, Nucl. Instrum. Methods Phys. Res. Sect. B 135 (1998) 355.
[176] Y.G. Shen, D.J. O'Connor, J. Yao, Appl. Surf. Sci. 125 (1998) 300.

[177] Y. Wu, H.S. Tao, E. Garfunkel, T.E. Madey, N.D. Shinn, Surf. Sci. 336 (1995) 123.
[178] R.K. Schulze, T.N. Taylor, M.T. Paffett, J. Vac. Sci. Technol. A 12 (1994) 3054.
[179] Y.G. Shen, J. Yao, D.J. O'Connor, B.V. King, R.J. MacDonald, Phys. Rev. B 56 (1997) 9894.
[180] D.J. O'Connor, M. Draeger, A.M. Molenbroek, Y.G. Shen, Surf. Sci. 357–358 (1996) 202.
[181] Y.G. Shen, D.J. O'Connor, R.J. MacDonald, K. Wandelt, in: R.J. MacDonald, E. Taglauer, K.R. Wandelt (Eds.), Surface Science: Principles and Current Applications, Springer, Berlin, 1996, p. 115.
[182] D. Schaepers, H.H. Strehblow, Corros. Sci. 39 (1997) 2193.
[183] A.W. Stobbe-Kreemers, G.C. van Leerdam, J.P. Jacobs, H.H. Brongersma, J.J.F. Scholten, J. Catal. 152 (1995) 130.
[184] W. Yu, J.L. Sullivan, S.O. Saied, Surf. Sci. 352–354 (1996) 781.
[185] J.J.W.M. Rosink, J.P. Jacobs, H.H. Brongersma, AIP Conf. Proc. 378 (1996) 44.
[186] C. Xu, W.S. Oh, D.W. Goodman, J. Phys. Chem. B 104 (2000) 10310.
[187] M. de Ridder, A.G.J. Vervoort, R.G. van Welzenis, H.H. Brongersma, Solid State Ionics 156 (2003) 255.
[188] P.J. Scanlon, R.A.M. Bink, F.P.F. van Berkel, G.M. Christie, L.J. van IJzendoorn, H.H. Brongersma, R.G. van Welzenis, Solid State Ionics 112 (1998) 123.
[189] L. Zhang, M. Kuhn, U. Diebold, Surf. Sci. 371 (1997) 223.
[190] E. Platzgummer, M. Sporn, R. Koller, M. Schmid, W. Hofer, P. Varga, Surf. Sci. 453 (2000) 214.
[191] V. Stamenkovic, T.J. Schmidt, P.N. Ross, N.M. Markovic, J. Phys. Chem. B 106 (2002) 11970.
[192] E. Taglauer, R. Beikler, Vacuum 73 (2004) 9.
[193] R. Beikler, E. Taglauer, Nucl. Instrum. Methods Phys. Res. Sect. B 193 (2002) 455.
[194] Y.G. Shen, D.J. O'Connor, K. Wandelt, R.J. MacDonald, Surf. Sci. 331–333 (1995) 746.
[195] Y.G. Shen, D.J. O'Connor, K. Wandelt, Surf. Sci. 406 (1998) 23.
[196] Y.G. Shen, D.J. O'Connor, H. van Zee, K. Wandelt, R.J. MacDonald, Thin Solid Films 263 (1995) 72.
[197] J. Yoshihara, J.M. Campbell, C.T. Campbell, Surf. Sci. 406 (1998) 235.
[198] G. Gilarowski, J. Mendez, H. Niehus, Surf. Sci. 448 (2000) 290.
[199] S. Terreni, M. Canepa, E. Magnano, P. Cantini, P. Pelori, L. Mattera, Nucl. Instrum. Methods Phys. Res. Sect. B 183 (2001) 97.
[200] P. Delichere, J.C. Bertolini, Surf. Interface Anal. 34 (2002) 116.
[201] L. Cornaglia, M. Houalla, J. Goldwasser, D.M. Hercules, Catal. Lett. 63 (1999) 131.
[202] Y.G. Shen, A. Bilic, D.J. O'Connor, B.V. King, Surf. Sci. 394 (1997) L131.
[203] T. Asahata, M. Onobu, A. Kondo, R. Shimizu, H.J. Kang, Jpn. J. Appl. Phys. 36 (1997) 7427.
[204] H.J. Kang, C.H. Kim, N.S. Park, D.J. O'Connor, R. MacDonald, Appl. Surf. Sci. 100–101 (1996) 329.
[205] E. Taglauer, J. du Plessis, G.N. van Wyk, in: R.J. MacDonald, E. Taglauer, K.R. Wandelt (Eds.), Surface Science: Principles and Current Applications, Springer, Berlin, 1996, p. 136.
[206] P. Druska, H.H. Strehblow, Surf. Interface Anal. 23 (1995) 440.
[207] C. Li, T. Asahata, R. Shimizu, J. Appl. Phys. 77 (1995) 3439.
[208] T. Neidhart, M. Sporn, M. Schmid, P. Varga, Nucl. Instrum. Methods Phys. Res. Sect. B 101 (1995) 127.
[209] A. Tolstogouzov, S. Daolio, C. Pagura, Nucl. Instrum. Methods Phys. Res. Sect. B 217 (2004) 246.
[210] A.M. Lam, Y.J. Zheng, J.R. Engstrom, Chem. Phys. Lett. 292 (1998) 229.
[211] A.M. Lam, Y.J. Zheng, J.R. Engstrom, Appl. Phys. Lett. 73 (1998) 2027.
[212] J. Kuntze, S. Speller, W. Heiland, P. Deurinck, C. Creemers, A. Atrei, U. Bardi, Phys. Rev. B 60 (1999) 9010.
[213] V.A. Bondzie, S.C. Parker, C.T. Campbell, J. Vac. Sci. Technol. A 17 (1999) 1717.
[214] V.A. Bondzie, S.C. Parker, C.T. Campbell, Catal. Lett. 63 (1999) 143.
[215] W.C.A.N. Ceelen, M. de Ridder, B. Moest, A.W. Denier van der Gon, H.H. Brongersma, Surf. Sci. 430 (1999) 146.
[216] W.C.A.N. Ceelen, B. Moest, M. de Ridder, L.J. van IJzendoorn, A.W. Denier van der Gon, H.H. Brongersma, Appl. Surf. Sci. 134 (1998) 87.
[217] P. Dolle, R. Baudoing-Savois, M. De Santis, M.C. Saint-Lager, M. Abel, J.C. Bertolini, P. Delichere, Surf. Sci. 518 (2002) 1.
[218] I. Spolveri, A. Atrei, U. Bardi, M. Torrini, G. Rovida, V. Martynyuk, M. Vasiliev, Surf. Sci. 419 (1999) 303.
[219] C. Creemers, P. Deurink, Surf. Interface Anal. 25 (1997) 177.
[220] M. Canepa, E. Magnano, A. Campora, P. Cantini, M. Salvietti, L. Mattera, Surf. Sci. 352–354 (1996) 36.
[221] C. Schmidt, H.H. Strehblow, J. Electrochem. Soc. 145 (1998) 834.
[222] C. Creemers, Surf. Sci. 360 (1996) 10.
[223] F. Yubero, A.R. Gonzalez-Elipe, S. Tougaard, Surf. Sci. 457 (2000) 24.
[224] P. Schieffer, M.C. Hanf, C. Krembel, G. Gewinner, Surf. Sci. 446 (2000) 175.
[225] P. Schieffer, C. Krembel, M.C. Hanf, G. Gewinner, Phys. Rev. B 55 (1997) 13884.
[226] V.D. Hildenbrand, C.J.M. Denissen, A.J.H.P. van der Pol, A.H.C. Hendriks, C. van der Marel, J.H.M. Snijders, Y. Tamminga, H.H. Brongersma, M.M. Viitanen, J. Electrochem. Soc. 150 (2003) H147.
[227] B.N. Grgur, N.M. Markovic, P.N. Ross Jr., J. Phys. Chem. B 102 (1998) 2494.
[228] A.C. Michel, L. Lianos, J.L. Rousset, P. Delichere, N.S. Prakash, J. Massardier, Y. Jugnet, J.C. Bertolini, Surf. Sci. 416 (1998) 288.
[229] P. Weigand, B. Jelinek, W. Hofer, P. Varga, Surf. Sci. 301 (1994) 306.
[230] W. Hebenstreit, G. Ritz, M. Schmid, A. Biedermann, P. Varga, Surf. Sci. 388 (1997) 150.
[231] J.C. Bertolini, P. Delichere, P. Hermann, Surf. Interface Anal. 24 (1996) 34.
[232] J.R. Kitchin, N.A. Khan, M.A. Barteau, J.G. Chen, B. Yakshinskiy, T.E. Madey, Surf. Sci. 544 (2003) 295.
[233] C. Dong, L. Zhang, U. Diebold, T.E. Madey, Surf. Sci. 322 (1995) 221.
[234] P. Hermann, J.M. Guigner, B. Tardy, Y. Jugnet, D. Simon, J.C. Bertolini, J. Catal. 163 (1996) 169.
[235] H.J. Kang, R.H. Roberts, D.J. O'Connor, R.J. MacDonald, Surf. Sci. 302 (1994) 363.
[236] P. Miegge, J.L. Rousset, B. Tardy, J. Massardier, J.C. Bertolini, J. Catal. 149 (1994) 404.
[237] V.N. Semenov, V.G. Glebovsky, H.H. Brongersma, Vacuum 47 (1996) 1193.
[238] X. Bao, M. Muhler, Th. Schedel-Niedrig, R. Schlögl, Phys. Rev. B 54 (1996) 2249.
[239] T. Janssens, C. Huyghebaert, W. Vandervorst, A. Gildenpfennig, H.H. Brongersma, Appl. Surf. Sci. 203–204 (2003) 30.
[240] J. Zhu, J.G. Van Ommen, A. Knoester, L. Lefferts, J. Catal. 230 (2005) 291.
[241] A.G.J. Vervoort, P.J. Scanlon, M. de Ridder, H.H. Brongersma, R.G. van Welzenis, Nucl. Instrum. Methods Phys. Res. Sect. B 190 (2002) 813.
[242] A. Kytökivi, E.L. Lakomaa, A. Root, H. Österholm, J.P. Jacobs, H.H. Brongersma, Langmuir 13 (1997) 2717.
[243] H.P. Steinrück, F. Pesty, L. Zhang, T.E. Madey, Phys. Rev. B 51 (1995) 2427.
[244] T.J. Schmidt, N.M. Markovic, V. Stamenkovic, P.N. Ross Jr., G.A. Attard, D.J. Watson, Langmuir 18 (2002) 6969.
[245] R. Koller, Y. Gauthier, C. Klein, M. De Santis, M. Schmid, P. Varga, Surf. Sci. 530 (2003) 121.
[246] B. Moest, S. Helfensteyn, P. Deurinck, M. Nelis, A.W. Denier van der Gon, H.H. Brongersma, C. Creemers, B.E. Nieuwenhuys, Surf. Sci. 536 (2003) 177.
[247] E. Platzgummer, M. Sporn, R. Koller, S. Forsthuber, M. Schmid, W. Hofer, P. Varga, Surf. Sci. 419 (1999) 236.
[248] E. Platzgummer, M. Sporn, R. Koller, M. Schmid, W. Hofer, P. Varga, Surf. Sci. 423 (1999) 134.
[249] W.C.A.N. Ceelen, A.W. Denier van der Gon, M.A. Reijme, H.H. Brongersma, I. Spolveri, A. Atrei, U. Bardi, Surf. Sci. 406 (1996) 264.
[250] V. Stamenkovic, M. Arenz, B.B. Blizanac, K.J.J. Mayrhofer, P.N. Ross, N.M. Markovic, Surf. Sci. 576 (2005) 145.
[251] V.R. Stamenkovic, M. Arenz, B.B. Blizanac, P.N. Ross, N.M. Markovic, J. New Mater. Electrochem. Syst. 7 (2004) 125.
[252] V.R. Stamenkovic, M. Arenz, C.A. Lucas, M.E. Gallagher, P.N. Ross, N.M. Markovic, J. Amer. Chem. Soc. 125 (2003) 2736.

[253] U. Diebold, L. Zhang, J.F. Anderson, P. Mrozek, J. Vac. Sci. Technol. A 14 (1996) 1679.
[254] T. Kawano, Y. Takai, R. Shimizu, Jpn. J. Appl. Phys. 39 (2000) 577.
[255] R. Cortenraad, S.N. Ermolov, V.N. Semenov, A.W. Denier van der Gon, V.G. Glebovski, S.I. Bozhko, H.H. Brongersma, J. Cryst. Growth 222 (2001) 154.
[256] S.C. Lee, Y. Irokawa, M. Inoue, R. Shimizu, Surf. Sci. 359 (1996) 198.
[257] N.R. Gleason, F. Zaera, J. Catal. 169 (1997) 365.
[258] G.C. Herdt, A.W. Czanderna, J. Vac. Sci. Technol. A 15 (1997) 513.
[259] M. Prevost, Y. Barbaux, L. Gengembre, B. Grzybowska, J. Chem. Soc. Faraday Trans. 92 (1996) 5103.
[260] H.H. Brongersma, A. Gildenpfennig, A.W. Denier van der Gon, R.D. van de Grampel, W.P.A. Jansen, A. Knoester, J. Laven, M.M. Viitanen, Nucl. Instrum. Methods Phys. Res. Sect. B 190 (2002) 11.
[261] R.D. van de Grampel, W. Ming, A. Gildenpfennig, W.J.H. van Gennip, J. Laven, J.W. Niemantsverdriet, H.H. Brongersma, G. de With, R. van der Linde, Langmuir 20 (2004) 6344.
[262] M.A. Reijme, A.W. Denier van der Gon, M. Draxler, A. Gildenpfennig, F.J.J. Janssen, H.H. Brongersma, Surf. Interface Anal. 36 (2004) 1.
[263] M.W.G. Ponjee, M.A. Reijme, A.W. Denier van der Gon, H.H. Brongersma, B.M.W. Langeveld-Voss, Polymer 43 (2002) 77.
[264] J.M.A. Harmsen, W.P.A. Jansen, J.H.B.J. Hoebink, J.C. Schouten, H.H. Brongersma, Catal. Lett. 74 (2001) 133.
[265] Z. Paal, P. Tetenyi, M. Muhler, U. Wild, J.M. Manoli, C. Potvin, J. Chem. Soc. Faraday Trans. 94 (1998) 459.
[266] F.M. Mulcahy, J. Goldwasser, A. Proctor, M. Houalla, D.M. Hercules, Surf. Interface Anal. 24 (1996) 306.
[267] V. Sazo, L. Gonzales, J. Goldwasser, M. Houalla, D.M. Hercules, Surf. Interface Anal. 23 (1995) 367.
[268] W.P.A. Jansen, M. Ruitenbeek, A.W. Denier van der Gon, J.W. Geus, H.H. Brongersma, J. Catal. 196 (2000) 379.
[269] F. Richter, H. Papp, Th. Götze, G.U. Wolf, B. Kubias, Surf. Interface Anal. 26 (1998) 736.
[270] M.M. Viitanen, W.P.A. Jansen, R.G. van Welzenis, H.H. Brongersma, D.S. Brands, E.K. Poels, A. Bliek, J. Phys. Chem. B 103 (1999) 6025.
[271] M. Borrell, A. Jentys, P. Varga, Microchim. Acta 125 (1997) 389.
[272] A. Renouprez, J.F. Faudon, J. Massardier, J.L. Rousset, P. Delichere, G. Bergeret, J. Catal. 170 (1997) 181.
[273] S. Labich, E. Taglauer, H. Knözinger, Top. Catal. 14 (2001) 153.
[274] J.N. Fiedor, M. Houalla, A. Proctor, D.M. Hercules, Surf. Interface Anal. 23 (1995) 234.
[275] N. Vaidyanathan, M. Houalla, D.M. Hercules, Surf. Interface Anal. 26 (1998) 415.
[276] V.V. Guliants, R. Bhandari, H.H. Brongersma, A. Knoester, A.M. Gaffney, S. Han, J. Phys. Chem. B 109 (2005) 10234.
[277] L.C.A. van den Oetelaar, O.W. Nooij, S. Oerlemans, A.W. Denier van der Gon, H.H. Brongersma, L. Lefferts, A.G. Roosenbrand, J.A.R. van Veen, J. Phys. Chem. B 102 (1998) 3445.
[278] J.L. Rousset, A.J. Renouprez, A.M. Cadrot, Phys. Rev. B 58 (1998) 2150.
[279] J.L. Rousset, A.M. Cadrot, L. Lianos, A.J. Renouprez, Eur. Phys. J. D 9 (1999) 425.
[280] M. Gaudry, et al., Phys. Rev. B 67 (2003) 155409.
[281] D. Hecht, H.H. Strehblow, J. Electroanal. Chem. 436 (1997) 109.
[282] S. Daolio, C. Pagura, A. Tolstogouzov, Appl. Surf. Sci. 222 (2004) 166.
[283] H. Niehus, E. Bauer, Surf. Sci. 47 (1975) 222.
[284] M.J. Ashwin, D.P. Woodruff, Surf. Sci. 244 (1991) 247.
[285] M. Beckschulte, E. Taglauer, Nucl. Instrum. Methods Phys. Res. Sect. B 78 (1993) 29.
[286] R. Cortenraad, A.W. Denier van der Gon, H.H. Brongersma, G. Gaertner, A. Manenschijn, Appl. Surf. Sci. 146 (1999) 69.
[287] S.P. Chenakin, V.T. Cherepin, I.Yu. Panichkin, A.L. Pivovarov, Appl. Phys. A 62 (1996) 175.
[288] J.T. Mayer, U. Diebold, T.E. Madey, E. Garfunkel, J. Electron Spectrosc. Relat. Phenom. 73 (1995) 1.
[289] R. Bergmans, Ph.D. Thesis, Eindhoven University of Technology, The Netherlands, 1996, p. 59.